NASA SP-239

KINETICS AND THERMODYNAMICS IN HIGH-TEMPERATURE GASES

A conference held at
LEWIS RESEARCH CENTER
Cleveland, Ohio
March 19, 1970

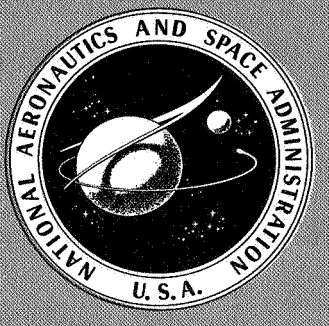

NATIONAL AERONAUTICS AND SPACE ADMINISTRATION

NASA SP-239

KINETICS AND THERMODYNAMICS IN HIGH-TEMPERATURE GASES

A conference held at
Lewis Research Center, Cleveland, Ohio
March 19, 1970

Prepared by Lewis Research Center

Scientific and Technical Information Division
OFFICE OF TECHNOLOGY UTILIZATION 1970
NATIONAL AERONAUTICS AND SPACE ADMINISTRATION
Washington, D.C.

For sale by the Clearinghouse for Federal Scientific and Technical Information
Springfield, Virginia 22151 – Price $3.00

FOREWORD

The Lewis Research Center is the National Aeronautics and Space Administration principal field installation for research and development of advanced aerospace propulsion and power generation systems. While much of the work at Lewis in these areas is applied research, a balanced effort must include basic, creative research. Such an effort establishes the base from which come future engineering applications.

Aircraft and rocket propulsion and, to a lesser extent, power generation involve the chemistry and physics of combustion and the properties of gases at high temperatures. NASA and its predecessor, the National Advisory Committee for Aeronautics, have long maintained a basic research program in these fields. The results of this work are published as NASA reports and in the technical journals, but an occasional technical conference further assists in communicating with others in the scientific fraternity. Therefore, this conference is presented to describe selected topics of Lewis work in the kinetics and thermodynamics of combustion and high-temperature gases.

Bruce T. Lundin
Director

CONTENTS

I. COMPLEX CHEMICAL EQUILIBRIUM CALCULATIONS

Sanford Gordon

Many of the chemical and flow processes taking place in rockets and airbreathing engines occur at high temperatures (of the order of, say, 2000 to 5000 K). At these temperatures, for example, molecules break up into atoms or free radicals, some species react to form new species, or neutral species ionize. The result is that we often have to deal with mixtures containing many kinds of chemical species. If we want to know theoretical properties of these complex mixtures, such as thermodynamic or transport properties, it is first necessary to calculate the equilibrium composition of the mixtures.

For a number of years Lewis has been working with equilibrium calculations for a wide variety of chemical systems. To carry out these calculations, we have developed mathematical procedures and computer programs (refs. 1 to 7).

Based on our experience, we could discuss many aspects of the equilibrium calculation; however, this paper is concerned only with the following topics: (1) a comparison between two formulations for chemical equilibrium and (2) a comparison of some thermodynamic derivatives for reacting and nonreacting systems.

TWO FORMULATIONS FOR CHEMICAL EQUILIBRIUM

The two formulations currently used for obtaining chemical equilibrium compositions will be referred to as the equilibrium constant method and the free-energy minimization method. The equilibrium constant method has been in use for many years and is the one usually described in thermodynamic texts (e.g., ref. 8). The free-energy minimization method was suggested in 1958 (ref. 9) and is not as well known. Both methods are based on the same principle for the condition of chemical equilibrium, namely, minimum free energy. This principle can be expressed mathematically as

$$\delta G\Big|_{T,P} = 0 \tag{1}$$

where G is the Gibbs free energy, T is temperature, and P is pressure. Equa-

tion (1) says that at constant temperature and pressure the condition necessary for thermodynamic equilibrium is that the Gibbs free energy be stationary with respect to all independent variations in composition.

Depending on the details of how equation (1) is developed (ref. 7), we can end up with either the equilibrium constant method or the free-energy minimization method. Rather than reviewing these details here, I will illustrate these methods by means of a few examples.

Equilibrium Constant Method

One reaction. - The simplest example of an equilibrium problem is one involving two species. For example, for molecular and atomic hydrogen (H_2 and H), we can write down the following reaction

$$\frac{1}{2} H_2 \rightleftharpoons H \tag{2}$$

(Hydrogen is the working fluid of a nuclear rocket engine and therefore the equilibrium composition of this system at various conditions is of practical interest.)

For every reaction we have an equilibrium constant K which can be expressed in two ways. The first way relates K to thermodynamic data:

$$K = e^{-\Delta G^{o}/RT} \tag{3}$$

where ΔG^{o} is the change in standard state free energy across the reaction, and R is the gas constant. Values for K as a function of temperature can be found in tables of thermodynamic data such as in references 10 and 11. The second way K may be expressed is in terms of a function of composition. For equation (2) we can relate the constant K obtained from equation (3) as follows:

$$K = \frac{p_H}{p_{H_2}^{1/2}} \tag{4}$$

where p_H and p_{H_2} are the partial pressures of H and H_2, respectively. To obtain compositions, auxiliary equations are usually used in addition to equilibrium equations. In this case we can make use of the pressure equation (Dalton's law for ideal gases)

$$P = p_H + p_{H_2} \tag{5}$$

where P is the system pressure. Combining equations (4) and (5) gives the quadratic espression

$$p_H^2 + K^2 p_H - K^2 P = 0 \tag{6}$$

Equation (6) can be solved in closed form. However, a closed-form solution is usually possible only with simple problems such as illustrated here. For example, for T = 3000 K and P = 1 atmosphere, with the value K = 0.1574 from reference 10, equation (6) gives $p_H = 0.145$, and from equation (5) $p_{H_2} = 0.855$. These numerical values will be used again in later discussion.

Several reactions. - The hydrogen-fluorine system provides an illustration of a somewhat more complicated equilibrium problem. This system is an extremely energetic propellant with which Lewis has done pioneering work (e.g., ref. 12). The problem here is to determine the equilibrium composition among the following five species: H_2, F_2, H, F, and HF. Other species, such as polymers of HF could also be considered but they will be omitted in this example. The species selected have the following set of reactions:

$$\left.\begin{aligned} \tfrac{1}{2} H_2 &\rightleftarrows H \\ \tfrac{1}{2} F_2 &\rightleftarrows F \\ \tfrac{1}{2} H_2 + \tfrac{1}{2} F_2 &\rightleftarrows HF \end{aligned}\right\} \tag{7}$$

Corresponding to these reactions are the following equilibrium constant equations:

$$\left.\begin{aligned} K_H &= \frac{p_H}{p_{H_2}^{1/2}} \\ K_F &= \frac{p_F}{p_{F_2}^{1/2}} \\ K_{HF} &= \frac{p_{HF}}{p_{H_2}^{1/2} p_{F_2}^{1/2}} \end{aligned}\right\} \tag{8}$$

In addition to these equilibrium equations and a pressure equation (such as eq. (5)), mass balance equations may be used in the form

$$\sum_j a_{ij} n_j - b_i^o = 0 \tag{9}$$

where a_{ij} are the number of gram-atoms of the i^{th} element in the j^{th} species, n_j are moles of species j, and b_i^o are gram-atoms of element i per gram of mixture.

Other than the fact that there are more equations to solve, there are two important differences between this example and the previous example. The first difference involves the use of components. For our purpose here, components are just some selected species, one for each chemical element, in terms of which all the remainder may be written. In this example, H_2 and F_2 were selected as components. For systems which involve many species, the use of components is the simplest way to specify reactions systematically. Components are a unique feature of the equilibrium constant method. As we shall see later, the free-energy minimization method does not use components.

The second important difference between this example and the first example is that now the solution cannot be obtained in closed form. This means that we must resort to some graphical, trial and error, or iterative procedure. There are numerous ways in which the details of solving the problem may vary (based on one's chemical intuition and selection of mathematical techniques). The fact that there are so many ways to solve the problem may explain why so many papers are written on this subject. (See ref. 7 for a partial list.) Often the success of a method depends on essentially knowing the answers already or at least quite a bit of the chemistry involved for a particular chemical system.

Many reactions. - The third example of the equilibrium constant method involves many species. The system selected to illustrate this complex equilibria situation is a solid rocket propellant containing the following ingredients: hydrocarbon binder (with some oxygen and sulfur), ammonium perchlorate, aluminum, and magnesium oxide. This system contains eight chemical elements: C, H, O, N, Al, Mg, Cl, and S. Currently, there are 140 possible combustion species (including 18 condensed and 32 ionized species) in the Lewis library of thermodynamic data that are formed from these eight elements.

Now, how should one go about handling the mathematics of solving about 140 simultaneous nonlinear equations? There are two approaches to this problem. One approach, as indicated in the discussion of the previous example, is to study the chemistry of this specific problem and then to work out specific techniques and procedures to solve this particular chemical system.

A second approach, which is the approach we have adopted, is to generalize the problem. This means that methods are developed and used which are equally applicable to any chemical system (refs. 1 to 7). In order to insure that these general methods will actually lead to a solution, attention must be given to mathematical details such as iteration techniques, convergence controls, and singularities.

So far, several examples of varying degrees of complexity have been discussed, all of which can be solved by the equilibrium constant method. Now we will look at the free energy method.

Free-Energy Minimization Method

The concept of minimum free energy as the criterion for equilibrium can be illustrated graphically as shown in figure I-1. We are again dealing with the first example selected to illustrate the use of equilibrium constants, that is, the determination of the equilibrium composition of a mixture of H_2 and H at T = 3000 K and P = 1 atmosphere. Figure I-1 is a plot of the free energy of the mixture G versus the partial pressure of H_2. (We could equally well have used p_H as the abscissa.) The minimum value of G occurs at $p_{H_2} = 0.855$ which is exactly the value obtained by the equilibrium constant method. This graphical example illustrates how one might apply the principle of minimum free energy as the criterion for chemical equilibrium. However, as soon as the problem becomes even slightly more complicated than this simple example, the graphical method becomes impractical or, more usually, impossible to use.

Therefore, we must use equations. As is often true in minimization problems, the function to be minimized is subject to certain constraints. In this case, G is to be minimized subject to the mass balance constraints given by equation (9). Equation (1) then becomes

$$\delta\left[G + \sum_i \lambda_i \left(\sum_j a_{ij} n_j - b_i^o\right)\right]_{T,P} = 0 \tag{10}$$

where λ_i are Lagrangian multipliers. After performing some mathematical details (ref. 7), one ends up with

$$\left(\frac{G^o}{RT}\right)_j + \ln p_j + \frac{1}{RT} \sum_i \lambda_i a_{ij} = 0 \tag{11}$$

The equations in equation (11) (one for each species) are analogous to the equilibrium constant equations used in the equilibrium constant method. This will be illustrated by applying equation (11) to the hydrogen-fluorine problem used previously and comparing these with the analogous equation (8).

For the five species, H_2, F_2, H, F, and HF, equation (11) gives

$$\left.\begin{aligned}
\ln p_{H_2} &= \left[\left(-G^o\right)_{H_2} + 2\lambda_H \right] \Big/ RT \\
\ln p_{F_2} &= \left[\left(-G^o\right)_{F_2} + 2\lambda_F \right] \Big/ RT \\
\ln p_H &= \left[\left(-G^o\right)_H + \lambda_H \right] \Big/ RT \\
\ln p_F &= \left[\left(-G^o_F\right) + \lambda_F \right] \Big/ RT \\
\ln p_{HF} &= \left[\left(-G^o_{HF}\right) + \lambda_H + \lambda_F \right] \Big/ RT
\end{aligned}\right\} \qquad (12)$$

For the purpose of comparison, equation (8) may be written in logarithmic variables and terms slightly rearranged as follows:

$$\left.\begin{aligned}
\ln p_H &= \ln K_H + \frac{1}{2} \ln p_{H_2} \\
\ln p_F &= \ln K_F + \frac{1}{2} \ln p_{F_2} \\
\ln p_{HF} &= \ln K_{HF} + \frac{1}{2} \ln p_{H_2} + \frac{1}{2} \ln p_{F_2}
\end{aligned}\right\} \qquad (13)$$

At least two points might be made concerning equations (12) and (13). First, equation (12) has more equations than equation (13) because the Lagrangian multipliers λ_H and λ_F are variables which must be solved for simultaneously with the composition variables. Second, before equation (13) can even be written, a set of reactions for the system (eq. (7)) must first be specified. In contrast, no reactions are required for equation (12), nor, as a matter of fact, can reactions be used if they are specified.

At this point it would seem reasonable to inquire whether or not there are any features in the two sets of equations (12) and (13) which would make one formulation

preferable to the other. Superficially it appears that the equilibrium constant method (eq. (13)) might be preferable simply because fewer equations and fewer variables are involved. However, if generalized methods of solution are used, the two formulations reduce to the same number of iterative equations (ref. 3). On the other hand, based on experience with both formulations, we have found that the equilibrium constant method has some disadvantages not found in the free-energy method. These disadvantages are

(1) There is more bookkeeping. First, components must be selected, then reactions must be written in terms of these components (or, equivalently, arrays of stoichiometric coefficients in terms of components must be calculated) and, finally, equilibrium constants for these reactions must be generated. None of this is necessary with the free-energy method.

(2) Numerical difficulties can and do occur when components become extremely small. For example, F_2 is a bad choice for a component for an initial mixture of $3H_2 + F_2$ at 500 K and P = 1 atmosphere, inasmuch as equilibrium calculations give $p_{F_2} = 10^{-58}$. In order to avoid this and other problems which result from using components, some investigators (ref. 13) have suggested switching components in the middle of a calculation. However, with the free-energy method one does not use components in the first place and therefore this type of difficulty never arises.

(3) The possibility of condensed phases complicates the equilibrium calculations. A commonly used procedure is to complete the calculations assuming that only gases are present and then to test whether a condensed phase should, in fact, have been included. Simple tests are available with both formulations.

With the equilibrium constant method, the condensed phase should be included if the following condition is met:

$$\ln p_{vap} > \ln K \tag{14}$$

where $\ln K$ is based on the vaporization reaction for some species A

$$A(condensed) \rightleftharpoons A(vapor) \tag{15}$$

However, equation (14) cannot be used if there is no vapor phase, as in the case of $Al_2O_3(c)$. This fact can result in much special handling and programming for species such as $Al_2O_3(c)$ (refs. 4 and 5).

With the free-energy method, by contrast, the following simple criterion for inclusion of a condensed phase can be used which does not depend on the presence of the corresponding gas phase:

$$G_j^o(c) + \sum_i a_{ij}\lambda_i < 0 \tag{16}$$

(4) It is more difficult to extend the generalized method of solution for nonideal equations of state when using the equilibrium constant method than when using the free-energy method (refs. 6 and 7).

THERMODYNAMIC DERIVATIVES

We know that some confusion exists about thermodynamic derivatives because of the numerous inquiries we receive concerning them. This confusion often occurs because the person does not distinguish clearly the difference between reacting and nonreacting systems.

We will use specific heat and the isentropic exponent to illustrate the problem. The question we are asked most often is "For a given composition at a specified temperature and pressure, how can there be two values of specific heat?" The explanation is made simple by an examination of figure I-2. Two curves are shown plotted of enthalpy as a function of temperature. By definition, specific heat is the slope of these curves:

$$C_p = \left(\frac{\partial h}{\partial T}\right)_P \tag{17}$$

We will assume that the equilibrium mixture of hydrogen is the same as that used for our first example of chemical equilibrium ($p_{H_2} = 0.855$ and $p_H = 0.145$ for $T = 3000$ K and $P = 1$ atm).

Now consider what happens if a flow process takes us from our starting thermodynamic state to another thermodynamic state, for example, $T = 2500$ K and $P = 1$ atmosphere. If the flow process is rapid relative to the chemical reaction rate, then the chemical process can be considered nonreacting. This process is sometimes referred to as a "frozen" composition process. The upper curve in figure I-2 exemplifies the nonreacting situation. The drop in enthalpy shown by this curve is due just to the change of temperature from 3000 to 2500 K. However, if the flow process is very slow relative to the reaction rate, then composition has time to adjust to new equilibrium values corresponding to the new thermodynamic state. This process is called a reacting or equilibrium composition process and is illustrated by the lower curve in figure I-2. In this case the change in enthalpy is due to two factors. One factor, as before, is the change in temperature, and the second factor is the change in composition. It can be seen that a change in compo-

sition may affect enthalpy more than a change in temperature.

How does all this relate to specific heat? Well, two curves pass through the point at T = 3000 K corresponding to the two flow processes just discussed. Since specific heat is just the slope of these curves, it is clear that there certainly can be two values of specific heat for the same thermodynamic conditions.

Figure I-3 shows specific heat for the hydrogen system as a function of temperature for the two conditions of reacting and nonreacting systems. At 3800 K and 1 atmosphere, the equilibrium value of 44 calories per gram per K is nine times the frozen value of 4.8 calories per gram per K. For lower pressures, the factor between the two values can be 20 or more (ref. 14). The large differences in these values point up the importance of distinguishing between reacting and nonreacting processes.

Isentropic Exponent

In many textbooks on fluid dynamics (see ref. 15, for example), the isentropic exponent is given the symbol γ and defined as the ratio of specific heat at constant pressure to specific heat at constant volume

$$\gamma = \frac{C_p}{C_v} \tag{18}$$

Based on this definition, various isentropic relations may be written such as

$$PV^{\gamma} = P_o V_o^{\gamma} = \text{Constant} \tag{19}$$

$$\frac{T}{T_o} = \left(\frac{P}{P_o}\right)^{(\gamma-1)/\gamma} \tag{20}$$

$$a = \sqrt{\gamma nRT} \tag{21}$$

However, equations (19) to (21) are valid only if we are dealing with a nonreacting (frozen) system. In the case of a reacting (equilibrium) system, the correct thermodynamic expression for isentropic exponent γ_s is

$$\gamma_s \equiv -\left(\frac{\partial \ln P}{\partial \ln V}\right)_S = \left(\frac{\partial \ln P}{\partial \ln \rho}\right)_S \tag{22}$$

The relations corresponding to equations (19) to (21) are now

$$PV^{\gamma_S} = P_o V_o^{\gamma_S} = \text{Constant} \tag{23}$$

$$\frac{T}{T_o} = \left(\frac{P}{P_o}\right)^{(\partial \ln T/\partial \ln P)_S} \tag{24}$$

$$a = \sqrt{\gamma_S nRT} \tag{25}$$

where

$$\left(\frac{\partial \ln T}{\partial \ln P}\right)_S = \left(\frac{\gamma - 1}{\gamma}\right)\left[-\frac{\left(\frac{\partial \ln V}{\partial \ln P}\right)_T}{\left(\frac{\partial \ln V}{\partial \ln T}\right)_P}\right] \tag{26}$$

The volume derivatives in equation (26) are discussed in reference 7. Equations (23) to (25) may give considerably different values than the corresponding equations (19) to (21). For example, using data given in reference 14, the correct expression for equilibrium velocity of sound (eq. (25)) gives 5343 feet per second, whereas the incorrect expression (eq. (21)) gives 5873 feet per second, a value which is too high by 10 percent.

Figure I-4 illustrates, by means of an unusual example, that the isentropic exponent is not the ratio of specific heats. Figure I-4 is for a chemical system containing beryllium oxide as one of the products of combustion. The curve is a plot of $\ln P$ versus $\ln \rho$ for the isentropic expansion from combustion conditions to lower pressures and temperatures. At the combustion point (high temperature) the beryllium oxide is in the liquid phase. During isentropic expansion the temperature drops until the freezing point of beryllium oxide is reached. The temperature remains at the freezing point, while the liquid is being converted to the solid phase. The dashed part of the curve indicates the region where both the liquid and solid phases of beryllium oxide exist and where the temperature remains constant.

The slope of the curve can be obtained both graphically and analytically. Reference 7 gives an analytic expression for the slope γ_S when just entropy is constant:

$$\gamma_s = \frac{C_p}{-C_p\left(\frac{\partial \ln V}{\partial \ln P}\right)_T - nR\left(\frac{\partial \ln V}{\partial \ln T}\right)_P^2} \tag{27}$$

In the two solid sections of the curve, the analytic values obtained by means of equation (27) match the graphical values to all figures shown. However, where temperature as well as entropy is constant, equation (27) cannot be applied because it contains derivatives with respect to temperature ($(\partial \ln V/\partial \ln T)_P$ and C_p) which are not defined for constant temperature. For constant entropy and temperature, the following expression for the slope was derived:

$$\gamma_{s,T} \equiv \left(\frac{\partial \ln P}{\partial \ln \rho}\right)_{S,T} = \frac{-1}{\left(\frac{\partial \ln V}{\partial \ln P}\right)_T} \tag{28}$$

This analytic expression also gives values which match the graphical slopes to all figures shown in the dashed part of the curve in figure I-4. The interesting fact in this analysis is that in the region of constant entropy and temperature $\gamma_{s,T} = 0.996$. Inasmuch as the ratio of specific heats can never be less than 1, this unusual example demonstrates that, indeed, the isentropic exponent is not the ratio of specific heats.

COMPUTER PROGRAM

The computer program developed at Lewis to carry out complex chemical equilibria calculations has the following capabilities:

(1) It calculates equilibrium compositions, thermodynamic mixture properties (such as enthalpy and entropy), and thermodynamic derivatives for any of the following assigned pairs of thermodynamic state functions: (T, P), (T, V), (H, P), (U, V), (S, P), and (S, V).

(2) It is a general program designed to handle any chemical system for which thermodynamic data are available.

(3) It considers gas and condensed phases and currently includes thermodynamic data for 402 species.

(4) It contains subroutines for the following applications: constant pressure or volume combustion, theoretical rocket performance, shock wave calculations, and Chapman-Jouguet detonations.

Inquiries concerning this program may be addressed to the author or to Mrs. Bonnie McBride of Lewis.

REFERENCES

1. Huff, Vearl N.; Gordon, Sanford; and Morrell, Virginia E.: General Method and Thermodynamic Tables for Computation of Equilibrium Composition and Temperatures of Chemical Reactions. NACA Rep. 1037, 1951.
2. Gordon, Sanford; Zeleznik, Frank J.; and Huff, Vearl N.: A General Method for Automatic Computation of Equilibrium Compositions and Theoretical Rocket Performance of Propellants. NASA TN D-132, 1959.
3. Zeleznik, Frank J.; and Gordon, Sanford: An Analytical Investigation of Three General Methods of Calculating Chemical-Equilibrium Compositions. NASA TN D-473, 1960.
4. Zeleznik, Frank J.; and Gordon, Sanford: A General IBM 704 or 7090 Computer Program for Computation of Chemical Equilibrium Compositions, Rocket Performance, and Chapman-Jouguet Detonations. NASA TN D-1454, 1962.
5. Gordon, Sanford; and Zeleznik, Frank J.: A General IBM 704 or 7090 Computer Program for Computation of Chemical Equilibrium Compositions, Rocket Performance, and Chapman-Jouguet Detonations. Supplement 1 - Assigned Area-Ratio Performance. NASA TN D-1737, 1963.
6. Zeleznik, Frank J.; and Gordon, Sanford: Equilibrium Computations for Multicomponent Plasmas. Can. J. Phys., vol. 44, no. 4, Apr. 1966, pp. 877-893.
7. Zeleznik, Frank J.; and Gordon, Sanford: Calculation of Complex Chemical Equilibria. Ind. Eng. Chem., vol. 60, no. 6, June 1968, pp. 27-57. (See also Applied Thermodynamics. American Chemical Society Publications, 1968, p. 303).
8. Kirkwood, John G.; and Oppenheim, Irwin: Chemical Thermodynamics. McGraw-Hill Book Co., Inc., 1961.
9. White, W. B.; Johnson, S. M.; and Dantzig, G. B.: Chemical Equilibrium in Complex Mixtures. J. Chem. Phys., vol. 28, no. 5, May 1958, pp. 751-755.
10. Anon.: JANAF Thermochemical Tables. The Dow Chemical Co., Midland, Mich., Dec. 31, 1960 to June 30, 1969.

11. McBride, Bonnie J.; Heimel, Sheldon; Ehlers, Janet G.; and Gordon, Sanford: Thermodynamic Properties to 6000° K for 210 Substances Involving the First 18 Elements. NASA SP-3001, 1963.

12. Douglass, H. W.; Hennings, G.; and Price, H. G., Jr.: Experimental Performance of Liquid Hydrogen and Liquid Fluorine in Regeneratively Cooled Rocket Engines. NASA TM X-87, 1959.

13. Feldmann, H. F.; Simons, W. H.; and Bienstock, D.: Calculating Equilibrium Compositions of Multiconstituent, Multiphase, Chemical Reacting Systems. Rep. BM-RI-7257, Bureau of Mines, May 1969.

14. Svehla, Roger A.: Thermodynamic and Transport Properties for the Hydrogen-Oxygen System. NASA SP-3011, 1964.

15. Shapiro, Ascher H.: Dynamics and Thermodynamics of Compressible Fluid Flow. Vol. 1. Ronald Press Co., 1953.

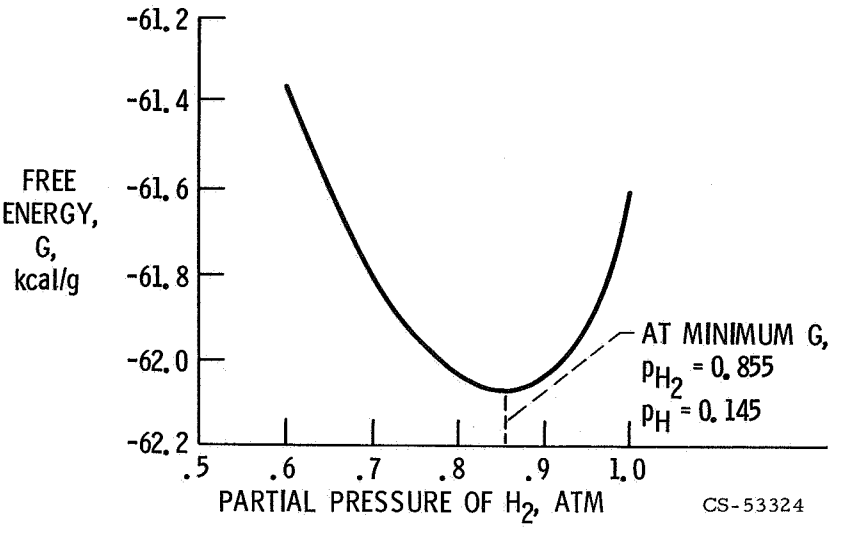

Figure I-1. - Example of minimum free energy as criterion for equilibrium. Mixture of H_2 and H at T = 3000 K and P = 1 atmosphere.

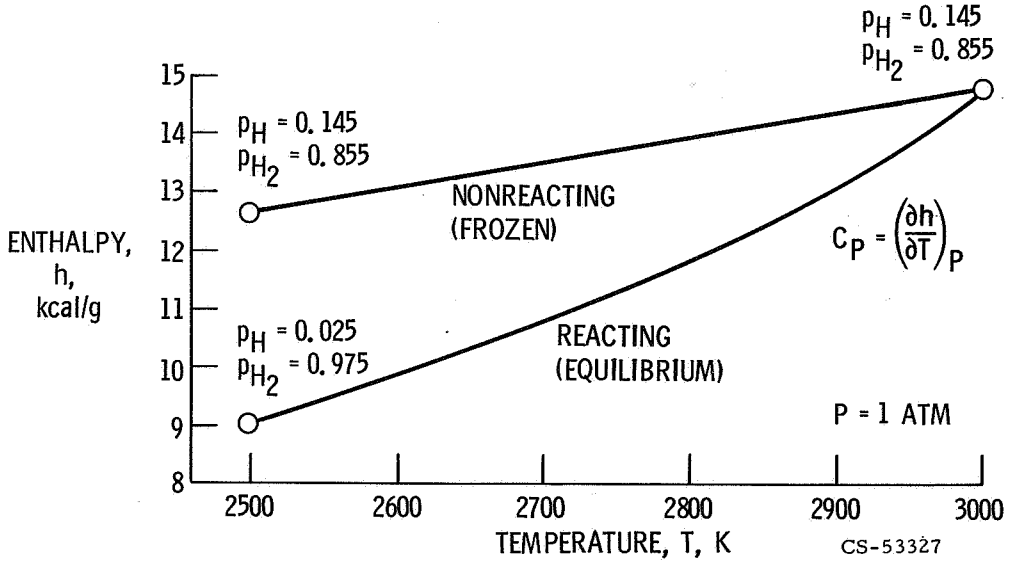

Figure I-2. - Example of how two values of specific heat C_p may exist at one point (same temperature, pressure, and composition).

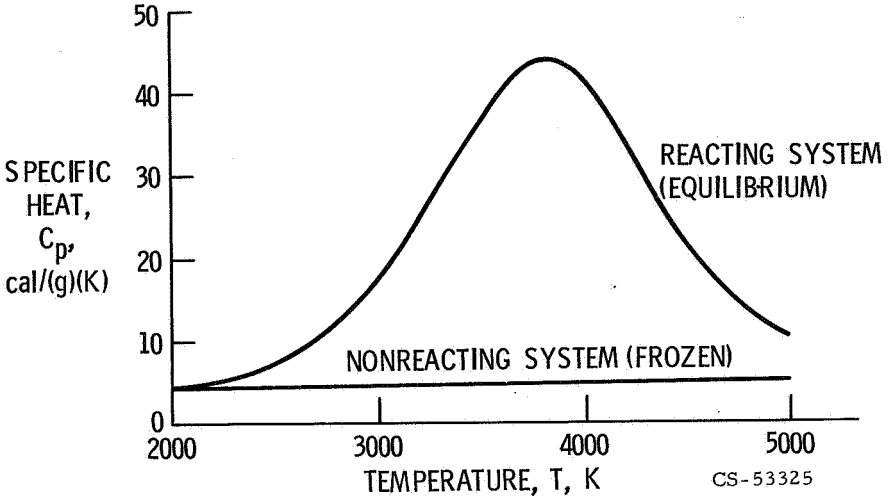

Figure I-3. - Comparison of specific heat for reacting and nonreacting systems. Mixture of H_2 and H at P = 1 atmosphere.

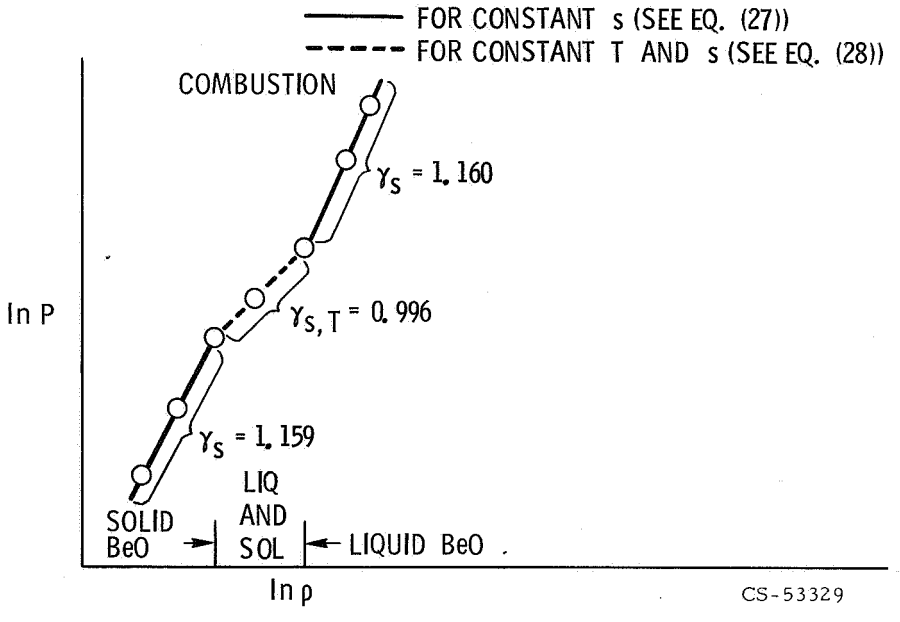

Figure I-4. - Isentropic exponent for usual situation of constant entropy, γ_s, and for special situation of constant entropy and temperature $\gamma_{s,T}$.

II. CALCULATION OF THE EQUILIBRIUM PROPERTIES OF PLASMAS

Sheldon Heimel

The calculation of the equilibrium properties of plasmas is an important subject because many physical situations in space technology involve plasmas. For example, the entry of a high-speed probe into a planetary atmosphere causes shock-ionization. The proper design of a heat shield for such a probe and the choice of an entry pattern requires knowledge of chemical compositions and thermodynamic properties of plasmas (ref. 1). Other situations involving plasma properties are rocket exhausts, thermionic diodes, and magnetohydrodynamic power generators (ref. 2).

The topics that will be covered in this paper are as follows:

(1) The place of plasma calculations in the context of equilibrium calculations

(2) The problems involved in plasma calculations, both theoretical and practical

(3) The effect of the assumptions used in the calculations, as illustrated by hydrogen and lithium plasmas

(4) The effect of the composition model for the atmosphere of the planet Jupiter on its high-temperature properties

PLACE OF PLASMA CALCULATIONS IN CONTEXT OF EQUILIBRIUM CALCULATIONS

In the first paper of this conference, Mr. Gordon discussed the calculation of the thermodynamic properties of combustion gases. When ionized, some combustion gases can be treated by a very simple model, known as the Saha model (ref. 3). Later on, this model is used as a basis for comparison with a more rigorous model of a plasma.

The Saha gas can be illustrated by considering the single-step ionization

$$A^{O} \rightleftharpoons A^{+} + e^{-} \qquad (1)$$

The Saha assumptions are

(1) The ground state makes the chief contribution to the electronic partition function of the ion and atom.

(2) The mass of the ion is approximately equal to the mass of the atom.

(3) The effect of the electric field on the ionization potential (IP) is negligible. This means that the isolated-atom or classical IP can be used.

In a rigorous sense, the mass-action law for equation (1) states

$$\frac{N_+N_-}{N_o} = \frac{Q_+Q_-e^{-I_{eff}/kT}}{Q_o} \tag{2}$$

where N is the number of particles of a kind described by the subscript, Q is the partition function of a particular species, I_{eff} is the effective IP, k is the Boltzmann constant, and T is the absolute temperature in degrees Kelvin. (The subscripts $+$, $-$, and o refer to the unipositive ion, the electron, and the neutral atom, respectively.)

If the Saha assumptions are applied to equation (2), it becomes

$$\frac{N_+N_-}{N_o} \approx \frac{(g_1)_+Q_-e^{-I/kT}}{(g_1)_-} \tag{3}$$

where g_1 is the ground-state statistical weight (multiplicity) of the species referred to by the subscript and I is the classical ionization potential.

COMPARISON OF COMBUSTION GASES AND PLASMAS

In regard to the third assumption, the Saha gas is not a plasma in the sense of the present discussion because the microfields from the charged particles have negligible effects. The plasmas to be discussed do have significant interactions. A plasma will be defined as an ionized gas which is macroscopically neutral but which is nonneutral over a distance which does not exceed the Debye length.

There are additional differences between combustion gases and plasmas. The usual temperature range for combustion gases is 300 to 5000 K; that for plasmas is above 3000 K. The main constituents of combustion gases are molecules and atoms. Plasmas consist chiefly of atoms, ions, and electrons. The effective IP

of a combustion gas is the isolated-atom IP; that for a plasma is the isolated-atom IP reduced by the effects of electrical interactions.

There is also a difference in the kind of chemical potential used for the two gases. (The chemical potential of a species is the increase in the Gibbs free energy of the gaseous mixture produced by the addition of one mole of the species involved.) For a combustion gas, the ideal-gas chemical potential is used. For a plasma, the ideal-gas chemical potential is increased by a term describing the Coulombic forces.

The electronic levels to be considered for a combustion gas are the first few levels. Those for a plasma are all the theoretically predicted levels up to the reduced IP.

THEORETICAL CONSIDERATIONS FOR PLASMA CALCULATIONS

The last feature of the comparison implies that, for a plasma, levels past the reduced IP are not considered in the electronic partition function. If they were included, the partition function would increase without limit (or diverge). This problem of divergence will be discussed shortly.

A related problem that arises in plasma calculations is the lowering of the IP. This problem comes about because it is easier to ionize a species immersed in an electric field. The question is: How much does the IP decrease?

A third problem is that of the missing levels: The literature does not supply all the levels needed for practical calculations.

The final problem is the perturbation or displacement of levels by the microfields. Since this effect has been shown to be small, it will not be discussed further (refs. 4 to 6).

Once the Coulombic effects have been described adequately, the thermodynamic consequences follow logically (ref. 7). These consequences are the reduction of pressure in the equation of state and the corrections to the ideal-gas properties, for example, heat capacity, enthalpy, and entropy, called the excess functions.

DIVERGENCE OF ELECTRONIC PARTITION FUNCTION

Divergence of the electronic partition function can be better understood by considering the electronic partition function for the simple case of the hydrogen atom, namely,

$$Q_{el} = \sum_{n=1}^{\infty} g_n e^{-\epsilon_n/kT} \tag{4}$$

where n is the principal quantum number, g is the statistical weight, and ϵ is the electronic energy. For the hydrogen atom, $g_n = 2n^2$ and values for ϵ are obtained from the Rydberg-Ritz equation.

Table II-1 gives representative principal quantum numbers up to 1000 and their corresponding radii in centimeters. The radii were computed from the formula (ref. 8)

$$a_n = a_o n^2 \tag{5}$$

where a_n is the radius for the n^{th} principal quantum number and a_o is the Bohr radius. If principal quantum numbers from one to infinity were used, the sum in equation (4) would diverge, and the radius calculated from equation (5) would increase without limit. However, at a principal quantum number of 1000, the radius is 10^{-2} centimeter, which is unrealistically large. Thus, one should be able to terminate the sum at some principal quantum number below 1000.

What, then, is the role of orbital size at different temperatures with regard to termination of the partition function? The answer lies in the interplay of orbital size a_n and the size of the contribution of individual energy levels

$$g_n e^{-\epsilon_n/kT}$$

to the sum. At a typical combustion gas temperature of 3000 K (see table II-1), not only does each excited state ($n > 1$) up to the unrealistic radius make a negligible contribution, but the totality of these contributions is negligible. In other words, the sum is insensitive to the exact radius at which it is cut off. If the sum is terminated almost anywhere below $n = 1000$, Q_{el} would still be 2. However, at a typical plasma temperature of 30 000 K, table II-1 shows that each excited state makes a significant contribution to the sum. Therefore, the sum is sensitive to the exact location of the cutoff. Practical experience indicates that, at 30 000 K, ionization is important. Therefore Coulombic forces must be included in a suitable criterion for cutoff.

Several methods that have been proposed for approximating cutoff are as follows:

Inglis-Teller (ref. 9)

$$n^* = \frac{10^{3.11}}{n_e^{2/15}} \tag{6}$$

Ecker-Weizel (ref. 10), Margenau-Lewis (ref. 11), and Kaeppeler-Baumann (ref. 12)

$$n^* \approx 2.75 \times 10^4 \left(\frac{T}{n_e}\right)^{1/4} \tag{7}$$

Gurvich (ref. 13)

$$n^* = 2.461 \left(\frac{T}{P}\right)^{1/6} \tag{8}$$

Bethe (ref. 8)

$$r^* = \left(\frac{3}{4\pi \Sigma n_i}\right)^{1/3} \tag{9}$$

Debye-Hückel (ref. 14)

$$\Delta I = (z_i + 1)\kappa e^2 \tag{10}$$

$$n^* = \left[\frac{(z_i + 1)IP_H}{\Delta I}\right]^{1/2} \tag{11}$$

$$\kappa^2 = \frac{4\pi e^2 \Sigma n_i z_i^2}{kT} \tag{12}$$

Admittedly, there is no exact procedure for terminating the electronic partition function. However, the Debye-Hückel theory of electrolytes has been selected for use in the present work because it yields a consistent set of corrections to the chemical potentials, thermodynamic functions, and equation of state (ref. 14).

The symbols used in the equations for the Debye-Hückel theory are as follows:

ΔI	lowering of ionization potential
z_i	charge number of the charged species i
κ	inverse Debye length
e	electron charge
n^*	maximum principal quantum number
IP_H	ionization potential of hydrogen atom
n_i	particle density of the charged species i
k	Boltzmann constant

The ionization potential of hydrogen is used in the expression for n^* since it is assumed that the high-lying levels are hydrogenic.

LOWERING OF IONIZATION POTENTIAL

Figure II-1 shows the physical basis of the reduction of the ionization potential (ref. 3). The potential energy is plotted against distance of the electron from the nucleus. The upper portion of the figure shows that to transform an isolated atom A^0 in its ground state into an unexcited ion A^+ and an electron e^-, the energy $I_{classical}$ is required. The lower plot shows how an external field perturbs the potential energy curves. Therefore, the same transformation in an electric field requires less energy. This can be interpreted as a lowering of the ionization potential ΔI. In a plasma, an atom is exposed to the action of the Coulomb fields of the ions and electrons (the electric microfields). Therefore, a lowering of the ionization potential is to be expected.

The important thing about ΔI is that it defines the highest energy level to be included in the electronic partition function. The lower dashed line in the lower plot can be interpreted as the highest level to be used.

MISSING LEVELS PROBLEM

Practical calculations require a knowledge of all electronic energy levels up to the reduced IP. However, the spectroscopic data (ref. 15) are incomplete in two respects: first, for each principal level given, the literature does not supply the fine structure of sublevels predicted by wave mechanics, and second, it does

not supply enough of the principal levels for practical calculations (ref. 16). Figure II-2 shows a specific example of the effects of including such levels.

In this figure, the particle density of neutral helium is plotted versus the electronic partition function at 40 000 K and 0.01 atmosphere. The circles enclose energy-level diagrams which symbolize what kinds of levels were used at each point. In the first energy-level diagram only observed principal levels (n = 1, 2, 3) and sublevels were used. In the second diagram the missing sublevels belonging to the observed principal levels were interpolated In the third diagram both types of levels were extrapolated up to the reduced IP. As one would surmise, the more numerous the levels used in the sum, the higher the partition function and particle density.

NECESSITY FOR ITERATIVE CALCULATIONS

In addition to the theoretical problems discussed in the previous sections, there are practical considerations governing the actual calculation. The main difficulty in performing the calculation is the prior knowledge of particle densities in the plasma required by the Debye-Hückel theory (eq. (12)). To overcome this difficulty, a composition is assumed. This allows the computation of a trial value of the Debye length and thus lowering of the ionization potential. For each species, energy levels are summed up to its reduced ionization potential, thus yielding a truncated partition function. New particle densities are then calculated and compared with the previous estimates. If the two sets of estimates do not agree within a specified tolerance, iteration is continued until they do. At the point of convergence, the thermodynamic properties and their derivatives are calculated.

EFFECT OF ASSUMPTIONS USED

Obviously, the Saha model does not require this type of iteration because no IP lowering is used. But, how realistic are the Saha assumptions as compared with the Debye-Hückel theory? Before detailed answers are given, some trends can be predicted from the mass-action law.

In the Saha model, I_{eff} is calculated as if ionization were negligible. Since high pressure represses ionization, the Saha model would be expected to do well at high pressure. In the Saha model, Q_o is calculated as if excited states of the atom made no contribution. This would be true at low temperature. In general,

then, the Saha model would be expected to be more realistic at high pressure and low temperature.

The next two figures present curves of the ratio of the particle density of the neutral atom using the Saha model to the same quantity for the Debye-Hückel theory. This ratio is derived by dividing equation (1) by the Saha equation (2). The quantities that cancel are the partition function of the electron and the classical ionization potential. Among the quantities that do remain is the IP lowering. Detailed calculations show that for high pressures, the ratio of particle densities is close to 1, but may be either greater or less than 1.

The predicted trends will now be checked against the results of calculations for hydrogen and lithium.

Figure II-3 gives the ratio of particle densities of hydrogen for both models as a function of pressure, with temperature as a parameter. A temperature of 10 000 K is low enough so that the Saha model is realistic at all pressures. At 20 000 K, it does well only at the higher pressures. At 40 000 K, the Saha model is not realistic at any pressure. Thus, the discrepancies between the two models follow the expected trend.

Figure II-4 gives the ratio of particle densities of lithium. Again, the discrepancies are in the expected direction. The discrepancies are much smaller than those for hydrogen, partly because lower temperatures were used. The reason that some of the ratios are greater than 1 at the high pressures is that $\Delta I/kT$ is significant.

EFFECT OF COMPOSITION MODEL OF JUPITER'S ATMOSPHERE ON ITS HIGH-TEMPERATURE PROPERTIES

The possible effects of not making a careful calculation of plasma properties have now been presented. The results given by the method selected will now be given for the atmosphere of Jupiter. Figure II-5 is a plot of dimensionless heat capacity versus pressure for ionized mixtures of hydrogen and helium at 40 000 K. Hydrogen and helium are the chief constituents of the Jovian atmosphere. The temperature of 40 000 K is typical for an entry probe at flight speeds of 140 000 and 190 000 feet per second. The heat capacity is calculated for three composition models, namely, atomic hydrogen-helium ratios (H/He) of 2, 5, and 10. Previously this ratio was throught to be 2 (ref. 17). The latest observations of Jupiter show that H/He exceeds 5 (ref. 18). Since helium is the key unknown in the Jovian atmosphere, it may be necessary to send sacrificial probes into it to determine

the helium content more precisely (ref. 1).

In summary, the problems involved in calculating the properties of plasmas have been discussed. A practical method for dealing with these problems has been presented. The calculation of the properties of the Jovian atmosphere is simply one application of the rigorous method used to treat plasmas.

REFERENCES

1. Gilligan, J. E.: Thermophysical Aspects and Feasibility of a Jupiter Atmospheric Entry. Rep. S-4, IIT Research Inst. (NASA CR-93814), Jan. 1968.
2. Fuhs, A. E.: Instrumentation for High Speed Plasma Flow. AGARDograph 96, Gordon and Breach Science Publishers, 1965.
3. Cooper, J.: Plasma Spectroscopy. Reports on Progress in Physics. Vol. 29, Pt. 1. A. C. Steckland, ed., Inst. Physics and Physical Soc., London, 1966, pp. 35-130.
4. Aller, Lawrence H.: Astrophysics: The Atmospheres of the Sun and Stars. Second ed., Ronald Press Co., 1963.
5. Michels, A.; et al.: Arc Discharge in He and H_2 Under High Pressure. Coll. Intern. Centre Natl. Recherche Sci., Paris, no. 77, 1959, pp. 267-281.
6. Cooper, J.: Summary of Discussions. The Lowering of the Ionization Potential and Related Problems of the Equilibrium Plasma. J. Cooper, ed. Rep. 79, Joint Inst. for Lab. Astrophysics, July 15, 1966, pp. 193-199.
7. Zeleznik, Frank J.; and Gordon, Sanford: Equilibrium Computations for Multicomponent Plasmas. NASA TN D-2806, 1965.
8. Bethe, H. A.: The Specific Heat of Air up to 25 000° C. Rep. OSRD 20.869, Office of Scientific Research and Development, Feb. 9, 1942.
9. Inglis, D. R.; and Teller, E.: Ionic Depression of the Series Limit in One-Electron Spectra. Astrophys. J., vol. 90, 1939, pp. 439-448.
10. Ecker, G.; and Weizel, W.: Zustandssumme und Effektive Ionisierungsspannung eines Atoms in Inneren des Plasmas. Ann. d. Physik, vol. 17, nos. 2-3, 1956, pp. 126-140.
11. Margenau, Henry; and Lewis, Marvin: Structure of Spectral Lines from Plasmas. Rev. Mod. Phys., vol. 31, no. 3, July 1959, pp. 569-615.

12. Kaeppeler, H. J.; and Baumann, G.: Irreversible Stochastic Thermodynamics and the Transport Phenomena in a Reacting Plasma. Forschungsinstitut fur Physik der Strahlantriebe e. V., Stuttgart (AFOSR-TR-57-20, DDC No. AD-120462), Nov. 1956.

13. Gurvich, L. V.; and Kvlividze, V. A.: Thermodynamic Functions of Monatomic and Diatomic Gases over a Wide Temperature Range. I. Thermodynamic Functions of Ideal Monatomic Gases. Russian J. Phys. Chem., vol. 35, no. 8, Aug. 1961, pp. 822-827.

14. Griem, Hans R.: Plasma Spectroscopy. McGraw-Hill Book Co., Inc., 1964.

15. Moore, Charlotte E.: Atomic Energy Levels. Circ. 467, National Bureau of Standards. Vol. I - June 15, 1949; Vol. II - Aug. 15, 1952; and Vol. III - May 1, 1958.

16. McChesney, M.: Equilibrium Shock-Wave Calculations in Inert-Gas, Multiply Ionized Debye-Hückel Plasmas. Can. J. Phys., vol. 42, no. 12, Dec. 1964, pp. 2473-2494.

17. Nelson, H. F.; and Goulard, R.: Equilibrium Radiation from Isothermal Hydrogen-Helium Plasmas. J. Quant. Spectrosc. Radiat. Transfer, vol. 8, 1968, pp. 1351-1372.

18. Owen, Tobias; and Mason, Harold P.: New Studies of Jupiter's Atmosphere. J. Atmospheric Sci., vol. 26, no. 5, pt. 1, Sept. 1969, pp. 870-873.

TABLE II-1. - ELECTRONIC PARTITION OF HYDROGEN ATOM

[See eq. (4).]

Principal quantum number, n	1	10	100	1000
Radius, cm	10^{-8}	10^{-6}	10^{-4}	10^{-2}
Contribution to sum, $g_n e^{-\epsilon_n/kT}$:				
For combustion gas at 3000 K	2	10^{-21}	10^{-19}	10^{-17}
For plasma at 30 000 K	2	1	10^{2}	10^{4}

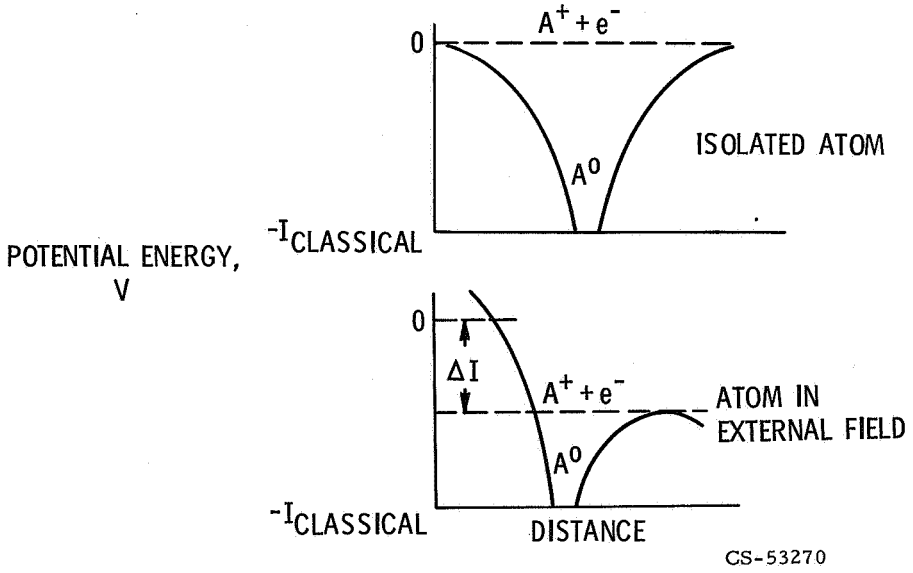

Figure II-1. - Lowering of ionization potential.

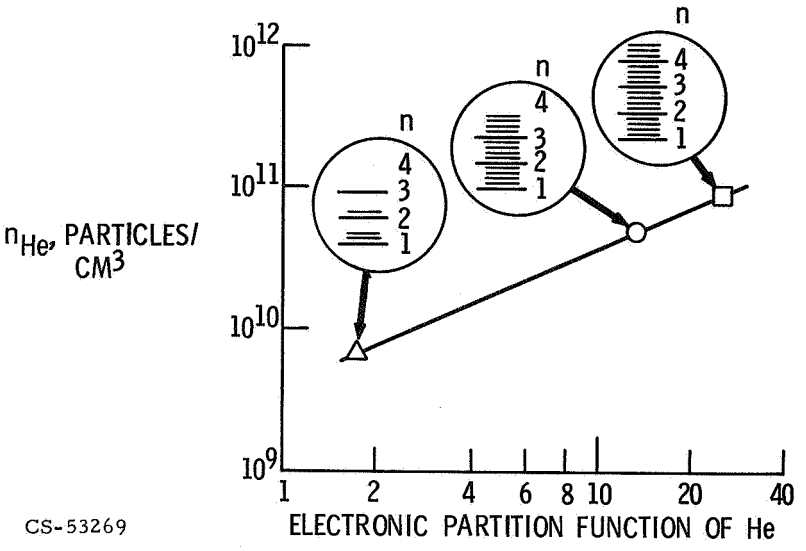

Figure II-2. - Effect of missing energy levels on properties of helium atom. T = 40 000 K; P = 0.01 atmosphere.

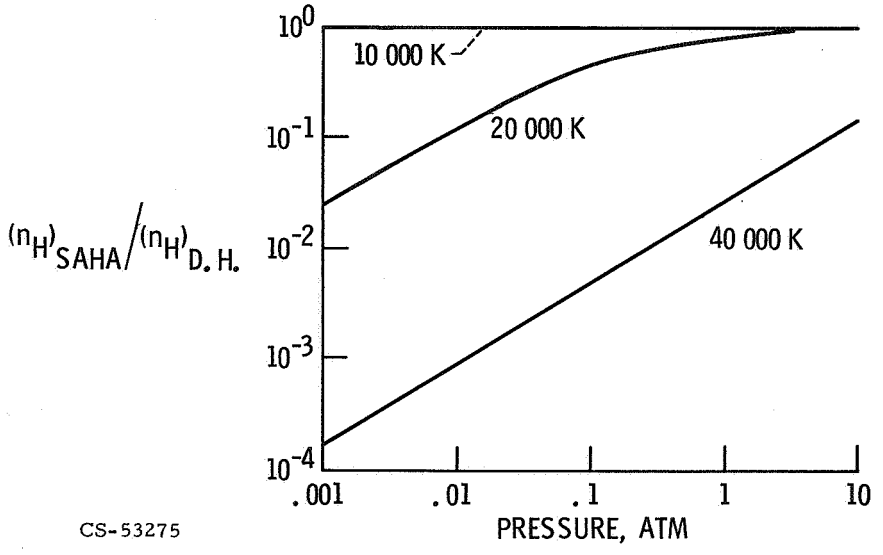

Figure II-3. - Ratio of hydrogen atom number densities using Saha and Debye-Hückel assumptions.

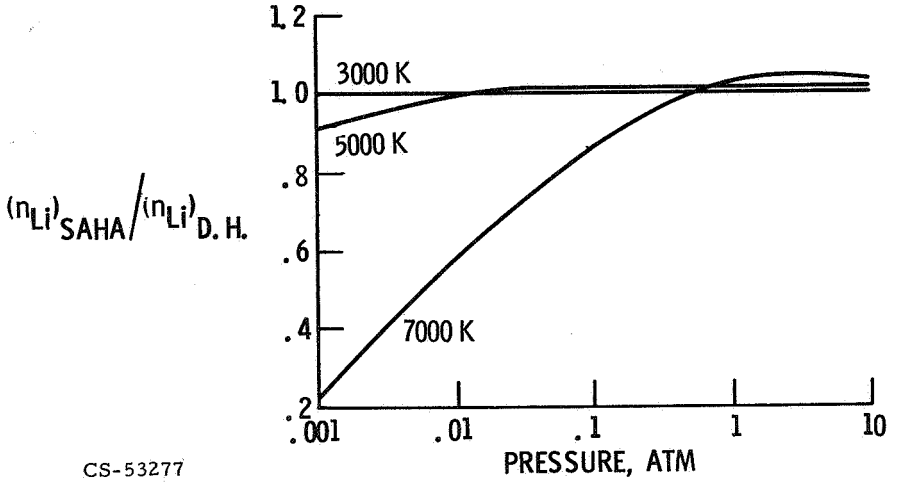

Figure II-4. - Ratio of lithium atom number densities using Saha and Debye-Hückel assumptions.

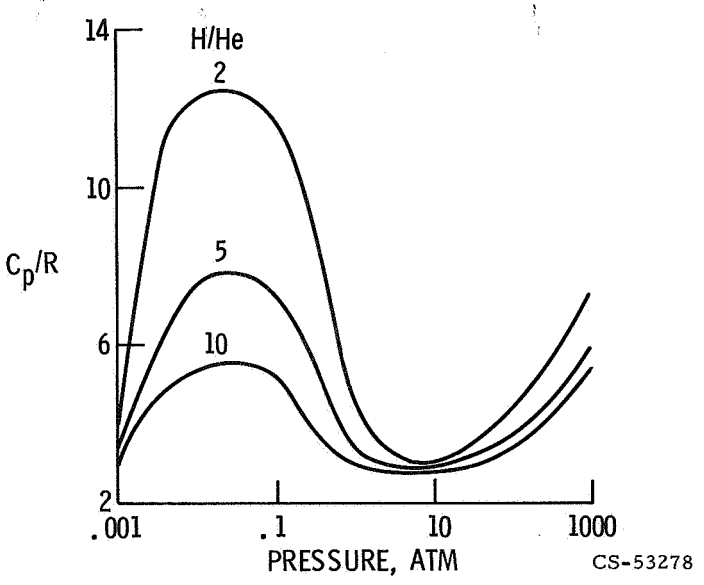

Figure II-5. - Effect of Jovian model on heat capacity at 40 000 K.

III. THERMODYNAMICS OF THE INTERNAL COMBUSTION ENGINE

Frank J. Zeleznik

The ubiquitous automobile has played both the role of hero and villian during the course of its history. At the present time it is being cast as the villian with increasing frequency because it has been indicted as a major source of air pollution. It is just this characterization that is responsible for our renewed interest in the automobile.

When we speak of the automobile as a source of air pollution, we really mean the heart of the automobile, the internal combustion engine. The prototype of the modern internal combustion engine was first successfully operated by Nicholas August Otto in 1876. In spite of its long history, the internal combustion engine is still poorly understood in terms of the details of the physical processes that take place during its operations.

The internal combustion engine operates on what is known as the Otto cycle, and Otto cycle calculations have been with us for many years (ref. 1). The emphasis in earlier calculations was usually on the performance rather than on the pollution aspects. Performance characteristics can often be estimated reasonably accurately even with a considerable degree of simplification. We are interested in the pollution aspects of the internal combustion engine, and therefore the calculations must be performed with more care.

Our extensive experience with equilibrium calculations places us in a position to carry out such careful calculations (ref. 2). We have just recently begun such an analysis, and its objective is the prediction of exhaust gas properties. I will describe our progress by first reviewing the Otto cycle, and then I will illustrate the effect of various assumptions on the calculated results.

DESCRIPTION OF OTTO CYCLE

The typical four-stroke Otto cycle is schematically indicated in figure III-1. Here we see that the internal combustion engine can be simply thought of as a cylinder with one end closed and the other end fitted with a moveable piston. An inlet

port at the closed end admits a combustible mixture into the cylinder, while an exhaust port permits burned gas to escape. The operation of such an engine may be simultaneously represented by these sketches and by a pressure volume chart as in figure III-2. The four-stroke cycle begins with the piston at the top, corresponding to minimum volume. As the volume increases, the intake valve opens and allows a fuel-air mixture to enter the engine at ambient conditions. When the volume has increased to its maximum value, the intake valve closes, and the piston reverses its direction. This reduces the volume, compresses the combustible mixture, and raises its temperature and pressure above the ambient values. When the volume has once more been decreased to its minimum value, the combustible mixture is ignited by a spark plug and the combustion process quickly raises the temperature and pressure by an additional amount. The increased pressure changes the direction of the piston once more, thus expanding the combustion gases. As the hot combustion gases expand, they do work on the piston and also lose some of their energy by heat transfer to the cooled walls. Near the end of the expansion stroke the temperature and pressure are considerably lower than their values at combustion. Nevertheless, at the end of the expansion stroke the pressure is usually somewhat higher than the ambient pressure. At this point the exhaust valve opens and the pressure is suddenly lowered to the ambient value; this is accompanied by a surge of gas out through the exhaust port. Concurrently the piston once more reverses direction and begins to expel the combustion gases that still remain in the cylinder. Not all of the remaining gas is expelled during this exhaust stroke of the piston since at least a portion of it will remain in the cavity that serves as a combustion chamber. This residual gas will dilute the fresh fuel mixture that will enter the cylinder as the next four-stroke cycle commences.

THERMODYNAMIC SIMULATION OF OTTO CYCLE

We shall now attempt to simulate the actual Otto cycle by thermodynamic calculations. It should be understood from the outset that thermodynamics alone cannot supply a truly realistic picture of the Otto cycle. At some point it becomes necessary to abandon a wholly thermodynamic analysis by including important rate processes such as heat transfer and chemical kinetics. However, thermodynamic analysis is a useful first step in the simulation since it supplies some insight into the operation of the Otto cycle and helps a person to form a judgement about the relative importance of some of the parameters. Therefore, in all the calculations to be discussed below, we assumed that combustion takes place instantaneously and essentially at constant volume and that there is no heat transfer. The fuel,

called gasoline, is a mixture of 25 percent benzene, 25 percent octane, and 50 percent dodecane by weight. Also the engine operates at a compression ratio of 8:1.

A first attempt at a simulation of this cycle is illustrated in table III-1. To simplify the calculation, we assume that there is no pressure drop below the ambient pressure during the intake stroke; that is, throttling is negligible. Further we assume that the fuel is fully vaporized and that none of the burned gas from the previous cycle remains in the engine. We also assume that the combustion products remain in chemical equilibrium.

Here we see the specific volume, pressure, and temperature in the engine at five points in the cycle. The five points correspond to the numbers in figure III-2 and are the conditions at (1) the start of the compression stroke, (2) the end of the compression stroke, (3) the start of the expansion stroke, (4) the end of the expansion stroke, and (5) the end of isentropic blowdown to ambient pressure. This calculation represents a considerable idealization of the actual processes taking place in the internal combustion engine. A somewhat more realistic calculation is shown in table III-2, where we have modified the calculation to allow the fuel to partially vaporize in the intake manifold and permitted residual exhaust gases to remain in the engine from cycle to cycle. Additionally it seems experimentally that the concentration of nitric oxide, one of the air pollutants, is unaffected by the expansion, and its concentration remains fixed at the combustion values. This cycle calculation is labeled as B, while the previous calculations of table III-1 are labeled as A. As can be seen, there is a discernible difference between the results of the two calculations.

We can introduce one more element of reality while still remaining wholly within the thermodynamic framework. The additional factor, throttling, is the pressure drop that occurs as the fuel-air mixture passes through the intake system. The appearance of the throttled Otto cycle on a pressure-volume chart is shown in figure III-3. The cross-hatched area represents that part of the cycle that corresponds to the unthrottled cycle. A cycle calculation for a throttled engine is shown in table III-3, where the numbering of points is consistent with the numbering in figure III-3. The throttled cycle calculation is labeled as C, while A once more corresponds to the initial cycle calculation presented as table III-1. Here we see that throttling produces substantial differences from the idealized cycle. This is particularly true of the pressure.

The presence of residual exhaust gases considerably complicates Otto cycle calculations. The reason for this is that the properties of the residual gas are not known until the cycle has been completed. Thus, to initiate a cycle calculation it is necessary to assume the properties of the exhaust gas for the first cycle and

then repeatedly traverse the cycle until the calculation converges. This, in effect, simulates the startup of an automobile; equivalently this can be taken as an indication of the time required for the disappearance of the effects due to large perturbations in the operation of the engine. The exhaust gas temperature corresponding to calculation C is shown in table III-4 as a function of the number of times the cycle is traversed. We see that the effect of the initial exhaust gas properties persists for about three cycles.

OTTO CYCLE AND AIR POLLUTION

The cycle calculations, in their present form, are idealizations but they do shed light on the air pollution problem. In dealing with automobile air pollution, we are concerned with the emission of hydrocarbons, oxides of nitrogen, and carbon monoxide. The production of all of these species is influenced by wall quenching; that is, the contact of the hot gases with the cool cylinder walls. However, sampling experiments (ref. 3) indicate that only something of the order of 1 mass percent of the cylinder contents is directly affected by wall quenching. Thus thermodynamics should give a reasonable estimate of pollutant concentrations in the exhaust. With this in mind let us compare the pollutant concentration in exhaust gases from two fuels, natural gas and gasoline. A great deal has recently been said about the possibility of reducing air pollution by using natural gas as a fuel. In table III-5 we see exhaust gas properties for the two fuels. In each case the cycle calculation corresponded to the throttled Otto cycle that is labeled C in table III-3. Here we see, for the assumptions made in the calculation, that gasoline produces approximately twice the amount of carbon monoxide and 35 percent more nitric oxides. Neither fuel shows any hydrocarbon, which indicates that exhaust hydrocarbons are a result of wall quenching.

The importance of wall quenching for the production of carbon monoxide and hydrocarbons suggests that these species might be eliminated merely by providing a suitable high temperature environment. One of the automotive emission control devices currently under development attempts to do just this. It is known as an exhaust manifold reactor or thermal reactor. Its purpose is to eliminate, by oxidation, any hydrocarbons and carbon monoxide that are exhausted by the automobile engine. Such a reactor is shown attached to an engine in figure III-4. Air is mixed with the exhaust gas at the exhaust port and allowed to react in the reactor. A more detailed sketch of a typical reactor is shown in figure III-5. We see that it is merely an insulated cylinder where sufficient residence time can be provided for the reactions to take place. The residence time is typically of the order

of 20 milliseconds. The effective operation of such a reactor is critically dependent on the temperature. This is shown in figure III-6, which presents the disappearance rate of carbon monoxide. The data were obtained by integrating a system of ordinary differential equations corresponding to 29 reversible chemical reactions. Although the oxidation of carbon monoxide proceeds quite rapidly at 1200 K, it goes relatively slowly at 900 K. As shown in table III-2 for the calculation labeled B, the exhaust gas temperature was 1246 K. This was the calculated exhaust temperature in the absence of any heat transfer. It is not difficult to imagine that, had we included heat transfer, the temperature would be considerably lower and could easily approach 900 K, where the reactor ceases to be effective.

None of the calculations that have been described include heat transfer effects. The presence of heat transfer makes the Otto cycle calculations time dependent in the sense that the Otto cycle conditions depend on the speed with which the cycle is traversed. We are currently working on the problem, but we have not yet reached the stage where we can present results for typical situations.

REFERENCES

1. Starkman, E. S.; Patterson, D. J.; and Taylor, C. Fayette; eds: Digital Calculations of Engine Cycles. Progress in Technology Series, Vol. 7. Society of Automotive Engineers, Inc.

2. Zeleznik, Frank J.; and Gordon, Sanford: Calculation of Complex Chemical Equilibria. Applied Thermodynamics. American Chemical Society Publications, 1968, p. 303.

3. Starkman, E. S.; Stewart, H. E.; and Zvonow, V. A.: An Investigation Into the Formation and Modification of Emission Precursors. Paper 690020, SAE, Jan. 1969.

TABLE III-1. - IDEALIZED OTTO CYCLE

RESULTS FOR UNTHROTTLED ENGINE

[Fuel, stoichiometric gasoline-air; compression ratio, 8; assumptions, fully vaporized fuel, no residual exhaust gas, chemical equilibrium.]

Point	Volume, cc/g	Pressure, atm	Temperature, K
1	849.9	1.0	300
2	106.2	16.93	667
3	106.2	77.88	2874
4	849.9	6.38	1915
5	3700.5	1.0	1308

TABLE III-2. - UNTHROTTLED OTTO

CYCLE CALCULATIONS

[Fuel, stoichiometric gasoline-air; compression ratio, 8.]

Point	Pressure, atm		Temperature, K	
	B (a)	A (b)	B (a)	A (b)
1	1.0	1.0	314	300
2	15.97	16.93	628	667
3	77.29	77.88	2851	2874
4	6.12	6.38	1828	1915
5	1 0	1.0	1246	1308

[a] Partial fuel vaporization; residual exhaust gases: oxides of nitrogen frozen; no throttling.

[b] No fuel vaporization; no residual exhaust gases; oxides of nitrogen in equilibrium; no throttling.

TABLE III-3. - THROTTLED OTTO CYCLE CALCULATIONS

[Fuel, stoichiometric gasoline-air; compression ratio, 8.]

Point	Pressure, atm		Temperature, K	
	C (a)	A (b)	C (a)	A (b)
1	0.50	1.0	343	300
2	7.90	16.93	678	667
3	34.82	77.88	2800	2874
4	2.79	6.38	1820	1915
5	1.0	1.0	1469	1308

[a] Partial fuel vaporization; residual exhaust gases; oxides of nitrogen frozen; throttling.

[b] No fuel vaporization; no residual exhaust gases; oxides of nitrogen in equilibrium; no throttling.

TABLE III-4. - CONVERGENCE RATE IN OTTO CYCLE CALCULATIONS

[Fuel, stoichiometric gasoline-air; compression ratio, 8; residual gas for first cycle, air at 300 K.]

Cycle	Temperature, K
1	1219.7
2	1472.5
3	1469.7
4	1469.3
5	1469.3

TABLE III-5. - EFFECT OF FUEL ON EXHAUST GAS PROPERTIES

[Stoichiometric fuel-air; compression ratio, 8; pressure, 1.0 atm.]

	Natural gas[a]	Gasoline[b]
	Mole fraction	
Ar	0.00842	0.00870
CO	.00300	.00574
CO_2	.09181	.12769
H_2	.00287	.00226
H_2O	.18621	.12260
NO	.00586	.00799
NO_2	.00000	.00001
N_2	.70184	.72501

[a] Temperature, 1393 K.

[b] Temperature, 1469 K.

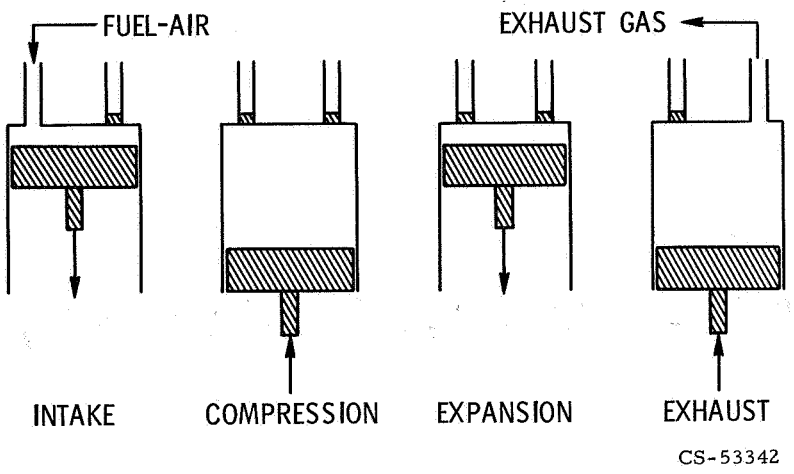

Figure III-1. - Schematic representation of Otto cycle.

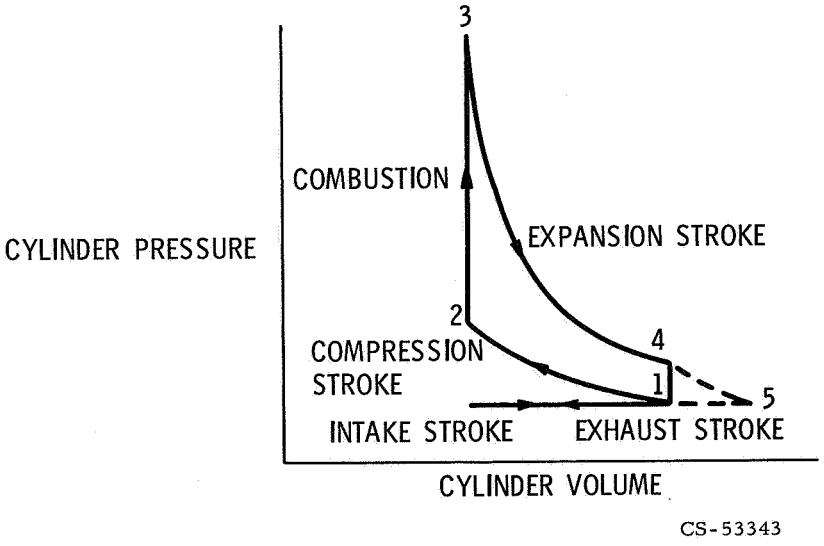

Figure III-2. - Pressure-volume diagram for unthrottled Otto cycle.

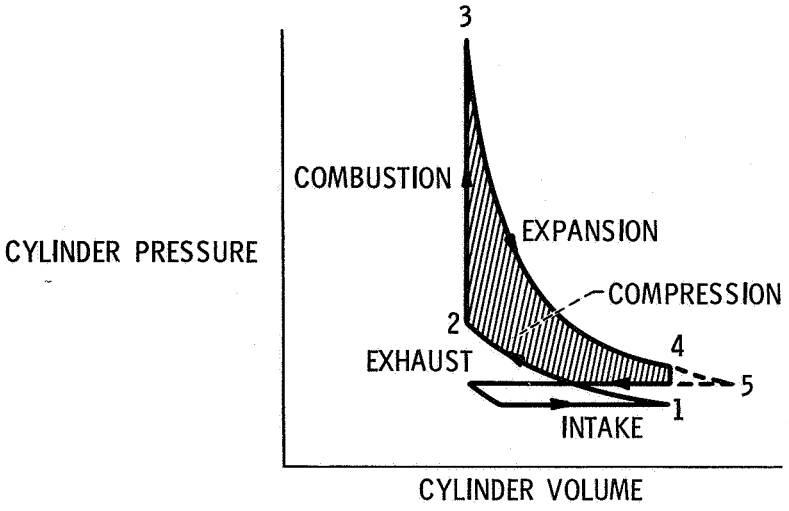

Figure III-3. - Pressure-volume diagram for throttled Otto cycle.

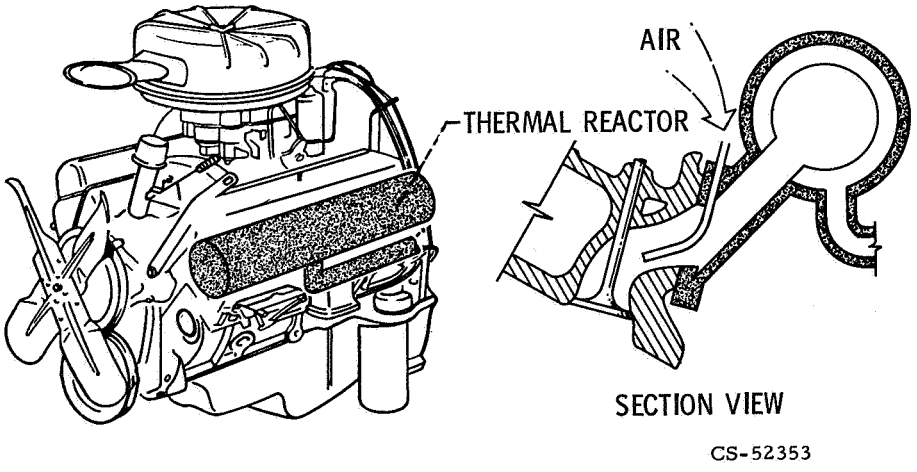

Figure III-4. - Thermal reactor installed on automobile engine.

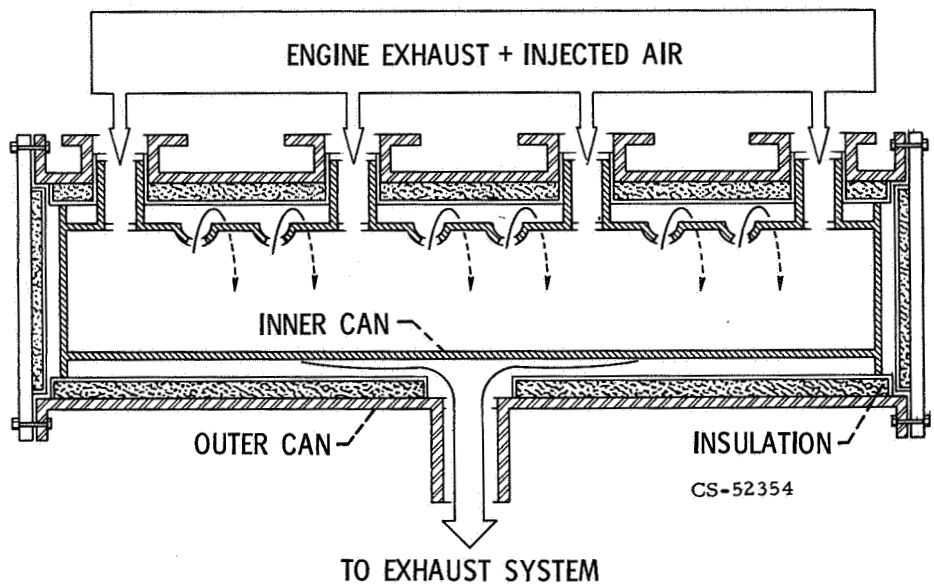

Figure III-5. - Typical thermal reactor.

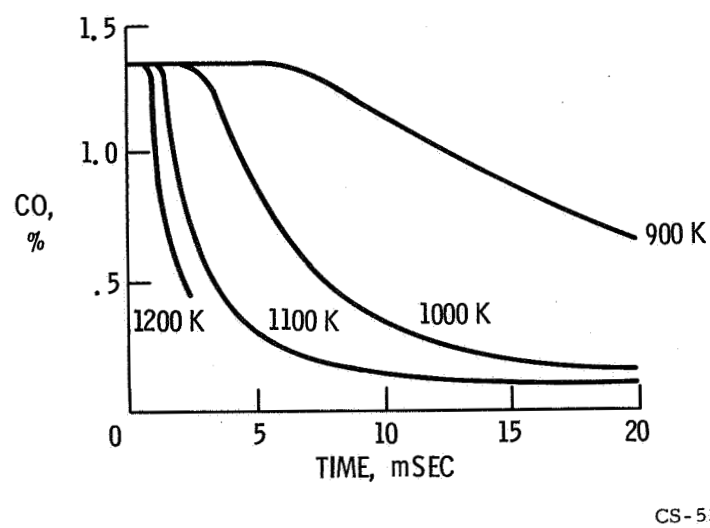

Figure III-6. - Oxidation rate of carbon monoxide in exhaust gas.

IV. TRANSPORT PROPERTIES OF HIGH TEMPERATURE GASES*

Richard S. Brokaw

The transport properties of dilute monatomic gases at low to moderate temperatures are now well understood; the rigorous Chapman-Enskog theory appears to provide an entirely adequate description for these gases. The theory applies to molecules with spherically symmetrical intermolecular force fields and hence is not strictly applicable to polyatomic gases. In practice, however, it turns out that theory gives a good account of the viscosities and diffusion coefficients of polyatomic gases and gas mixtures. The thermal conductivity poses a special problem, however, because internal energy modes - rotation, vibration, etc. - make a contribution to the heat flux. Here there has been recent progress - notably the work of Mason and Monchick (refs. 1 and 2) - so that we now have an improved understanding of the problem, sufficient for most practical purposes. For example, if we know the viscosity of a gas and something of its molecular properties (heat capacity, moments of inertia, dipole moment, if any) we should be able to predict its thermal conductivity within a few percent (except, perhaps, for strongly polar gases).

Consequently in this paper I take the position that we have an adequate theoretical framework for predicting transport properties of high temperature gases and that differences from room temperature gases arise as a consequence of phenomena not usually encountered at modest temperatures, for example, the presence of mobile chemical equilibria or the presence of atoms or free radicals which are valence unsaturated. As a starting point the next section discusses briefly transport properties of gases at moderate temperatures. That will be followed with a section on heat conduction in chemically reacting gas mixtures, and then a section on the effect of the "unusual" intermolecular forces between labile atoms and/or free radicals. The paper concludes with a discussion of some of the unique phenomena in ionized gases (plasmas).

---

*Also presented at the Third International Symposium on High Temperature Technology, Asilomar, California, 1967.

TRANSPORT PROPERTIES AT MODERATE TEMPERATURES

The rigorous Chapman-Enskog theory leads to the following expressions for the transport properties of dilute monatomic gases (ref. 3):

Viscosity

$$\eta = \frac{5}{16}\left(\frac{\sqrt{\pi mkT}}{\pi\sigma_\eta^2}\right) \tag{1}$$

Thermal conductivity

$$\lambda = \frac{25}{32}\left(\frac{\sqrt{\pi mkT}}{\pi\sigma_\eta^2}\right)\left(\frac{c_v}{m}\right) \tag{2}$$

Self-diffusion coefficient

$$D = \frac{3}{8}\left(\frac{\sqrt{\pi mkT}}{\pi\sigma_D^2}\right)\frac{1}{\rho} \tag{3}$$

These formulas involve well-known quantities such as the atomic mass m, the Boltzmann constant k, the temperature T, the heat capacity $c_v \left(=\frac{3}{2}k\right)$, and the density ρ. In addition, the formulas contain cross sections (or collision integrals) σ_η^2 and σ_D^2, and to compute these the intermolecular force law must be known. However, the potential appears explicitly in an integrand which is then averaged by three integrations. Consequently the collision integrals are not very sensitive to the details of the intermolecular potential.

Figure IV-1 compares experimental and calculated viscosity data for argon over a wide temperature range. The curve has been computed for the potential energy function shown in the inset in figure IV-1 (a combination of an inverse sixth power attractive potential, which has a theoretical basis in the dispersion forces, with an exponential repulsion). The potential has been chosen (ref. 4) to take account of equation-of-state and crystal properties as well as viscosity coefficients. For example, the interatomic distance in solid argon is 3.8 Å, (just inside the minimum of the potential energy curve at 3.866 Å). And the depth of the attractive well, 123.2 K, is consistent with argon's heat of sublimation of 0 K. The same

potential successfully describes the thermal conductivity (fig. IV-2) and self-diffusion coefficients (fig. IV-3) for argon.

For gas mixtures the expressions for the viscosity and thermal conductivity are algebraically complicated and contain cross sections characteristic of interactions between unlike molecules. In principle this requires a knowledge of the intermolecular potential between the unlike species; however, in practice, rough estimates based on empirical combination rules, which average potential parameters of the pure components, work reasonably well for the valence-saturated gases encountered at ordinary temperatures. With mixtures of polar and nonpolar gases the polar-nonpolar interactions are essentially of a nonpolar nature; hence, the unlike cross sections are smaller than might be inferred from a simple averaging of the cross sections of the pure components.

Experimental viscosities of nitrogen-hydrogen (ref. 5) and ammonia-hydrogen (ref. 6) mixtures are shown in figure IV-4. The solid lines have been computed using empirical combination rules to estimate the N_2 - H_2 and NH_3 - H_2 intermolecular potentials. The agreement between theory and experiment is generally good (although for NH_3 - H_2 mixtures the accord is even better if experimental diffusion coefficients are analyzed to estimate the NH_3 - H_2 potential; see ref. 7). The dashed curve for NH_3 - H_2 mixtures was calculated assuming the NH_3 - H_2 cross section to be the geometric mean of the NH_3 - NH_3 and H_2 - H_2 cross sections. This procedure (which works reasonably well for nonpolar mixtures) overestimates the cross section so that the predicted viscosities are too low.

Experimental thermal conductivities (ref. 8) for these same mixtures are shown in figure IV-5. The curves, calculated using Hirschfelder's (ref. 9) Eucken-type approximation for gas mixtures, agree reasonably well with experiment, although the errors are larger than in the case of viscosity. This is in part due to larger experimental errors, but may also be due to approximations in the theory. (But a more sophisticated theory for gas mixtures seems scarcely better, ref. 2.)

Thus we have adequate theory for predicting transport properties of dilute gases. The remainder of the paper will be devoted to the phenomena which do not usually arise in room temperature gases.

HEAT CONDUCTION IN CHEMICALLY REACTING GASES

At high temperatures many gases are partially dissociated and undergo a variety of chemical reactions. In reacting gases, heat transport may be considerably larger than in "frozen" (nonreacting) mixtures. Large amounts of heat can be carried as chemical enthalpy of molecules that diffuse because the gas composition

varies with temperature. For example, in a gas that absorbs heat by dissociating as the temperature is raised, heat is transported when a molecule dissociates in the high-temperature region and the fragments diffuse toward the cooler region. In the low-temperature region the fragments recombine and release the heat absorbed at high temperature.

When chemical reaction rates are very high, chemical equilibrium can be assumed to exist locally throughout a gas mixture. It is then possible, by differentiating the equilibrium relations, to relate the concentration gradients to the temperature gradient. In this event one can define an equilibrium thermal conductivity λ_e independent of apparatus geometry and scale:

$$\lambda_e = \lambda_f + \lambda_r \tag{4}$$

where λ_f is the conductivity in the absence of reaction (the frozen thermal conductivity) and λ_r is the augmentation due to the reactions.

A general expression for the thermal conductivity due to chemical reactions has been developed (refs. 9 and 10) that is applicable to mixtures involving any number of reactants, inert diluents, and chemical equilibria, provided chemical equilibrium exists locally in the temperature gradient. For a simple dissociation of the type $A \rightleftharpoons nB$ the thermal conductivity due to chemical reaction is

$$\lambda_r = \frac{D_{AB}P}{RT}\frac{\Delta H^2}{RT^2}\frac{x_A x_B}{(nx_A + x_B)^2} \tag{5}$$

Here D_{AB} is the binary diffusion coefficient between components A and B, ΔH is the heat of reaction, and x_A and x_B are the mole fractions of the components. Note that unless both species are present λ_r is zero. Furthermore, since, in a dissociating gas the composition varies with pressure, we expect the heat conductivity to vary with pressure also. This is in contrast to the behavior of nonreacting gases, for which the heat conductivity is independent of pressure.

Experimental (ref. 11) and theoretical (ref. 12) conductivities for the $N_2O_4 \rightleftharpoons 2NO_2$ system at one atmosphere are shown in figure IV-6. The dashed curve indicates the frozen conductivity. Thus λ_r is the major contribution to the heat conductivity; at the maximum (where the mass fractions of N_2O_4 and NO_2 are equal) the conductivity is comparable to that of a light gas such as helium and an order of magnitude greater than in the chemically frozen gas mixture.

The theoretical expression for a system involving two reactions has been tested (ref. 13) for the case of hydrogen fluoride vapor. At moderate pressures the

pressure-volume-temperature behavior of hydrogen fluoride can be described in terms of a monomer-hexamer equilibrium, while low pressure data suggest a dimer as well. Although the actual state of the vapor is uncertain, it appears that at low and moderate pressures the equilibria

$$2HF \rightleftharpoons (HF)_2 \qquad \Delta H_2 = 7.4 \text{ kcal}$$

$$6HF \rightleftharpoons (HF)_6 \qquad \Delta H_6 = 40.5 \text{ kcal}$$

serve to specify the system rather well.

Computed and experimental (ref. 14) thermal conductivities are compared in figure IV-7. The solid line was computed assuming both dimer and hexamer equilibria; whereas the dashed line was computed considering only the hexamer equilibrium. Note the extreme pressure dependence of the thermal conductivity. The maximum conductivity is more than three times that of hydrogen at the same temperature and some 33 times the frozen thermal conductivity expected in the absence of reaction. The inclusion of a dimer equilibrium markedly improves the agreement between theory and experiment in the low-pressure region.

The experimental studies on nitrogen tetroxide and hydrogen fluoride prove the validity of the theoretical expressions for thermal conductivity of reacting gases in chemical equilibrium. The theory has also been successfully applied to data for the $PCl_5 \rightleftharpoons PCl_3 + Cl_2$ equilibrium (ref. 15).

Thus far we have considered systems where the chemical reactions are so rapid that chemical equilibrium prevails locally at all points in the gas mixture. Let us now consider the reduction of heat transport caused by reduced reaction rates. A general expression has been derived (ref. 16) for the apparent thermal conductivity of reacting mixtures in which a single reaction proceeds at a finite rate. In contrast to systems where reaction rates are either very high or very low, it is found that heat conduction depends on the geometry and scale of the system and also the catalytic activity of the surfaces.

For a plane parallel plate geometry, with one surface noncatalytic and the other surface a perfect catalyst, the effective thermal conductivity is

$$\lambda^* = \frac{\lambda_e \lambda_f}{\lambda_f + \lambda_r \left[\dfrac{(\tanh \varphi)}{\varphi}\right]} \tag{6}$$

where

$$\varphi^2 \equiv \frac{\lambda_e}{\lambda_f \lambda_r} \frac{\Delta H^2}{RT^2} \mathcal{R} l^2$$

Here $\mathcal{R}$ is the chemical reaction rate at equilibrium (that is the total rate in either direction - not the net rate, which is zero, of course), and l is the distance between the plates. For simple systems it can be shown that

$$\varphi^2 = \frac{\lambda_e}{\lambda_f} \frac{\tau_{Diff}}{\tau_{Chem}} \tag{7}$$

If the diffusion time τ_{Diff} is short in comparison with the chemical relaxation time τ_{Chem}, $\varphi \to 0$, $\tanh \varphi/\varphi \to 1$, and $\lambda^* \to \lambda_f$. In other words, the concentration gradients are washed out by diffusion and the frozen conductivity is obtained. On the other hand if the chemical time is short, the concentration gradients are maintained, $\varphi \to \infty$, $\tanh \varphi/\varphi \to 0$, and $\lambda^* \to \lambda_e$.

The theory can be applied to low-pressure measurements (ref. 11) on the $N_2O_4 \rightleftharpoons 2NO_2$ system, as shown in figure IV-8. The upper and lower dashed curves are respectively, the computed equilibrium and frozen conductivities. The solid curve has been fitted to the data assuming negligible surface reaction and assuming that the rate constant for the dissociation reaction

$$N_2O_4 + M \to 2NO_2 + M$$

is 5.3×10^9 cubic centimeters per mole per second at 296 K. This is in reasonable agreement with values derived from ultrasonic absorption measurements by Sessler (ref. 17) and by Cher (ref. 18) who reported values of 4.7×10^9 and 4.1×10^9, respectively.

Thus we seem to have an adequate understanding of the effects of chemical reaction on heat conduction. This is fortunate, because these mobile chemical equilibria are frequently encountered in high temperature gas mixtures.

MULTIPLE INTERACTION CURVES AND PROPERTIES OF LABILE ATOMS AND FREE RADICALS

The discussion thus far has been concerned with systems in which it is assumed that a pair of colliding atoms or molecules can interact along only one potential energy curve. However, in collisions between atoms or free radicals pos-

sessing unpaired electron spins, multiple interaction curves are possible. For example, if two hydrogen atoms collide with spins opposed, they follow the $^1\Sigma$ attractive potential (which corresponds to the H_2 molecule); this occurs on one collision in four. On the other hand in three out of four collisions the spins are parallel and the atoms follow the antibonding $^3\Sigma$ repulsive potential. With other atoms these interactions can be much more complex: two ground state oxygen atoms can follow any of 18 different potential energy curves (ref. 19). It has been shown (ref. 20) that, when there are multiple interaction curves, the transport property formulas of classical kinetic theory remain valid but the collision integrals must be averaged over the different curves, with each one weighted according to its statistical weight.

These interactions between labile atoms or free radicals are usually much stronger than the interactions between valence saturated species, and this in turn has an effect on the transport properties. This is illustrated in figure IV-9 where the viscosities of atomic and molecular hydrogen are compared. The experimental viscosities for hydrogen atoms have been deduced by Browning and Fox (ref. 21) from their measurements on hydrogen atom-molecule mixtures, assuming an appropriate fit to Margenau's calculation (ref. 22) of the H - H_2 interaction. The experimental atom viscosities are in near-perfect agreement with the accurate quantal calculations of Buckingham, Browning, and Gal (ref. 23) shown as a solid line.

On the other hand, if one were to naively overlook the $^1\Sigma$ and $^3\Sigma$ potentials and assume weak forces analogous to the H_2 - H_2 and H - H_2 interactions, a considerably smaller H atom cross section would be predicted. The dashed curve in figure IV-9 shows such a prediction based on Lennard-Jones (12-6) potential force constants of $\sigma_{H-H} = 2.53$ Å, $(\epsilon/k)_{H-H} = 31.3$ K. (These values were obtained from the force constants $\sigma_{H-H_2} = 2.75$ Å, $(\epsilon/k)_{H-H_2} = 32.27$ K (ref. 24), and $\sigma_{H_2-H_2} = 2.968$ Å, $(\epsilon/k)_{H_2-H_2} = 33.3$ K (ref. 25) by inverting the usual combining rules for the potential parameters (ref. 26).)

Thus the effects due to multiple interaction curves seem well-understood and we find a satisfying agreement between theory and experiment in the case of atomic hydrogen. Of course in high temperature gas mixtures involving many different atoms and radicals the situation may be complex indeed, and it might be necessary to consider hundreds of interactions for a truly rigorous calculation of transport properties. (A reasonably complete treatment for the nitrogen-oxygen system, for high temperature air, includes more than 30 interactions (ref. 27).) The potential curves for many interactions are known only poorly, if at all - especially some of

the repulsive interactions. And the repulsive interactions play an important role because of the high multiplicities which are frequently associated with such states.

TRANSPORT PROPERTIES OF IONIZED GASES

At temperatures in the neighborhood of 10 000 K and moderate pressures almost all gases are to some extent ionized. Such gases possess unusual properties because of the presence of the very light electrons and because of the very long range Coulomb interaction between the charged species.

The precise experimental determination of the transport properties of plasmas is extremely difficult; hence the usual interplay between theory and accurate experimentation is lacking. Consequently the theory must be developed with sophistication and care.

For unionized gases the lowest nonzero Chapman-Enskog approximation provides a generally adequate description of the transport properties (with the possible exception of the coefficients of thermal diffusion). Consequently some have applied these lowest approximations to ionized gases, although calculations (ref. 28) for the Lorentzian gas should have suggested the possibility of slow convergence in the case of plasmas. Ahtye (ref. 29) realized that higher approximations were required and the matter has been further and extensively explored by Devoto (refs. 30 and 31).

Some of Devoto's (ref. 31) results for argon at atmospheric pressure are presented in figure IV-10, which shows the ratios of the lowest nonzero Chapman-Enskog approximations to the highest approximations calculated by Devoto. The ratios are plotted against temperature, with a secondary scale showing the degree of ionization α. The ratio of the first to second approximation for viscosity $[\eta]_1/[\eta]_2$ is within 1 percent of unity at low temperatures and drops off to about 0.89 as the gas approaches complete ionization. This is about the same as the ratio Devoto calculated (ref. 30) for a fully ionized hydrogen plasma (0.833) and indicates that the first approximation is not sufficient for accurate calculations at high degrees of ionization. The accuracy of the second approximation is not known, but it is probably within 1 or 2 percent, if the result for the Lorentzian gas is any guide (ref. 28).

The ratio of the second to fourth approximation for the translational thermal conductivity $[\lambda]_2/[\lambda]_4$ (the first Chapman-Enskog approximation is zero) drops to about 0.43 at high temperature, showing that $[\lambda]_2$ is seriously in error ($[\lambda]_2/[\lambda]_4$ for fully ionized hydrogen is 0.438 (ref. 30)). Devoto finds $[\lambda]_3/[\lambda]_4$ within 3 percent of unity, so that $[\lambda]_4$ must be accurate indeed.

The ratio $[\sigma]_1/[\sigma]_4$ indicates that the first approximation to the electrical conductivity is inadequate under any circumstances. At high temperatures the higher approximations converge rapidly (at 10 000 K the second approximation is within 5 percent of the fourth) but at low temperatures even the fourth approximation seems not to have converged on the true value. For example at 4000 K, $[\sigma]_2/[\sigma]_4 = 0.63$ and $[\sigma]_3/[\sigma]_4 = 0.82$.

Thus it seems that accurate calculations for ionized gases require the higher Chapman-Enskog approximations, which are algebraically complicated. It would be very desirable to develop simpler expressions; Devoto (ref. 31) has done some work in this direction.

A partially ionized gas contains at least three species: ions, electrons, and the parent atoms. In order to describe the transport properties, cross sections for all the pair interactions must be obtained. Let us consider argon as an example. The interactions are Ar - Ar, Ar - e, Ar - Ar^+, Ar^+ - Ar^+, e - e, and Ar^+ - e.

If we regard the argon-argon cross section as "normal", all the other cross sections are in one way or another abnormal or peculiar. Argon atoms are very transparent to electrons so the atom-electron cross section is unusually small (about 0.5 to, perhaps, 7 Å (ref. 2) compared with 13 to 15 Å for the Ar-Ar cross section (ref. 32)). On the other hand the argon atom-ion cross sections appear unusually large. One might at first assume that the atom-ion cross section would be comparable to the atom-atom cross section. However, when an ion encounters its parent atom, resonant charge transfer occurs; this gives rise to an exchange force which increases the elastic collision cross sections (by about 80 percent in the case of argon (ref. 32)). But charge exchange has a further effect on the diffusion or mobility of ions. This resonant exchange is probable on grazing collisions between ions and their parent atoms, and a grazing collision with charge transfer is equivalent to a head-on collision without charge transfer insofar as the transport of charge is concerned.

To a good approximation the contribution of the ionization equilibrium to the heat conductivity is (refs. 9 and 33)

$$\lambda_r \cong \frac{D_{Ar\text{-}Ar^+}^{P}}{RT} \frac{\Delta H^2}{RT^2} \frac{x_{Ar} x_{Ar^+}}{(x_{Ar} + x_{Ar^+})^2} \tag{8}$$

Here ΔH is now the heat of ionization while x_{Ar} and x_{Ar^+} are the mole frac-

tions of atoms and ions; the atom-ion diffusion coefficient $D_{Ar\text{-}Ar^+}$ is small because of the large charge transfer cross section.

The consequences of the small atom-electron cross section and large atom-ion cross section are apparent in figure IV-11, where the thermal conductivity of argon at atmospheric pressure is plotted as a function of temperature. An auxiliary scale shows the degree of ionization α. The curves for the equilibrium and translational heat conductivity were computed by Devoto (ref. 31), and the curve for atomic argon was calculated by Amdur and Mason (ref. 34). The experimental data below 5000 K (solid symbols) are derived from shock tube heat transfer studies (refs. 35 and 36), and the data in the 8000 to 12 000 K range (open symbols) were deduced from arc temperature profiles (ref. 37).

Note that the heat conductivity in slightly ionized argon is considerably larger than in the unionized gas. For example at 9300 K where the gas is only 1 percent ionized the heat conductivity is about 80 percent higher than in atomic argon. This is in part due to the small electron mass and in part due to the small argon-electron cross section.

Note too that at higher temperatures the ionization reaction contributes to the heat conductivity; for example, at 13 500 K the equilibrium conductivity λ_e is about 75 percent larger than the translational conductivity, λ_{trans}. However, this is a rather small increase, in comparison with the eight-to tenfold increase in heat conductivity caused by the dissociation of diatomic molecules (ref. 9). The reason, of course, is the very small ion-atom diffusion coefficient which is in turn a consequence of the large resonant charge transfer cross section.

The ion-ion, electron-electron, and ion-electron interactions are all coulombic, an extremely strong and long range interaction, which makes these cross sections very large; in fact if the collision integrals are evaluated for the simple coulomb potential, they are found to diverge (ref. 38). This difficulty is most easily circumvented by cutting off the integration for the cross section at some large distance such as the mean interparticle distance, or better yet, at the Debye length

$$d = \left(\frac{kT}{8\pi n_e e^2} \right)^{1/2} \tag{9}$$

where n_e is the number density of electrons and e is the electronic charge. This procedure is justified by the argument that the electrical charge of distant particles

is effectively screened or neutralized by nearby particles of opposite charge.[1]

However, it seems preferable to introduce the assumption of screening at the outset and describe the charged particle interactions by the screened coulomb potential,

$$\varphi_{ij} = \pm \frac{e^2}{r} \exp\left(\frac{-r}{d}\right) \tag{10}$$

The plus sign applies for ion-ion and electron-electron interactions, and the minus sign applies for the ion-electron interaction. Liboff (ref. 39) and Kihara (ref. 40) have developed analytic expressions for the collision integrals for this potential which are valid at high temperatures, and recently Mason, Munn, and Smith (ref. 41) have done the necessary numerical work to evaluate the integrals for low temperatures as well.

Normally, intermolecular potentials depend on intermolecular distance, and, in the case of polyatomic molecules, on the angular orientation of the molecules. The screened coulomb potential is unique, however, in that the potential itself depends on both temperature and pressure, since the Debye length d is a function of temperature and the charged particle density.

This leads to pressure-dependent cross sections, which is also unique. For example, Liboff's expression for the cross section which is important in determining viscosity is

$$\sigma_\eta^2 = \left(\frac{e^2}{kT}\right)^2 \left[\frac{3}{4} \ln\left(\frac{kT}{e^2}\right) - \frac{1}{4} \ln(8\pi n_e) + \ln 2 - \gamma\right] \tag{11}$$

($\gamma = 0.577$ = Euler's constant); the other cross sections are similar, but with different numerical constants. When the degree of ionization is small, n_e is proportional to the square root of the pressure, whereas in the fully ionized gas n_e varies directly with the pressure. In either case, the cross sections increase as

[1] Following Ahtye and Devoto, equation (9) considers both electrons and ions effective in screening; if electrons only are considered, then $d = (kT/4\pi n_e e^2)^{1/2}$. It would seem reasonable to include screening by the ions in calculating a property such as viscosity, which is determined largely by the heavy ions. On the other hand, for the heat conductivity, determined mostly by the rapid motions of the electrons, the slow-moving ions probably do not screen effectively. (Private communication from Dr. F. A. Lyman.)

the pressure is lowered so that the viscosity and translational thermal conductivity should increase with increasing pressure.

This effect is shown in figure IV-12, where the viscosity of argon is plotted as a function of temperature for a number of pressures. Most of the calculations are due to Ahtye (ref. 29) (solid curves); his results at atmospheric pressure agree reasonably closely with Devoto's (ref. 31) computations (dashed curve). Two features are noteworthy. First, at high temperatures the viscosity is pressure dependent, because of the dependence of the shielded coulomb cross sections on electron density. Second, the high temperature viscosities are low, a consequence of the enormous size of the shielded coulomb cross sections.

Two concluding observations about the transport properties of ionized gases are in order: First, What about quantum effects? Mason, Munn, and Smith (ref. 41) have considered this question and conclude that quantum corrections are important in high density plasmas (say, $n_e > 10^{20}$ cm^{-3}) at all temperatures; above 10^6 K quantum effects are important in low density plasmas too. Second, Mason and Sherman (ref. 42) have made estimates of cross sections for symmetric resonant charge exchange between ions differing by one in electronic charge (processes such as $Ar^+ + Ar^{++} \rightarrow Ar^{++} + Ar^+$). They find that at most temperatures and electron densities of interest these cross sections are negligible in comparison with the screened coulomb cross sections for diffusion. This means that resonant charge transfer between ions will not affect the thermal conductivity of plasmas by depressing the rate of diffusive transport of ionization energy. This is in contrast to the situation in partially ionized gases, where, as we have already seen, ion-neutral exchange is important. Thus it appears that theory is adequate for calculating properties of multiply ionized plasmas, provided only that quantum effects are negligible, and the shielded coulomb potential is appropriate for describing interactions between charged particles $\left(T^3/n_e > 10^{-7}\ (^oK\ cm)^3\right)$.

CONCLUDING REMARKS

I hope the foregoing sections convince the reader that we do indeed have the theoretical tools for estimating high temperature transport properties. We must be certain that we consider all important aspects - effects due to chemical reactions, multiple interaction curves, and, in partially ionized gases, charge transfer and the long range coulomb forces. In ionized gases we must also take account of the higher Chapman-Enskog approximations, and in this regard algebraic simplifications would be most welcome. Then too, for many interactions between valence unsaturated atoms or free radicals the multiple intermolecular potentials

are unknown. But this is a problem of quantum chemistry and not a concern of transport theory per se.

REFERENCES

1. Mason, E. A.; and Monchick, L.: Heat Conductivity of Polyatomic and Polar Gases. J. Chem. Phys., vol. 36, no. 6, Mar. 15, 1962, pp. 1622-1639.

2. Monchick, L.; Pereira, A. N. G.; and Mason, E. A.: Heat Conductivity of Polyatomic and Polar Gases and Gas Mixtures. J. Chem. Phys., vol. 42, no. 9, May 1, 1965, pp. 3241-3256.

3. Hirschfelder, Joseph O.; Curtiss, Charles F.; and Bird, R. Byron: Molecular Theory of Gases and Liquids. John Wiley & Sons, Inc., 1954, p. 527.

4. Mason, Edward A.; and Rice, William E.: The Intermolecular Potentials for Some Simple Nonpolar Molecules. J. Chem. Phys., vol. 22, 1954, pp. 843-851.

5. Trautz, Max; and Baumann, P. B.: Viscosity, Heat Conductivity and Diffusion in Gas Mixtures. II. The Viscosities of Hydrogen, Nitrogen and Hydrogen-Carbon Monoxide Mixtures. Ann. Physik, vol. 2, 1929, pp. 733-736.

6. Trautz, Max; and Heberling, Robert: Viscosity, Heat Conductivity and Diffusion in Gas Mixtures. XVII. The Viscosity of Ammonia and Its Mixtures with Hydrogen, Nitrogen, Oxygen, Ethylene. Ann. Physik, vol. 10, 1931, pp. 155-177.

7. Brokaw, Richard S.; Svehla, Roger A.; and Baker, Charles E.: Transport Properties of Dilute Gas Mixtures. NASA TN D-2580, 1965.

8. Gray, P.; and Wright, P. G.: The Thermal Conductivity of Mixtures of Nitrogen, Ammonia and Hydrogen. Proc. Roy. Soc. (London), ser. A, vol. 263, no. 1313, Sept. 5, 1961, pp. 161-188.

9. Butler, James N.; and Brokaw, Richard S.: Thermal Conductivity of Gas Mixtures in Chemical Equilibrium. J. Chem. Phys., vol. 26, no. 6, June 1957, pp. 1636-1643.

10. Brokaw, Richard S.: Thermal Conductivity of Gas Mixtures in Chemical Equilibrium. II. J. Chem. Phys., vol. 32, no. 4, Apr. 1960, pp. 1005-1006.

11. Coffin, Kenneth P.; and O'Neal, Cleveland, Jr.: Experimental Thermal Conductivities of the $N_2O_4 \rightleftharpoons 2NO_2$ System. NACA TN 4209, 1958.

12. Brokaw, Richard S.; and Svehla, Roger A.: Viscosity and Thermal Conductivity of the $N_2O_4 \rightleftharpoons 2NO_2$ System. J. Chem. Phys., vol. 44, no. 12, June 15, 1966, pp. 4643-4645.

13. Brokaw, R. S.: Energy Transport in High Temperature and Reacting Gases. Planetary Space Sci., vol. 3, 1961, pp. 238-252.

14. Franck, E. U.; and Spalthoff, W.: Abnormal Heat Conductivity of Gaseous Hydrogen Fluoride. Naturwissenschaften, vol. 40, 1953, p. 580.

15. Chakraborti, P. K.: Thermal Conductivity of Dissociating Phosphorous Pentachloride. J. Chem. Phys., vol. 38, no. 3, Feb. 1, 1963, pp. 575-577.

16. Brokaw, Richard S.: "Thermal Conductivity" and Chemical Kinetics. J. Chem. Phys., vol. 35, no. 5, Nov. 1961, pp. 1569-1580.

17. Sessler, G.: Schallausbreitung in Teilweise Dissoziiertem, Gasförmigen Distickstofftetroxyd. Acustica, vol. 10, 1960, pp. 44-59.

18. Cher, Mark: Rate of Dissociation of N_2O_4 by Ultrasonic Absorption Measurements. J. Chem. Phys., vol. 37, no. 11, Dec. 1, 1962, pp. 2564-2570.

19. Vanderslice, Joseph T.; Mason, Edward A.; and Maisch, William G.: Interactions Between Ground State Oxygen Atoms and Molecules: O-O and O_2-O_2. J. Chem. Phys., vol. 32, no. 2, Feb. 1960, pp. 515-524.

20. Mason, Edward A.; Vanderslice, Joseph T.; and Yos, Jerrold M.: Transport Properties of High-Temperature Multicomponent Gas Mixtures. Phys. Fluids, vol. 2, no. 6, Nov.-Dec. 1959, pp. 688-694.

21. Browning, R.; and Fox, J. W.: The Coefficient of Viscosity of Atomic Hydrogen and the Coefficient of Mutual Diffusion for Atomic and Molecular Hydrogen. Proc. Roy. Soc. (London), ser. A, vol. 278, no. 1373, Mar. 24, 1964, pp. 274-286.

22. Margenau, Henry: The Forces Between a Hydrogen Molecule and a Hydrogen Atom. Phys. Rev., vol. 66, no. 11-12, Dec. 1-5, 1944, pp. 303-306.

23. Buckingham, R. A.; Fox, J. W.; and Gal, E.: The Coefficients of Viscosity and Thermal Conductivity of Atomic Hydrogen from 1 to 400° K. Proc. Roy. Soc. (London), ser. A., vol. 284, no. 1397, Feb. 23, 1965, pp. 237-251.

24. Clifton, David G.: Calculations of the Coefficient of Viscosity and the Coefficients of Diffusion for Dissociating Hydrogen. J. Chem. Phys., vol. 35, no. 4, Oct. 1961, pp. 1417-1420.

25. Hirschfelder, Joseph O.; Curtiss, Charles F.; and Bird, R. Byron: Molecular Theory of Gases and Liquids. John Wiley & Sons, Inc., 1954, p. 1110.

26. Hirschfelder, Joseph O.; Curtiss, Charles F.; and Bird, R. Byron: Molecular Theory of Gases and Liquids. John Wiley & Sons, Inc., 1954, eqs. 8.4-8 and 8.4-9, p. 567.

27. Yun, K. S.; and Mason, E. A.: Collision Integrals for the Transport Properties of Dissociating Air at High Temperatures. Phys. Fluids, vol. 5, no. 4, Apr. 1962, pp. 380-386.

28. Chapman, Sydney; and Cowling, T. G.: The Mathematical Theory of Non-Uniform Gases. Second ed., Cambridge Univ. Press, 1953, pp. 193-198.

29. Ahtye, Warren F.: A Critical Evaluation of Methods for Calculating Transport Coefficients of Partially and Fully Ionized Gases. NASA TN D-2611, 1965.

30. Devoto, R. S.: Transport Properties of Ionized Monatomic Gases. Phys. Fluids, vol. 9, no. 6, June 1966, pp. 1230-1240.

31. Devoto, R. S.: Transport Coefficients of Partially Ionized Argon. Phys. Fluids, vol. 10, no. 2, Feb. 1967, pp. 354-364.

32. Devoto, R. Stephen: Argon Plasma Transport Properties. Rep. SUDAER-217, Stanford Univ. (NASA CR-68297), Feb. 1965.

33. Meador, W. E., Jr.; and Staton, L. D.: Electrical and Thermal Properties of Plasmas. Phys. Fluids, vol. 8, no. 9, Sept. 1965, pp. 1694-1703.

34. Amdur, I.; and Mason, E. A.: Properties of Gases at Very High Temperatures. Phys. Fluids, vol. 1, no. 5, Sept.-Oct. 1958, pp. 370-383.

35. Smiley, Edward F., II: The Measurement of the Thermal Conductivity of Gases at High Temperatures with a Shocktube: Experimental Results in Argon at Temperatures Between 1000° K and 3300° K. PhD Thesis, Catholic Univ. of America, 1957.

36. Collins, D. J.; and Menard, W. A.: Measurement of the Thermal Conductivity of Noble Gases in the Temperature Range 1500 to 5000 Deg Kelvin. J. Heat Transfer, vol. 88, no. 1, Feb. 1966, pp. 52-56.

37. Knopp, C. F.; and Cambel, Ali Bulent: Experimental Determination of the Thermal Conductivity of Atmospheric Argon Plasma. Phys. Fluids, vol. 9, no. 5, May 1966, pp. 989-996.

38. Chapman, Sydney; and Cowling, T. G.: The Mathematical Theory of Non-Uniform Gases. Second ed., Cambridge Univ. Press, 1953, pp. 177-179.

39. Liboff, Richard L.: Transport Coefficients Determined Using the Shielded Coulomb Potential. Phys. Fluids, vol. 2, no. 1, Jan.-Feb. 1959, pp. 40-46.

40. Kihara, Taro: On the Coefficients of Irreversible Processes in a Highly Ionized Gas. J. Phys. Soc. Japan, vol. 14, no. 4, Apr. 1959, pp. 402-410.

41. Mason, E. A.; Munn, R. J.; and Smith, Francis J.: Transport Coefficients of Ionized Gases. Phys. Fluids, vol. 10, no. 8, Aug. 1967, pp. 1827-1832.

42. Mason, E. A.; and Sherman, Martin P.: Effect of Resonant Charge Exchange on Heat Conduction in Plasmas. Phys. Fluids, vol. 9, no. 10, Oct. 1966, pp. 1989-1991.

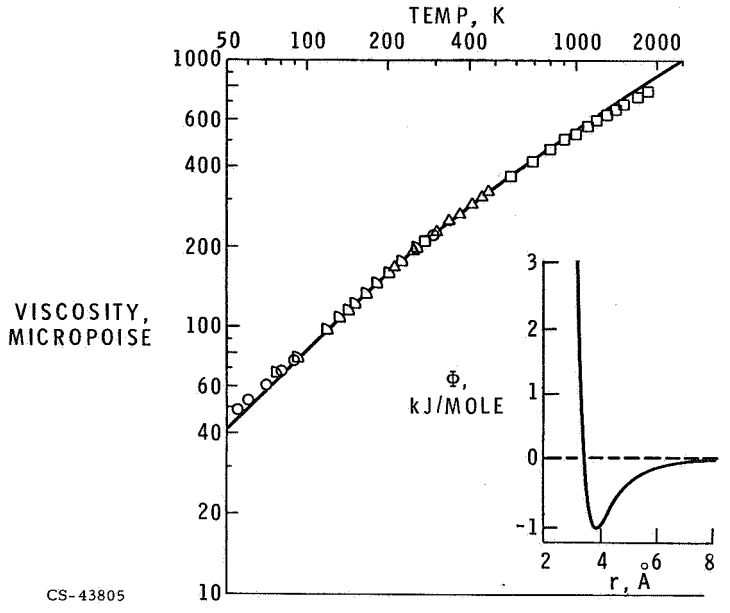

Figure IV-1. - Viscosity of argon. Comparison of theory and experiment.

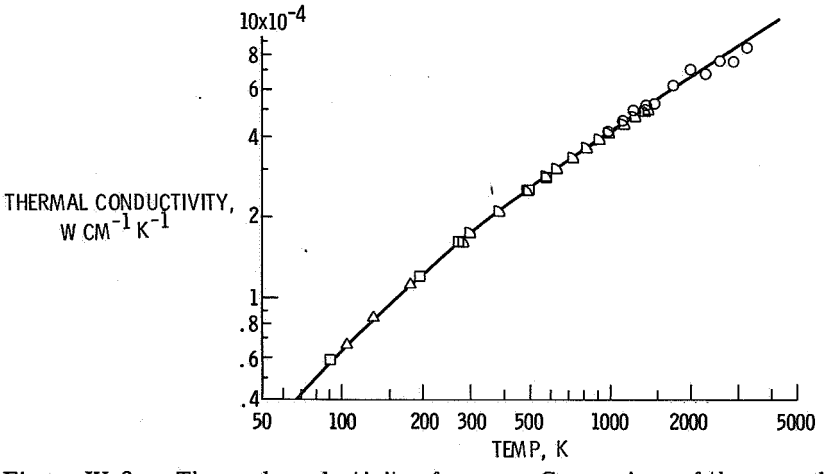

Figure IV-2. - Thermal conductivity of argon. Comparison of theory and experiment.

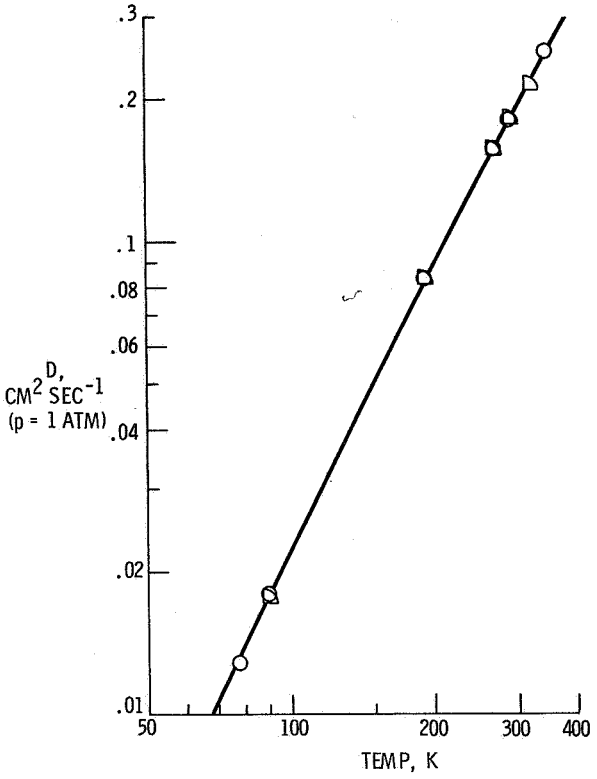

Figure IV-3. - Self-diffusion coefficient of argon. Comparison of theory and experiment.

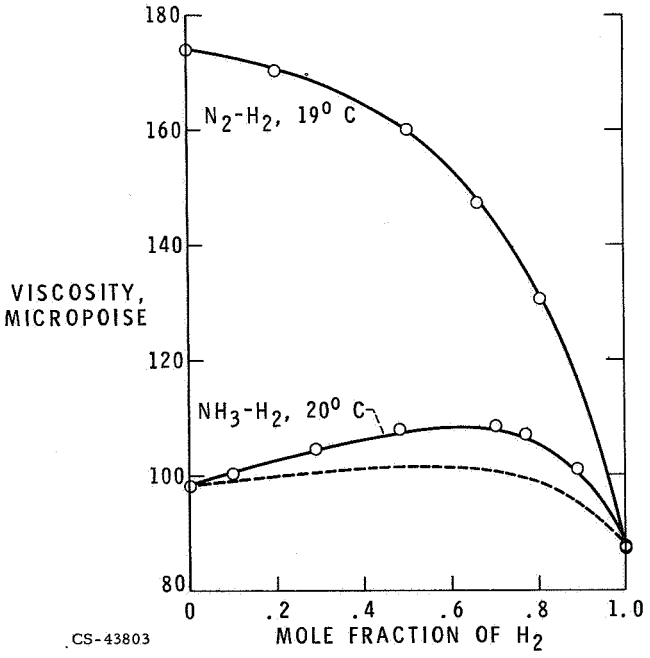

Figure IV-4. - Viscosity of gas mixtures. Comparison of theory and experiment.

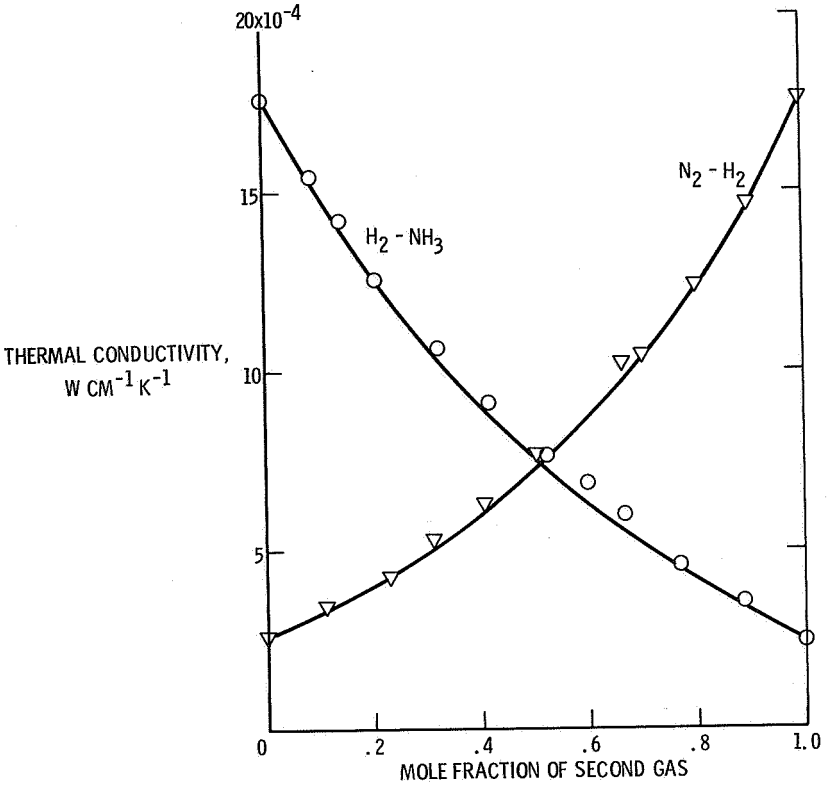

Figure IV-5. - Thermal conductivity of gas mixtures, 25.3° C. Comparison of theory and experiment.

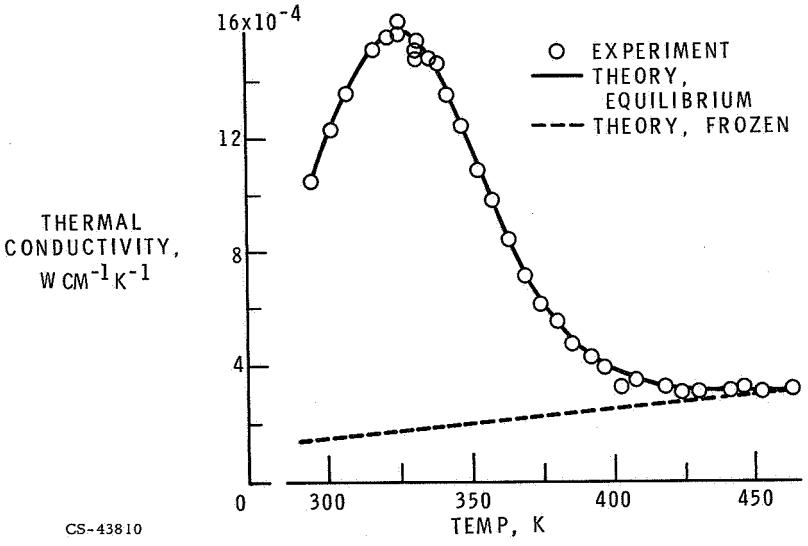

Figure IV-6. - Thermal conductivity of nitrogen tetroxide - nitrogen dioxide system. P = 1 atmosphere (ref. 12).

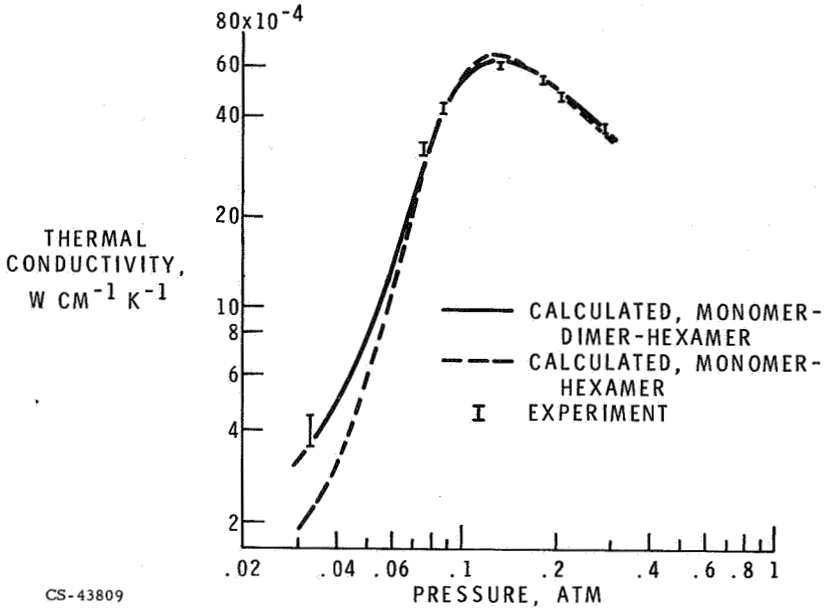

Figure IV-7. - Thermal conductivity of hydrogen fluoride vapor at 267.7 K.

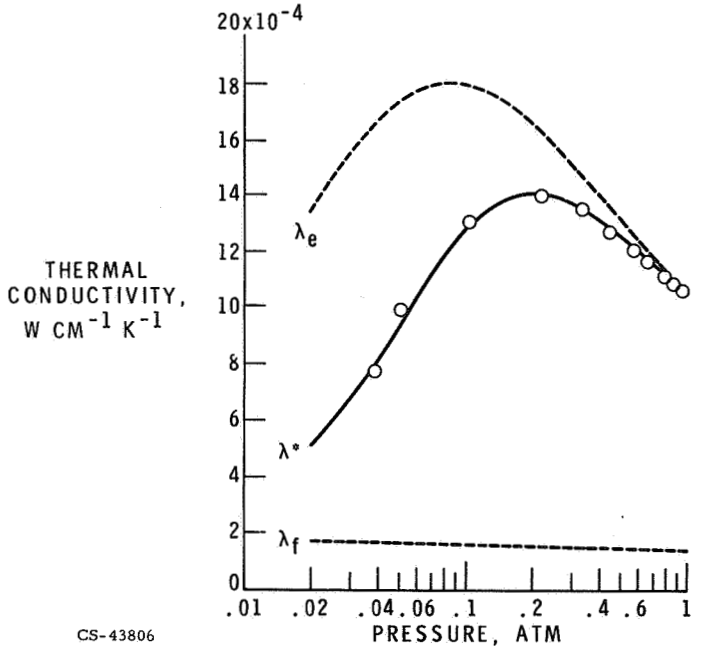

Figure IV-8. - Effect of chemical reaction rate on thermal conductivity of $N_2O_4 \rightleftharpoons 2NO_2$ system. T = 296 K (ref. 16).

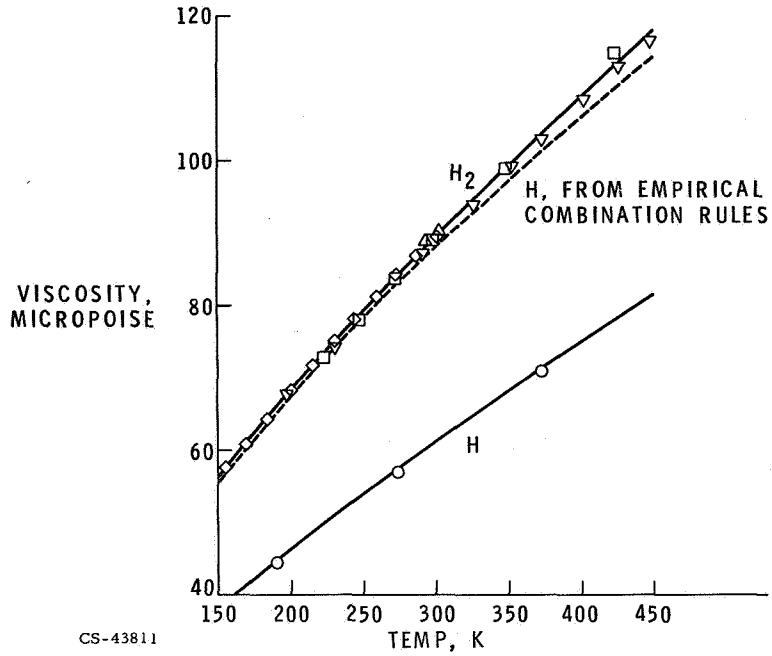

Figure IV-9. - Viscosities of atomic and molecular hydrogen.

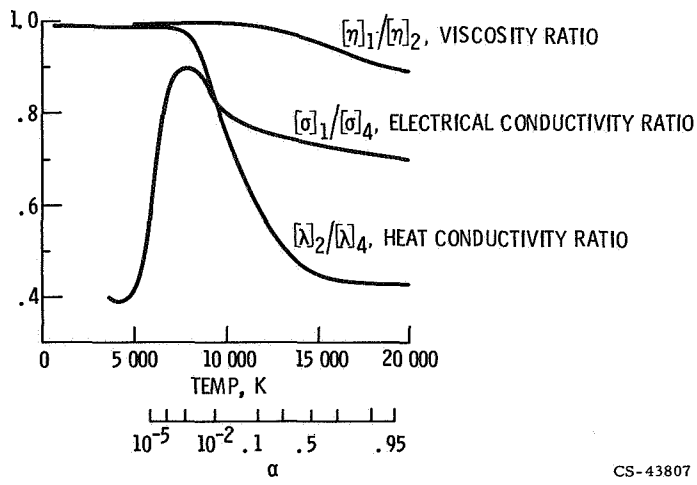

Figure IV-10. - Comparison of lowest Chapman Enskog approximations with higher approximations. (Argon, 1 atm.)

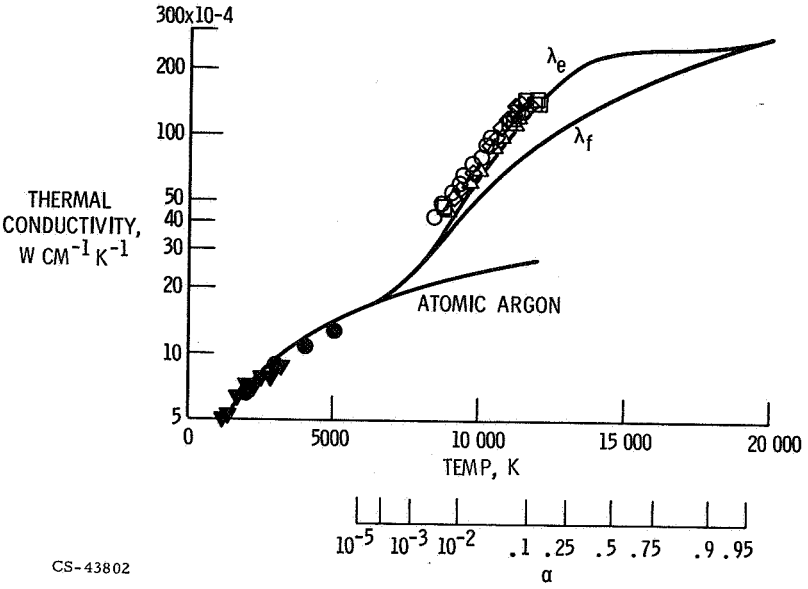

Figure IV-11. - Thermal conductivity of partially ionized argon (1 atm).

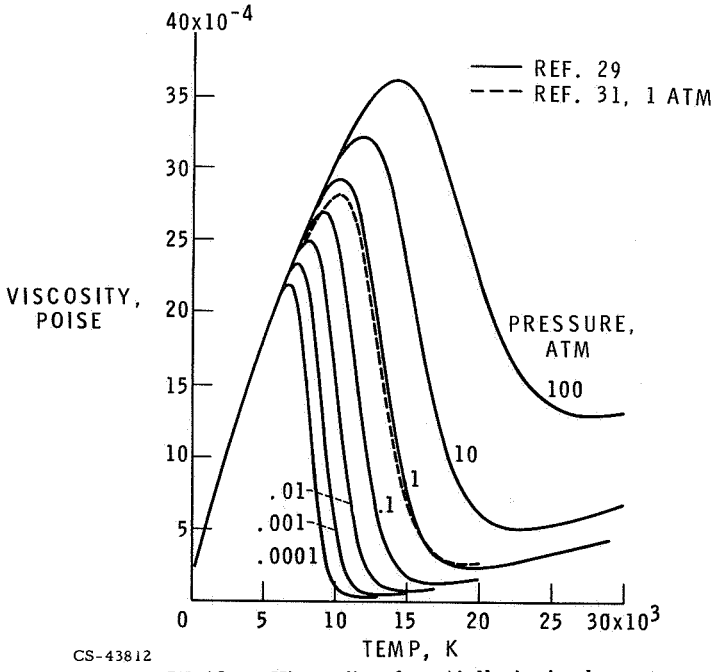

Figure IV-12. - Viscosity of partially ionized argon.

V. EXPERIMENTAL MEASUREMENTS OF DIFFUSION COEFFICIENTS FOR ATOMIC OXYGEN

Charles E. Baker

For the past several years there has been considerable interest at the Lewis Research Center in measuring the transport properties of gases. For example, the self-diffusion coefficient of gaseous ammonia as a function of temperature has recently been measured (ref. 1). Although there is still a lack of data for some systems, especially polar gases, the theoretical understanding of stable gas systems is satisfactory. The potential parameters obtained for a gas from one transport property can be used to calculate the other transport properties of the gas.

When molecules are subjected to the high temperatures found in such applications as combustion processes and space-vehicle reentry, unstable species such as free radicals and atoms are produced. Because of the importance of these unstable species to high-temperature transport properties (paper IV by R. S. Brokaw), our current experimental effort involves measuring the diffusion coefficient of atomic oxygen through various background gases.

There are several reasons for beginning our studies with atomic oxygen. It is a constituent of our atmosphere and thus is important in any process involving high-temperature air. In addition, it has been shown spectroscopically and by rocket release experiments that most oxygen above an altitude of 100 kilometers is in the atomic rather than molecular state. There are also some experimental reasons which make atomic oxygen a good first choice for study. These are discussed in the experimental section of this paper.

The conventional method for measuring the diffusion coefficient of stable species is illustrated by figure V-1. (This was the method employed in ref. 1.) Gases A and B are placed in cells separated by a removable diaphragm. Diffusion starts when the diaphragm is removed in such a way as to minimize disturbance of the interface. After a suitable time, the diaphragm is replaced, the resulting mixtures in the two cells analyzed, and the diffusion coefficient computed. Obviously such a method could not be used to measure the diffusion coefficient of, for example, atomic oxygen into molecular oxygen because of the rapid recombination of the oxygen atoms into oxygen molecules. Because of the experimental difficulties involved,

very little work has been reported on the diffusion of unstable atoms. Krongelb and Strandberg (ref. 2) measured the diffusion of atomic oxygen into molecular oxygen using the electron spin resonance (ESR) technique, which takes advantage of the unpaired electron in atomic oxygen. Using a similar technique, Wise and coworkers also measured the diffusion coefficient of atomic oxygen into molecular oxygen (ref. 3) as well as atomic hydrogen into molecular hydrogen (ref. 4). Morgan and Schiff used the concentration gradient produced by a catalytic sink to measure the diffusion coefficients of atomic oxygen (refs. 5 and 6), atomic nitrogen (ref. 6), and atomic hydrogen (ref. 7) through several background gases.

The method for determining atom diffusion coefficients that will be discussed in this paper uses recombination of the atoms of a partially dissociated gas on a catalytic surface placed in the gas flow. The essential features of the method are illustrated in figure V-2. A gas such as oxygen flows past the cavity of a microwave generator, and a few percent of the molecules are dissociated. The resulting mixture of atoms and molecules continues down the tube, flows past the catalytic probe, and then into high-speed pumps. The catalytic probe responds to the recombination of the atoms on its surface. The next section of this paper shows that an experiment of this type is capable of yielding information from which the diffusion coefficient of the atom through the background gas can be determined.

THEORETICAL BACKGROUND

The following steps must take place for an atom to recombine on a catalytic surface:

(1) Transport of the atom to the surface

(2) Adsorption of the atom by the surface

(3) Residence of the atom on the surface until recombination occurs

(4) Desorption of the resulting molecule from the surface

(5) Transport of this molecule away from the surface

Steps (1) and (5) may be regarded as transport effects, and steps (2) to (4) as kinetic effects. If the time for either step (1) or (5) is large compared with the time for the other steps, the process is transport or diffusion controlled. Similarly, if the time for one of the steps (2) to (4) is large, the process is kinetically or rate controlled. If the two effects have comparable times, the reaction is an intermediate one.

Hartunian and Liu (ref. 8) have considered the slow flow of a partially dissociated gas about a spherical catalytic probe and have shown that the averaged integrated heat flux to the surface (per unit area) is closely approximated by

$$\bar{q} = \rho C_0 h_R \left(\frac{D}{a}\right)\left(\frac{K}{1+K}\right) \tag{1}$$

where ρ is the density, C_0 is the atom concentration in the free stream, h_R is the specific heat of recombination of the atoms, D is the diffusion coefficient for the atom through the background gas, a is the probe radius, and $K = k_w/(D/a)$. In this last expression, k_w is the "true" rate constant for the surface recombination. From equation (1), when $K >> 1$,

$$\bar{q}_D = \rho C_0 h_R \frac{D}{a} \tag{2}$$

which is the diffusion-controlled limit. Similarly, when $K << 1$,

$$\bar{q}_R = \rho C_0 h_R k_w \tag{3}$$

which is the rate-controlled limit. Using equations (2) and (3), we can now rewrite equation (1) as

$$\frac{1}{\bar{q}} = \frac{1}{\bar{q}_D} + \frac{1}{\bar{q}_R} \tag{4}$$

Equation (4) makes the same kinds of predictions about whether a process is diffusion controlled or rate controlled as did the physical picture of the recombination process described at the beginning of this section. If the surface is a very active catalyst, that is, if k_w is large, $\bar{q}_R$ will be large, $1/\bar{q}_R$ will be small, and the process will be diffusion controlled. In other words, the surface is such an efficient catalyst that the atoms on the surface rapidly recombine; the overall process is limited only by the rate at which atoms are delivered to the surface. Conversely, if the surface is a poor catalyst, k_w, and hence $\bar{q}_R$, will be small, $1/\bar{q}_R$ will be large, and the process will be rate controlled. The same kind of reasoning holds for the D/a term, which changes with pressure and probe radius.

Equation (4) can also be written in the following form

$$\bar{q} = \bar{q}_R \left(1 + \frac{\bar{q}_R}{\bar{q}_D}\right)^{-1} \tag{5}$$

Substituting the values of $\bar{q}_R$ and $\bar{q}_D$ given in equations (2) and (3) yields

$$\bar{q} = \bar{q}_R \left(1 + k_w \frac{a}{D}\right)^{-1} \tag{6}$$

The reaction rate observed is a result of the interaction of the true reaction rate effects and the diffusional effects, and from equation (6) one may write an expression for an apparent reaction rate k_{w_a}

$$k_{w_a} = \frac{\bar{q}}{\rho C_0 h_R} = \frac{k_w}{1 + k_w \frac{a}{D}} \tag{7}$$

Inverting and using $D = D_0/p$, where $D = D_0$ at some reference pressure p_0 (1 torr in this paper), yields

$$\frac{1}{k_{w_a}} = \frac{\rho C_0 h_R}{\bar{q}} = \frac{1}{k_w} + \frac{ap}{D_0} \tag{8}$$

Equation (8) is the theoretical basis for this experimental method for obtaining atom diffusion coefficients. From the experimental measurements, k_{w_a} may be determined as a function of pressure and probe radius. According to equation (8), a plot of $1/k_{w_a}$ against ap should be a straight line with a slope of $1/D_0$ and an intercept of $1/k_w$.

EXPERIMENTAL APPARATUS AND PROCEDURE

The apparatus used in this work is based on a design described by Carson and Hartunian (refs. 9 and 10) and is shown schematically in figure V-3. The flow tube is constructed of 3-inch inside diameter Pyrex pipe which is commercially available. After passing through a suitable flowmeter and metering valve, the gas under investigation flows through the cavity of an 800-watt microwave generator operating at 2540 megahertz. The discharge produces a small percentage of oxygen atoms in the background gas. The resulting mixture of unstable species in a background of stable species flows down the tube approximately 9 feet before reaching the catalytic probes, then passes through a gate valve, and on to high-speed mechanical pumps. Located near the probe mount are a sidearm leading to a pressure gage, a titration probe needed for the oxygen atom determination, which is discussed

later, and a photomultiplier, also used in the oxygen atom determination.

The catalytic probes used in this work are thermistor beads which have been coated with about 1 micron of silver. On exposure to oxygen atoms, the silver surface is rapidly converted to a black silver peroxide. This surface is a nearly ideal catalyst for the recombination of oxygen atoms: it is very active, and this activity is essentially temperature independent. The availability of such an excellent catalyst was one of the reasons for starting our studies of atom diffusion with oxygen. The thermistor mount is also shown in figure V-3. Normally, thermistors of three different radii were mounted in the Lucite holder at half-radius, 120^{o} apart. All exposed metal surface, other than the catalytic surfaces, were coated with a varnish to prevent recombination on these surfaces.

In an experiment of this kind it is possible to operate the thermistor as a calorimeter probe or as an isothermal probe. In the calorimeter the heat released by the recombination of the atoms on the probe surface raises the temperature of the thermistor and, hence, reduces its resistance. This change in resistance or temperature of the thermistor that occurs when the microwave generator is turned on is a measure of the amount of recombination that is taking place on the probe surface. In contrast, the isothermal probe is operated at a constant overheat; the bridge circuit (ref. 11) of which the thermistor is a part, automatically maintains the thermistor at a constant temperature even though recombination may or may not be occurring on its surface. From the difference in power (reflected in a voltage change across the thermistor as indicated by a digital voltmeter) between the discharge "off" and the discharge "on" conditions, the heat flux to the probe surface due to atom recombination can be calculated. This method has the advantage over the calorimeter technique that radiation and conduction effects cancel.

The procedure for a typical experimental run is as follows. A flow is set up with the discharge off. The flow rate, resulting pressure, and voltage across the thermistor necessary for the given overheat are recorded. The microwave generator is then turned on, and the reduced voltage now required to maintain the thermistor at the given overheat noted. All the quantities necessary for the determination of the diffusion coefficient for the atoms through the background gas are now known except for the free-stream atom concentration.

The oxygen atom concentration in the free stream was determined by means of the two-step gas titration technique described by Reeves, Mannella, and Harteck (ref. 12). The reactions involved in this method are as follows:

$$NO_2 + O \xrightarrow{k_1} NO + O_2$$

$$NO + O \xrightarrow{k_2} NO_2 + h\nu$$

$$k_1 >> k_2$$

The second reaction is much slower than the first and the yellow-green light produced by it serves as an indicator for the titration. Because the intensity of this light is proportional to the product of the NO and O atom concentrations, a maximum in the intensity occurs. At this point the NO_2 concentration (and hence, the NO concentration) equals one-half the initial O atom concentration. Thus, the first step of this two-step titration involves adding NO_2 to the stream through the titration probe (shown in fig. V-3) until a maximum light intensity is registered by the photomultiplier. An NO_2 flow is difficult to meter because of the formation of N_2O_4 and because of its corrosiveness. Hence, no attempt is made to meter NO_2 in this first step. In step two of this technique, NO is now metered into the stream by means of a pressure-drop technique until the same light intensity (evidenced by the same output of the photomultiplier) is produced. The NO now equals one-half the NO concentration in step one because O atoms are no longer consumed to form NO. Thus, the NO concentration in step two equals one-fourth the initial O atom concentration. Step two may be regarded as merely an indirect way of metering NO_2. A plot of photomultiplier output against NO_2 flow rate for a typical titration of O atoms is shown in figure V-4.

EXPERIMENTAL RESULTS AND DISCUSSION

The results of some preliminary experiments at room temperature are shown in figure V-5. Here, the reciprocal of the apparent reaction rate constant k_{w_a} is plotted against the product of probe radius and pressure. Probes with radii of 0.015 and 0.05 centimeter were used in these measurements. With the exception of the point for the large probe at an ap value of about 2×10^{-2} centimeter-torr, the pressure was not varied greatly, ranging between 0.71 and 0.84 torr for the remaining points. The point outside this range was taken at a pressure of 0.42 torr. Equation (8) predicts that, if the experimental data are plotted as in figure V-5, the points should fall on a straight line. Despite some scatter in the data, it is quite obvious that this is indeed the case, and these results are encouraging.

A determination of the diffusion coefficient for oxygen atoms through argon at room temperature is shown in figure V-6. The gas flowing past the microwave cavity was a mixture of 1.8 percent oxygen in argon. Under these conditions most of the oxygen molecules are dissociated. However, because of both volume and wall recombination of the oxygen atoms, the oxygen atom concentration near the probes is only about 1 percent. The determinations for the large and small probes were at a pressure of 0.84 torr; the points for the medium probe were taken at 0.59 torr. The least-squares line through the points has a slope whose reciprocal gives a value for D_O of 224 square centimeters per second at the reference pressure of 1 torr.

How does this compare with other experimental values for the diffusion coefficient of oxygen atoms into argon? Morgan and Schiff (ref. 6), using a flow system but an otherwise different experimental method, report a value of 209 square centimeters per second for oxygen atoms into argon at 280 K. This corresponds to a diffusion coefficient of 229 square centimeters per second when the necessary temperature correction is made. These results are summarized in table V-1. The good agreement between the results obtained by different experimental methods is certainly encouraging. A value for the diffusion coefficient calculated from simple theory is also shown in table V-1. For this calculation the volume of the oxygen atom was assumed to be one-half that of the oxygen molecule

$$\sigma_O^3 = \frac{1}{2}\sigma_{O_2}^3$$

and the usual combining rules were then applied. The close agreement between rough theory and experiment for this system is probably fortuitous. There is no reason to expect such good agreement between experiment and simple theory for other systems involving unstable species.

CONCLUDING REMARKS

Results obtained on our work on atom diffusion thus far indicate that this method is capable of producing data from which diffusion coefficients can be extracted. Our plans for further work on atom diffusion include the diffusion of oxygen atoms into other background gases such as helium, oxygen, and nitrogen, as well as the diffusion of nitrogen atoms through similar gases. These measurements will then be extended to higher temperatures. Diffusion data over a suitable temperature range can be used to determine parameters for appropriate interaction potentials. Using these potential parameters and current theory, it is then possible

to calculate the other transport properties for the particular system involved. The importance of the interactions between stable and unstable species in high-temperature transport property calculations will be clearly seen in paper VI by R. A. Svehla.

REFERENCES

1. Baker, Charles E.: Self-Diffusion in Gaseous Ammonia. J. Chem. Phys., vol. 52, no. 4, Feb. 15, 1970, pp. 2159-2161.
2. Krongelb, S.; and Strandberg, M. W. P.: Use of Paramagnetic-Resonance Techniques in the Study of Atomic Oxygen Recombinations. J. Chem. Phys., vol. 31, no. 5, Nov. 1959, pp. 1196-1210.
3. Yolles, Robert S.; McCalley, Leonard; and Wise, Henry: Diffusion and Heterogeneous Reaction. XII. Measurements of O-O_2 Diffusion as a Function of Temperature. J. Chem. Phys., vol. 52, no. 2, Jan. 15, 1970, pp. 723-728.
4. Sancier, K. M; and Wise, H.: Diffusion and Heterogeneous Reaction. XI. Diffusion Coefficient Measurements for Gas Mixture of Atomic and Molecular Hydrogen. J. Chem. Phys., vol. 51, no. 4, Aug. 15, 1969, pp. 1434-1438.
5. Morgan, J. E.; and Schiff, H. I.: Use of Catalytic Probes to Determine Atom Concentrations and Atom Diffusion Coefficients. J. Chem. Phys., vol. 38, no. 11, June 1, 1963, pp. 2631-2634.
6. Morgan, J. E.; and Schiff, H. I.: Diffusion Coefficients of O and N Atoms in Inert Gases. Can. J. Chem., vol. 42, no. 10, Oct. 1964, pp. 2300-2306.
7. Khouw, B.; Morgan, J. E.; and Schiff, H. I.: Experimental Measurements of the Diffusion Coefficients of H Atoms in H_2 and in H_2-He and H_2-Ar Mixtures. J. Chem. Phys., vol. 50, no. 1, Jan. 1, 1969, pp. 66-70.
8. Hartunian, R. A.; and Liu, S. W.: Slow Flow of a Dissociated Gas About a Catalytic Probe. Phys. Fluids, vol. 6, no. 3, Mar. 1963, pp. 349-354.
9. Carson, B. H.; and Hartunian, R. A.: Oxygen Recombination on a Catalytic Sphere in the Continuum-Free Molecule Transition. Rep. TR-669 (6240-20)-17, Aerospace Corp. (SSD-TR-66-171, DDC No. AD-801277), June 1966.
10. Carson, Bernard H.: Experimental Studies of the Recombination of Glow-Discharged Oxygen on Catalytic Spheres. Ph. D. Thesis, Pennsylvania State Univ., 1965.

11. Lumley, J. L.: The Constant Temperature Hot-Thermistor Anemometer. Symposium on Measurement in Unsteady Flow. ASME, 1962, pp. 75-82.

12. Reeves, Robert R.; Mannella, Gene; and Harteck, Paul: Rate of Recombination of Oxygen Atoms. J. Chem. Phys., vol. 32, no. 2, Feb. 1960, pp. 632-633.

TABLE V-1. - COMPARISON OF SEVERAL VALUES OF DIFFUSION COEFFICIENT OF OXYGEN ATOMS INTO ARGON

Diffusion coefficient at 298 K and 1 torr, cm^2/sec	Source
224	This work
[a]229	Morgan and Schiff
230	Calculated from simple theory

[a]Corrected from 280 K.

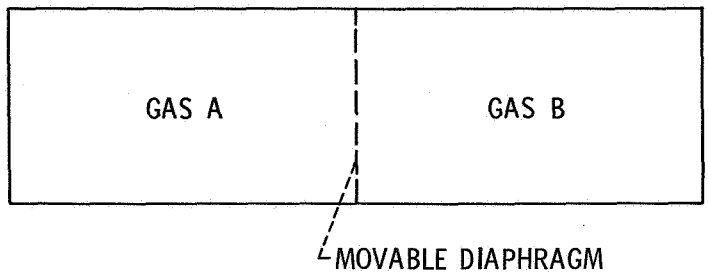

CS-53312

Figure V-1. - Conventional method for measuring diffusion coefficient of stable gases.

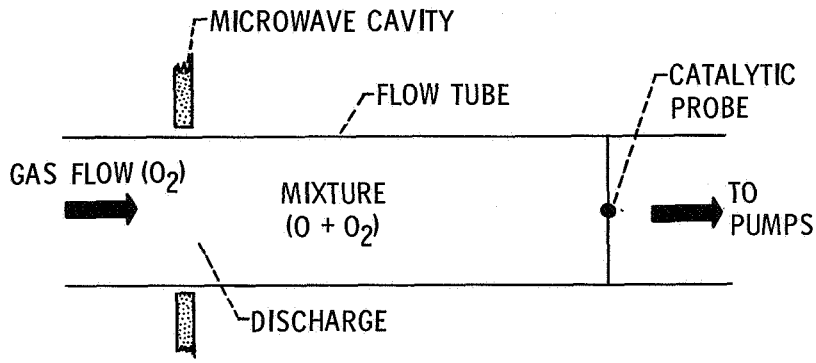

CS-53315

Figure V-2. - Atom recombination flow system.

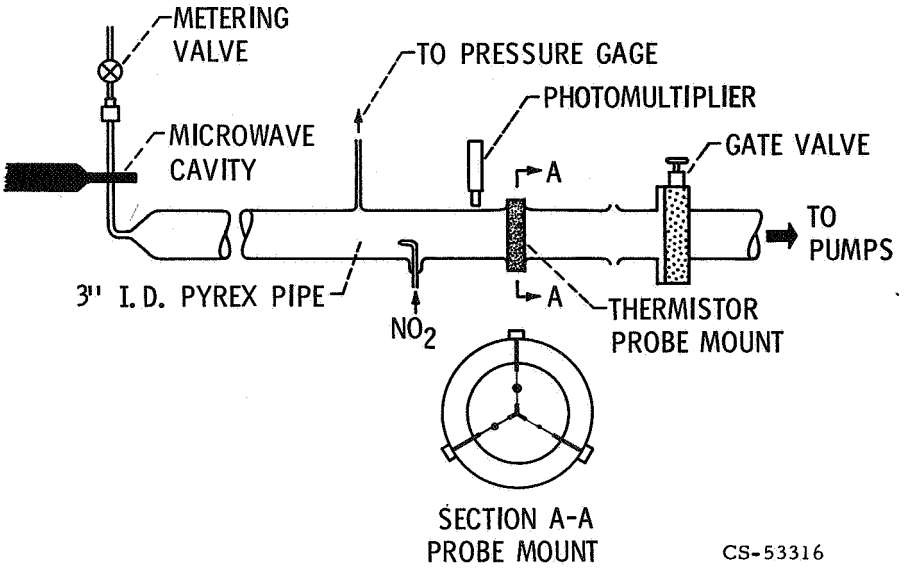

Figure V-3. - Atom recombination apparatus.

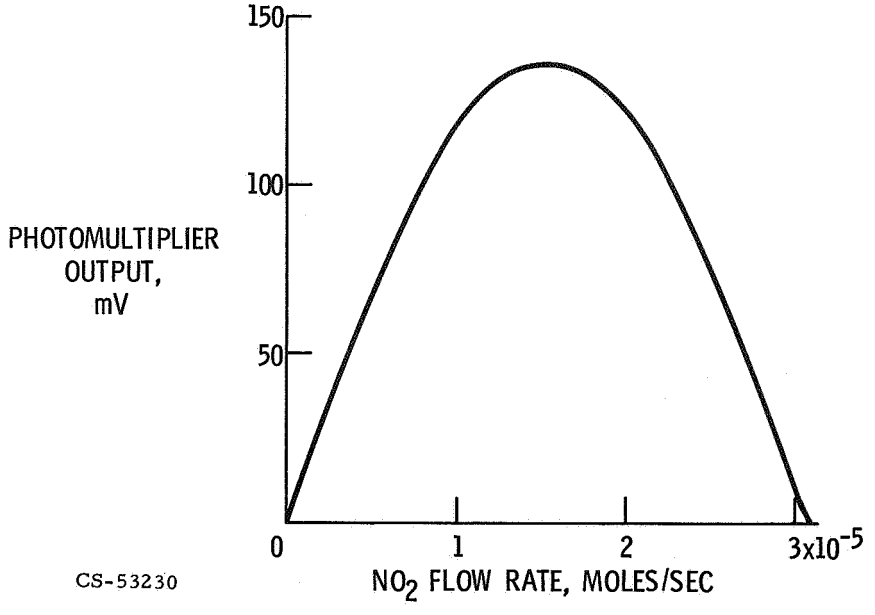

Figure V-4. - Light intensity variation during oxygen atom titration.

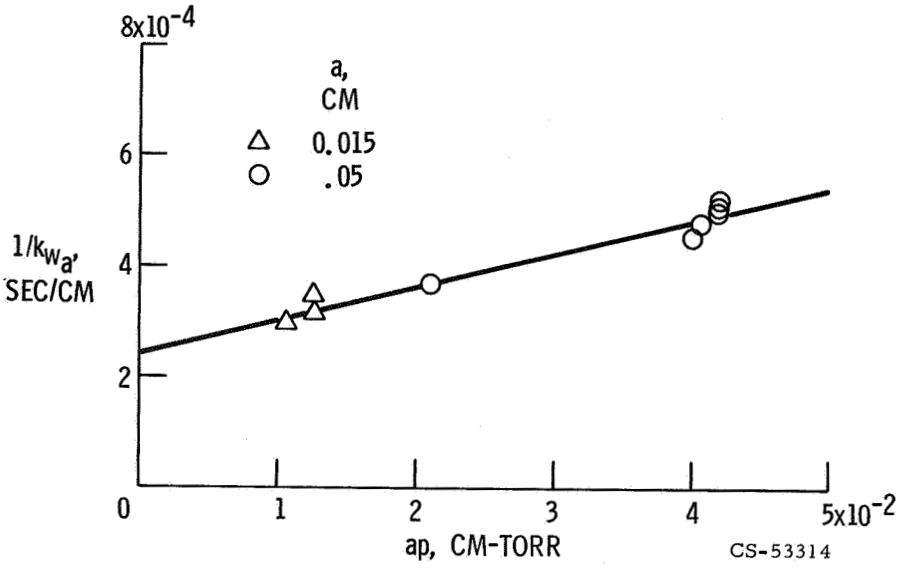

Figure V-5. - Dependence of apparent reaction rate on pressure and probe radius.

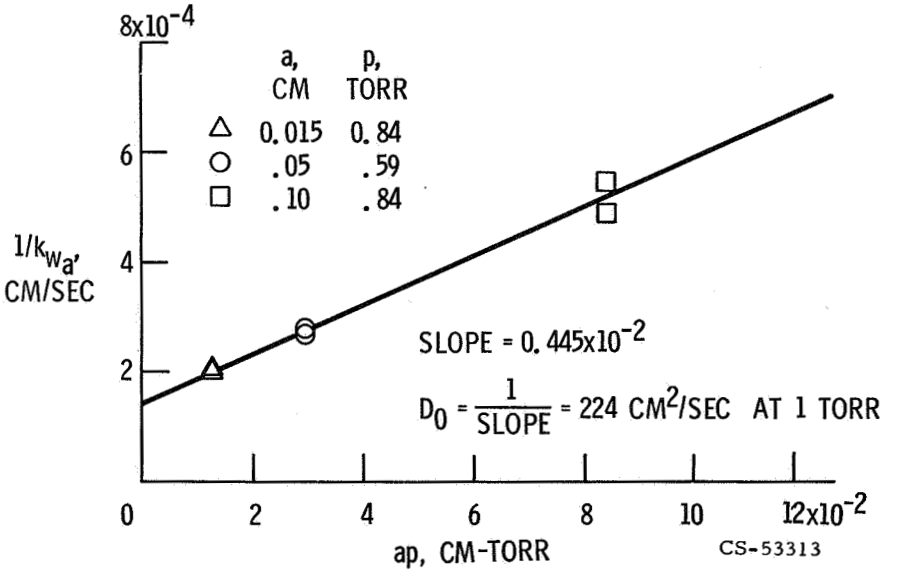

Figure V-6. - Determination of diffusion coefficient for oxygen atoms into argon at 298 K.

VI. TRANSPORT PROPERTIES OF COMPLEX MIXTURES

Roger A. Svehla

In the past much effort has gone into research of the theory and measurement of transport properties. Theory for the transport properties of dilute monatomic gases has been well established (refs. 1 and 2), and in recent years inroads have been made into the theory for polyatomic gases (refs. 3 and 4). But theory requires confirmation by experiment, and this has inspired a considerable effort in the measurement of the viscosity, thermal conductivity, and diffusion coefficients of gases. However, these efforts have been limited almost exclusively to pure gases and to binary or ternary mixtures. Measurements of transport properties of systems of many species are almost totally nonexistent. This leaves the problem of obtaining data for complex systems to the man with a pencil and paper or, better yet, a computer.

Yet despite the fact that our knowledge of transport properties for complex mixtures is considerably less than for pure gases or simple mixtures, this area is probably the one of most practical interest. Properties of complex mixtures are needed for heat- and mass-transfer calculations over wide ranges of pressure and temperature for many well-known processes. Some of the most common (and most important processes) occur during combustion in automobile, rocket, and jet engines. Others occur in the petroleum and chemical industries in hardware such as heat exchangers, absorbers, or gas pipelines.

EQUATIONS

Fortunately in spite of the dearth of experimental data, rigorous equations for mixtures are known (refs. 1 and 2). Thus, given the needed input, flavored with sufficient perseverance to do the arithmetic, we can get answers.

The problems in doing the arithmetic become apparent when we look at the equations for the viscosity and the thermal conductivity. First, consider the equation for the viscosity of a mixture of n gases:

$$\eta_{\text{mixture}} = \sum_{i=1}^{n} x_i \eta_i \tag{1}$$

where the x_i are the mole fractions. The η_i look something like partial viscosity contributions to the total viscosity. In fact, they are obtained by solving the following set of simultaneous linear equations

$$\sum_{j=1}^{n} c_{ij}\eta_j = x_i \qquad i=1, 2, \ldots, n \tag{2}$$

and the c_{ij} are given by

$$c_{ii} = \frac{x_i^2}{\eta_{ii}} + \sum_{\substack{k=1 \\ k\neq i}}^{n} \frac{2x_i x_k}{\eta_{ik}} \frac{M_i M_k}{(M_i + M_k)^2} \left(\frac{5}{3A_{ik}} + \frac{M_k}{M_i} \right) \tag{3a}$$

$$c_{ij} = -\frac{2x_i x_j}{\eta_{ij}} \frac{M_i M_j}{(M_i + M_j)^2} \left(\frac{5}{3A_{ij}} - 1 \right) \qquad i\neq j \tag{3b}$$

where

$$\eta_{ij} = \frac{5}{16N} \frac{\sqrt{\dfrac{2\pi M_i M_j RT}{(M_i + M_j)}}}{\pi \sigma^2_{\eta_{ij}}}$$

and

$$A_{ij} = \frac{\sigma^2_{\eta_{ij}}}{\sigma^2_{D_{ij}}}$$

where N is Avogadro's number, M_i the molecular weight, R the gas constant, and T the temperature. The $\sigma^2_{D_{ij}}$ can be interpreted as a binary diffusion cross section, and the $\sigma^2_{\eta_{ij}}$ as something like an average viscosity cross section be-

tween species i and j. If j = i, then η_{ij} simplifies to the expression for the viscosity of species i:

$$\eta_{ii} = \frac{5}{16N} \frac{\sqrt{\pi M_i RT}}{\pi \sigma^2_{\eta_{ii}}}$$

where $\pi\sigma^2_{\eta_{ii}}$ is the viscosity cross section of species i.

If the formulas for the coefficients (eqs. (3)) are examined, it is apparent that each η_i is approximately equal to the viscosity of species i, but becomes modified (sometimes quite substantially), by the presence of the other species, through the cross terms involving the η_{ij} and A_{ij}.

The thermal conductivity can be expressed as the sum of three terms:

$$\lambda_{mixture} = \lambda_{translational} + \lambda_{internal} + \lambda_{reaction} \tag{4}$$

Considering each term separately,

$$\lambda_{translational} = 4 \sum_{i=1}^{n} x_i \lambda_i \tag{5}$$

where the λ_i are found by solving a set of simultaneous linear equations, similar to those for the viscosity

$$\sum_{j=1}^{n} b_{ij} \lambda_j = x_i \qquad i = 1, 2, \ldots, n \tag{6}$$

and the b_{ij} are given by

$$b_{ii} = \frac{4x_i^2}{\lambda_{ii}} + \sum_{\substack{k=1 \\ k \neq i}}^{n} \frac{2x_i x_k \left(\frac{15}{2} M_i^2 + \frac{25}{4} M_k^2 - 3B_{ik} M_k^2 + 4A_{ik} M_i M_k \right)}{(M_i + M_k)^2 A_{ik} \lambda_{ik}} \tag{7a}$$

$$b_{ij} = -\frac{2x_i x_j M_i M_j}{(M_i + M_j)^2 A_{ij}\lambda_{ij}}\left(\frac{55}{4} - 3B_{ij} - 4A_{ij}\right) \qquad i \neq j \tag{7b}$$

where

$$\lambda_{ij} = \frac{25}{32N}\frac{\sqrt{\frac{\pi(M_i + M_j)RT}{2M_iM_j}}}{\pi\sigma^2_{\eta_{ij}}}\left(\frac{3R}{2}\right) = \frac{15}{4}R\left(\frac{M_i + M_j}{2M_iM_j}\right)\eta_{ij}$$

Notice that the calculation is very similar to that for the viscosity of a mixture, except that there is a little bit more algebra in obtaining the b_{ij} coefficients. We also have a new term called B_{ij}. This is another dimensionless grouping of cross sections similar to A_{ij}. However, no simple physical interpretation is available for B_{ij} as was for A_{ij}. But once we know the η_{ij} and A_{ij} we can calculate B_{ij} from theory. If $j=i$, then λ_{ij} simplifies to

$$\lambda_{ii} = \frac{25}{32N}\frac{\sqrt{\pi M_i RT}}{\pi\sigma^2_{\eta_{ii}}}\left(\frac{3R}{2M_i}\right) = \left(\frac{15R}{4M_i}\right)\eta_{ii}$$

which is the expression for a simple monatomic gas possessing only translational energy, such as argon. Therefore, the entire first term $\lambda_{translational}$ may be thought of as the contribution due to translational energy to the total conductivity.

The second term $\lambda_{internal}$ represents the contribution from internal energy modes, such as rotational, vibrational, and electronic, to the thermal conductivity. This is frequently expressed as

$$\lambda_{internal} = \sum_{i=1}^{n} \frac{\lambda_{i_{internal}}}{\sum_{j=1}^{n} \frac{D_{ii}}{D_{ij}}\frac{x_j}{x_i}} \tag{8}$$

which is the generalized Hirschfelder-Eucken expression (ref. 5) for a mixture. The D_{ij} are binary diffusion coefficients, the D_{ii} self-diffusion coefficients, and $\lambda_{i_{internal}}$ the internal contribution of species i. In the past a frequently used expression for $\lambda_{i_{internal}}$ is the Eucken expression

$$\lambda_{i_{internal}} = \rho_i D_{ii}\left(\frac{Cp_i}{R} - \frac{5}{2}\right)\frac{R}{M_i} \tag{9}$$

where ρ is the density and Cp the heat capacity. The expression, in effect, assumes that relaxation times for internal energy modes are very long. However, Monchick, Pereira, and Mason (ref. 3) have derived expressions to include finite relaxation times, which they express in terms of collision numbers. These relaxation effects enter into both the $\lambda_{translational}$ and $\lambda_{internal}$ terms, decreasing the first term and increasing the second. There is no need to belabor the point by reproducing the equations here. Suffice it to say that it merely increases the amount of algebra involved, but not the general nature of the solutions.

The final term corresponds to the contribution from the effects of chemical reaction (refs. 6 and 7)

$$\lambda_{reaction} = R \sum_{i=1}^{v}\left(\frac{\Delta H_i}{RT}\right)\lambda_{R_i} \tag{10}$$

where ΔH_i is the heat of reaction of reaction number i and v is the total number of reactions.

$$\Delta H_i = \sum_{k=1}^{n} a_{ik}H_k \qquad i = 1, 2, \ldots, v \tag{11}$$

In equation (11) the a_{ik} are the stoichiometric coefficients written for chemical reactions involving species Y_k as follows:

$$\sum_{k=1}^{n} a_{ik}Y_k = 0 \qquad i = 1, 2, \ldots, v \tag{12}$$

Similar to what we had previously, the λ_{R_i} are obtained by solving a set of simultaneous linear equations

$$\sum_{j=1}^{v} g_{ij}\lambda_{R_j} = \frac{\Delta H_i}{RT} \qquad i = 1, 2, \ldots, v \tag{13}$$

where

$$g_{ij} = \sum_{k=1}^{n-1} \sum_{l=k+1}^{n} \frac{RT}{PD_{kl}} x_k x_l \left(\frac{a_{ik}}{x_k} - \frac{a_{il}}{x_l}\right)\left(\frac{a_{jk}}{x_k} - \frac{a_{jl}}{x_l}\right) \qquad i, j = 1, 2, \ldots, v \tag{14}$$

Although these equations appear somewhat complicated, especially for systems of many species, at least they are straightforward. The main drawback is that they can be very lengthy. The time required to do calculations by hand becomes prohibitive for anything more complex than a binary or, perhaps, a ternary mixture. (The possibility of using approximate equations is one way of reducing the arithmetic. However, this line of attack has been investigated by others (refs. 8 and 9) and will not be repeated here.)

As a consequence, a computer program, coded in FORTRAN IV, was written at Lewis to calculate the properties of mixtures. The program is a combination of the NASA Lewis Computer Equilibrium Calculations Program (CECS) for calculating thermodynamic properties, together with a program for the transport property calculations. The CECS part of the program provides the composition needed in the transport calculations in addition to the thermodynamic properties. The types of problems the program is capable of handling include rocket combustion, properties across normal shock waves, Chapman-Jouguet detonations, and properties at assigned thermodynamic states. The program handles up to 100 chemical species in the thermodynamic calculations at any one time. In doing the transport calculations, the 20 most important gaseous species are used. This is done by selecting the 20 most important gaseous products and ignoring any remaining gaseous species and all liquids and solids. The composition is then normalized, based on those 20 gaseous species.

Questions concerning this program, which will be published later, may be directed to the author. Thermodynamic data for a large number of species are included in the program. Transport data are also included for a large number of

species and for a number of interactions between different species. When transport data are missing the program has built-in techniques to estimate the missing data.

HYDROCARBON-AIR COMBUSTION

As a typical problem, let us consider the interactions in hydrocarbon-air combustion:

(1) Species

$$H,\ Ar,\ N_2,\ H_2,\ O_2,\ CO,\ NO,\ CO_2,\ H_2O,\ N,\ O,\ OH$$

(2) Interactions between identical species

$$H\text{-}H,\ Ar\text{-}Ar,\ N_2\text{-}N_2,\ \ldots,\ \rightarrow \text{Total of } n = 12$$

(3) Interactions between different species

$$H\text{-}Ar,\ H\text{-}N_2,\ \ldots,\ N_2\text{-}H_2,\ \ldots,\ \rightarrow \text{Total of } \frac{n(n-1)}{2} = \frac{12(12-1)}{2} = 66$$

The most important species in this combustion system are listed in the approximate order of our knowledge of the transport properties, with the best known starting on the left. All the species are not important at any one time; some are important at low temperatures, while others are important at high temperatures. In general, more species become important at the higher temperatures as dissociation occurs.

Experimental transport data are available for most of the species. A large number of measurements have been made for the eight species starting with Ar and ending with H_2O. In fact, measurements of the viscosity of Ar, N_2, and H_2 have recently been reported for temperatures up to 2150 K (ref. 10). In addition, molecular beam scattering measurements are available for Ar, N_2, O_2, and H_2, which provide information for calculating the properties to considerably higher temperatures.

Little experimental transport data exist for the remaining species H, N, O, and OH. However, extensive theoretical calculations are available for the H-H interaction. In addition, spectroscopic measurements of H_2 provide information for the $^1\Sigma$ energy curve of the bound state. In view of this substantial amount of information about the H-H interaction, it seemed there was sufficient knowledge

to justify putting H first on the list. But, for N and O, information is much more scanty. No experimental transport data are available, and knowledge is pretty much limited to spectroscopic measurements, which provide information on the bound states. Finally, for OH no experimental transport data are available. We would either have to try to build up the information from data for the interactions between O and H, or try to estimate the data by some other technique.

Hydrocarbon-air interactions (2) and (3) break down into interactions for the pure species and interactions between different species. Of the 66 interactions between unlike species, there are experimental binary diffusion coefficient data for about 17 of the interactions and molecular beam scattering measurements for about 17 interactions. Some of the interactions have both diffusion data and beam scattering measurements, while others have neither. For those which have neither, one might apply some sort of combining rule, using the data of the pure species.

CALCULATED PROPERTIES

Figures VI-1 to VI-4 show some of the individual calculated properties for a stoichiometric mixture, plotted at constant pressure, for a range of pressures. In figure VI-1 the combustion temperature is indicated for combustion at 1 atmosphere, occurring at about 2400 K. With increasing pressure, or other types of combustion such as automobile or hypersonics, higher temperatures might be obtained. Notice that the enthalpy increases slowly and is pressure independent up to about 1700 K. This simply represents the increase in enthalpy of the four species N_2, CO_2, H_2O, and Ar. At higher temperature, dissociation starts to occur, resulting in an increasing number of species. There are as many as 11 important species under some conditions. Recall that the specific heat C_p is $(\partial h/\partial T)_p$, so that the slope of the curve is the specific heat at that pressure. This is illustrated in figure VI-2 by the solid upper curves referred to as equilibrium. In addition, there is a lower dashed curve called frozen, also sometimes referred to as nonreacting. This is simply the sum of the specific heats of the individual species each multiplied by its respective mole fraction. The difference between equilibrium and frozen is usually referred to as the specific heat due to chemical reaction and is caused by the change in composition with temperature.

This effect can be quite large. Under some conditions the equilibrium value may be as much as an order of magnitude greater than the frozen. Incidently, as one would expect, the frozen curve is also pressure dependent. However, the

variation with pressure is too slight to be observed on the scale plotted in the figure.

In contrast to the curves for the enthalpy and specific heat, the results for the viscosity show a rather well-behaved temperature dependence, as shown in figure VI-3. Also, the pressure dependence is so slight that there is almost no change in the viscosity from 0.01 to 100 atmospheres. This is in sharp contrast to the results for the thermal conductivity, shown in figure VI-4. The behavior of the thermal conductivity is quite similar to that for the specific heat. As was the case for the specific heat, the equilibrium value may be greatly in excess of the frozen value. Again the difference is due to the effect of chemical reaction, as given by equation (10). Since this effect is present in both the specific heat and the thermal conductivity, it would be expected that by taking a ratio of the two properties much of this effect would cancel. This would suggest looking at a quantity such as the Prandtl number. It is a dimensionless number frequently used in heat- and mass-transfer calculations and includes a ratio of these two properties. The equilibrium Prandtl number is shown in figure VI-5. It is obvious that the Prandtl number varies more slowly with temperature than any of the individual properties entering into its calculation, and more slowly with pressure than either the specific heat or thermal conductivity. In fact, over the entire range of variables, the Prandtl number varies from about 0.36 to 0.73, a factor of two, in sharp contrast with any of the individual properties. This is an interesting result in as much as heat- and mass-transfer calculations frequently involve dimensionless numbers, such as the Prandtl number. If one looks at the typical correlations which have been proposed, such as the following

$$Nu = k\,Re^{0.8}\,Pr^{1/3} \tag{15}$$

where

Nu Nusselt number, $h\ell/\lambda$

Re Reynolds number, $\ell u\rho/\eta$

Pr Prandtl number, $C_p\eta/\lambda$

and k is an adjustable constant determined by experiment, h the heat transfer coefficient, ℓ a characteristic dimension of the geometry, u the linear flow velocity, ρ the density, and the other properties the same as before.

Solving for the heat-transfer coefficient in equation (15) gives

$$h \alpha \frac{\lambda^{2/3} C_p^{1/3}}{\eta^{0.47}} \tag{16}$$

Expressing the heat-transfer coefficient in the form of equation (16) shows that the uncertainty in the coefficient is less than the uncertainty in an individual property because the exponents of the properties are less than one. Furthermore, by doing rigorous calculations for the viscosity and thermal conductivity, errors due to uncertainties in the transport cross sections are systematic rather than random. This results in some degree of cancellation of these errors when a ratio of these properties is taken (ref. 11). However, in contrast to the result of the Prandtl number, the effect of chemical reaction enters as a first-order effect on the heat-transfer coefficient, rather than tending to cancel, as in the Prandtl number. As a result, when the contribution due to chemical reaction is large, the heat-transfer coefficient can become considerably more sensitive to variations in the thermodynamic properties, than to variations in the transport properties. This is fortunate since, in general, thermodynamic properties are known more accurately than the corresponding transport properties.

The data points in figure VI-5 represent experimental measurements from the University of Minnesota (ref. 12) and were obtained by measuring the recovery factor for a flat plate. The recovery factor can be expressed as the square root of the Prandtl number. There appears to be satisfactory agreement with the calculations.

In conclusion, perhaps the whole problem of calculating the transport properties of gas mixtures might be summarized as follows. The calculation of complex mixtures requires a large quantity of input data including composition, transport data for the pure species, and transport data for the interactions between different species. In fact, accumulating these data is the most difficult part of the job. But, once having done this, then, with the aid of modern day computers, we are now in a position to handle even very complex mixtures in a straightforward fashion.

REFERENCES

1. Chapman, Sydney; and Cowling, T. G.: The Mathematical Theory of Non-Uniform Gases. Second ed., Cambridge Univ. Press, 1952.

2. Hirschfelder, Joseph O.; Curtiss, Charles F.; and Bird, R. Byron: Molecular Theory of Gases and Liquids. John Wiley & Sons, Inc., 1954.

3. Monchick, L.; Pereira, A. N. G.; and Mason, E. A.: Heat Conductivity of Polyatomic and Polar Gases and Gas Mixtures. J. Chem. Phys., vol. 42, no. 9, May 1, 1965, pp. 3241-3256.

4. Mason, E. A.; and Monchick, L.: Heat Conductivity of Polyatomic and Polar Gases. J. Chem. Phys., vol. 36, no. 6, Mar. 15, 1962, pp. 1622-1639.

5. Hirschfelder, Joseph O.: Generalization of the Eucken Approximation for the Heat Conductivity of Polyatomic or Chemically Reacting Gas Mixtures. International Union of Pure and Appl. Chem. and Inst. Mech. Eng. Joint Conference on Thermodynamic and Transport Properties of Fluids, 1958, pp. 133-141.

6. Butler, James N.; and Brokaw, Richard S.: Thermal Conductivity of Gas Mixtures in Chemical Equilibrium. J. Chem. Phys., vol. 26, no. 6, June 1957, pp. 1636-1643.

7. Brokaw, Richard S.: Thermal Conductivity of Gas Mixtures in Chemical Equilibrium. II. J. Chem. Phys., vol. 32, no. 4, Apr. 1960, pp. 1005-1006.

8. Brokaw, Richard S.: Approximate Formulas for the Viscosity and Thermal Conductivity of Gas Mixtures. J. Chem. Phys., vol. 29, no. 2, Aug. 1958, pp. 391-397.

9. Reid, Robert C.; and Sherwood, Thomas K.: The Properties of Gases and Liquids: Their Estimation and Correlation. Second ed., McGraw-Hill Book Co., Inc., 1966.

10. Guevara, F. A.; McInteer, B. B.; and Wageman, W. E.: High-Temperature Viscosity Ratios for Hydrogen, Helium, Argon, and Nitrogen. Phys. Fluids, vol. 12, no. 12, Dec. 1969, pp. 2493-2505.

11. Brokaw, R. S.: Energy Transport in High Temperature and Reacting Gases. Physical Chemistry in Aerodynamics and Space Flight. A. L. Myerson and A. C Harrison, eds., Pergamon Press, 1961, pp. 238-252.

12. Anderson, Kenneth M.; Pulkrabek, Willard W.; Ibele, Warren E.; and Eckert, E. R. G.: Measurement of Prandtl Number and Thermal Conductivity. Rep. HTL TR-88, Univ. Minnesota (NASA CR-54634), Dec. 15, 1968.

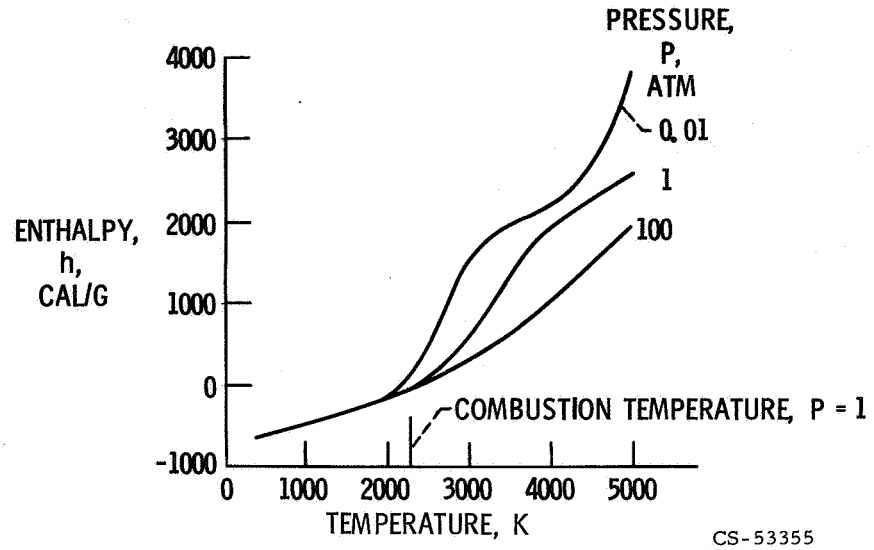

Figure VI-1. - Enthalpy of jet-fuel/air combustion products. Stoichiometric mixture.

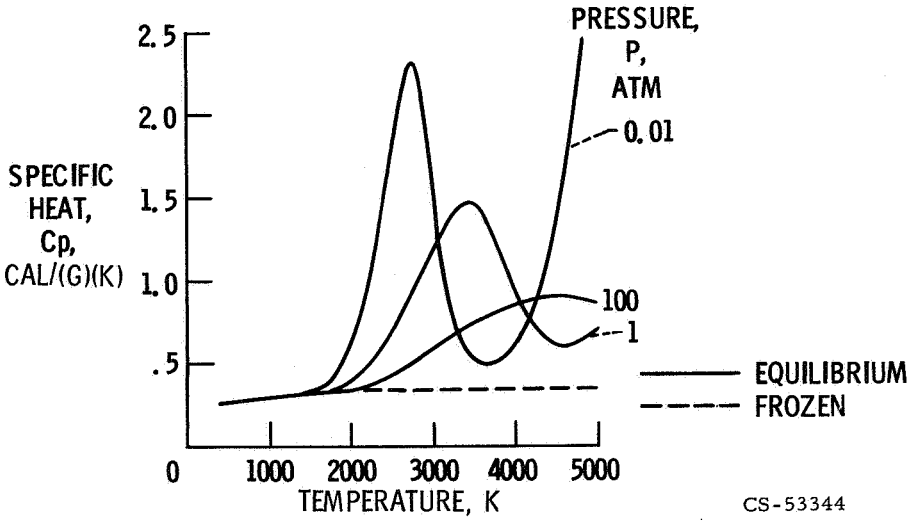

Figure VI-2. - Specific heat of jet-fuel/air combustion products. Stoichiometric mixture.

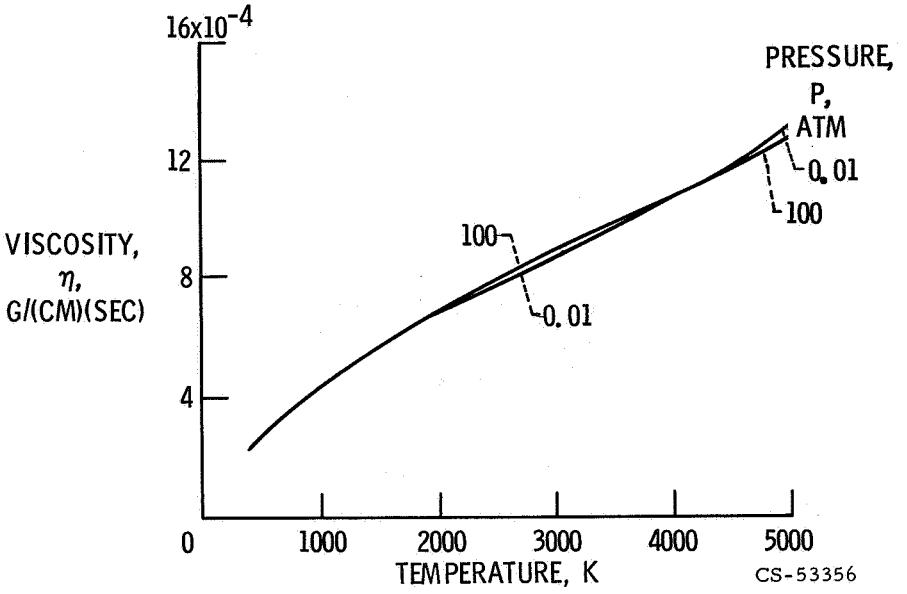

Figure VI-3. - Viscosity of jet-fuel/air combustion products. Stoichiometric mixture.

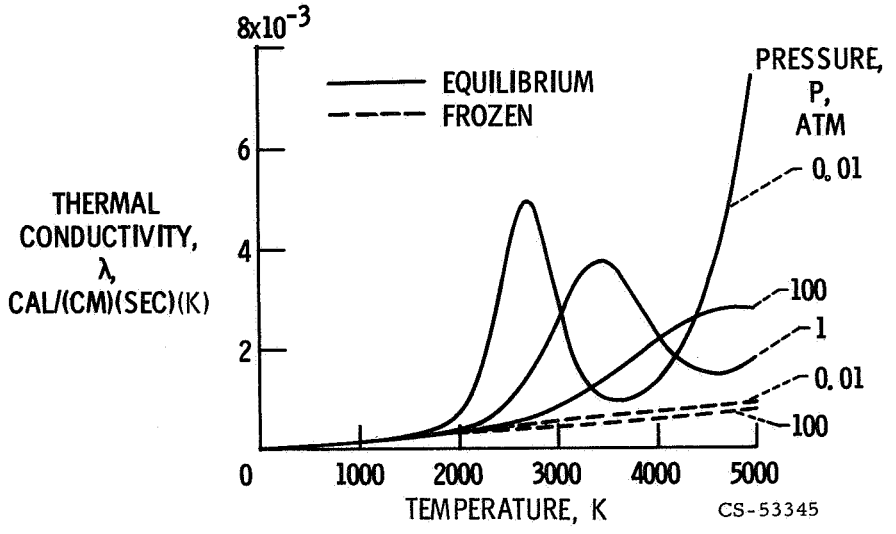

Figure VI-4. - Thermal conductivity of jet-fuel/air combustion products. Stoichiometric mixture.

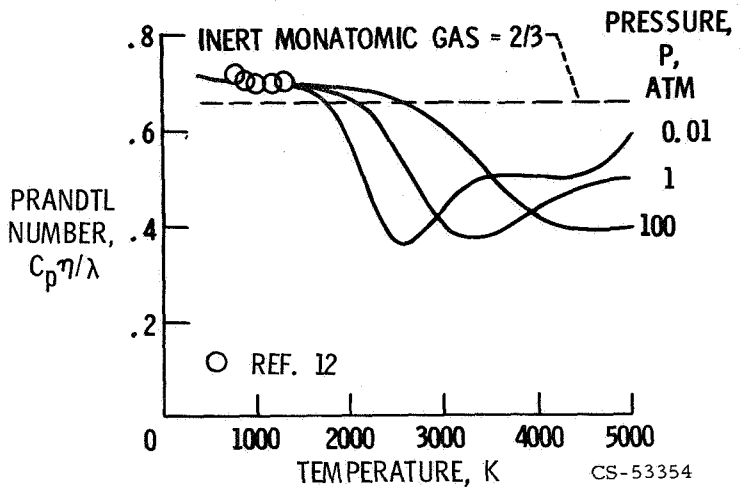

Figure VI-5. - Prandtl number of jet-fuel/air combustion products. Stoichiometric mixture.

VII. COMBUSTION CHEMISTRY

Frank E. Belles

This survey of combustion chemistry covers two aspects of the subject:

(1) What is known about the reactions involved; all of this work has been done at other laboratories.

(2) What is known about the rates of these reactions and how to learn more; Lewis Research Center is active in this field.

Everyone is well aware that flames can be used in countless ways without knowing anything at all about combustion chemistry. But when it is necessary to extract all possible performance from a combustion system, to understand the source and elimination of combustion-generated air pollutants, or to devise better ways to extinguish fires, then it also becomes necessary to know the important combustion reactions and their rates.

COMBUSTION REACTIONS

Experimental Approaches

Consider a typical flame burning in a mixture of hydrocarbon fuel and air or oxygen (fig. VII-1). There are two ways to study the chemistry occurring in such a flame.

The overall, or global, approach is to measure the burning velocity over a range of temperatures, pressures, and concentrations of fuel and oxygen. The results are expressed in terms of the rate of consumption of fuel and are fitted to an expression of the following form:

$$\frac{-dN_{fuel}}{dt} = A(N_{fuel})^b\left(N_{O_2}\right)^c \exp\left(\frac{-E}{RT}\right) \qquad (1)$$

Here N_{fuel} and N_{O_2} are concentrations, and A, b, c, and E (the apparent activation energy) are empirical constants. Such an expression would represent the results precisely if all the flames studied were dominated by a slow reaction that paced the chemistry. But under new conditions, outside the range of measurements

used to derive A, b, c, and E, equation (1) may become invalid if the same reaction no longer controls the chemistry. Furthermore, an empirical result such as equation (1) says nothing about the actual reactions that are responsible for the consumption of fuel. For both reasons, the global approach has limited value.

The second, more general, approach is to study only a few flames but in much greater detail. Starting about 15 years ago, a few groups began to measure profiles of temperature and composition in flames. This work - much of which was done at the Applied Physics Laboratory of the John Hopkins University - has provided most of the current understanding of flame chemistry. The intention here is not to go into this work exhaustively, but to convey its general flavor and then to present the chemistry that has been deduced from it.

Flame Profiles

What kind of temperature profile might one expect to find in a flame such as that in figure VII-1? An offhand conclusion might be that the highest temperature would occur in the thin, intensively luminous inner zone, which is so much brighter than the diffuse outer zone. Figure VII-2 shows that this is not the case. The profile in figure VII-2 was obtained at low pressure in a flat flame of methane burning in a large excess of air. Under such experimental conditions, the flame is thickened and the temperature is held down, so that reliable measurements can be made by means of a thermocouple.

There are three regions in this profile. First, starting at the mouth of the burner, there is a region of slow temperature rise due to heat transfer from the hotter part of the flame. This prepares the mixture for rapid reaction in the second region, which coincides with the zone of intense luminosity; here, the temperature jumps sharply. The feature of this profile that seemed rather surprising in 1954, when the work was done, was the existence of a third region in which a further, albeit more gradual, rise in temperature occurs. It is in this third region that the final temperature, corresponding to chemical equilibrium, is attained.

The greater significance of this work lies in the heat-release profile that can be derived from the temperature profile. In figure VII-3, the fraction of total heat release is plotted against distance. Far to the right, the temperature has reached its final value (fig. VII-2), all the heat has been released, and the fraction is unity. But when the gas leaves the luminous zone, only 60 percent of the heat has been released; the remaining 40 percent is released more slowly in the diffuse outer zone.

Friedman and Burke, who measured this profile, noted that this 60 to 40 distribution corresponds to conversion in the luminous zone of the hydrogen to water and of the carbon to carbon monoxide, with slow conversion to carbon dioxide, the final product, in the outer zone. Initially, this was a speculative idea. Later, the group at the Applied Physics Laboratory confirmed it by measuring composition profiles.

Figure VII-4 shows such a profile. It was measured in a flame of methane burning in excess oxygen at 0.1 atmosphere. (The difference in pressure as compared to that used in the work depicted in figs. VII-2 and VII-3 and the substitution of oxygen for air are irrelevant to the general conclusions.) The fraction of the total flow of moles of gas is plotted against distance for three constituents of the mixture. Methane starts out at between 7 and 8 percent of the unburned mixture and disappears in the luminous zone. Its carbon is converted to carbon monoxide, just as suspected. The luminous zone is thus the region of primary reaction. In the succeeding secondary zone, the carbon monoxide is gradually converted to the final product, carbon dioxide. Obviously, the chemistry is much faster in the primary than the secondary zone. The methane in this particular flame is destroyed in a fraction of a millisecond.

Other flame-sampling studies, including some in which reaction intermediates were measured, have established the reason for this behavior in terms of the detailed mechanism of reaction in oxygen rich methane flames. The conclusions drawn from studies of this particular class of flames are presented next, followed by a discussion of modifications in the reaction mechanism that occur in other combustion systems.

Combustion Scheme for Methane in Excess Oxygen

Figure VII-5(a) lists the reactions that occur in the primary (luminous) zone. Two of them are of utmost importance: the attack on oxygen by hydrogen atoms, and the initial reaction of the fuel with hydroxyl radicals.

As a result of this initial attack, the methane is converted to methyl radicals. These go through an intermediate stage of conversion to formaldehyde (OCH_2), which does not accumulate but is rapidly converted to carbon monoxide via the intermediate formation of formyl radical (HCO). The second step, involving HCO, has not been positively identified; the other reactant and product are therefore omitted and this step is merely indicated by the wavy arrow. Meanwhile, methane is also attacked to a certain extent by hydrogen atoms, and the molecular

hydrogen produced as well as the water formed in the main attack on methane engage in the last three reactions.

Examination of the reactions listed in figure VII-5(a) suggests the reason for the great speed of the chemical events that occur in the primary zone. Every reaction listed involves a chain carrier - a highly reactive atom or free radical. Moreover, every reaction produces at least one chain carrier. But four of the reactions (marked with asterisks) produce two. As a result, this chain of reactions yields more chain carriers than are consumed, and the extra ones can begin new chains. Thus, the primary zone is a region of chain-branching reaction, which is characteristically a very fast process.

The first reaction listed in figure VII-5(a) is crucially important. Not only is it the means by which oxygen is attacked, but it is also the reaction that begins the process of chain branching. Furthermore, it is a key reaction because it happens to be very slow at low temperatures. There are two reasons for this. First, the reaction is quite endothermic and therefore has a very low rate at temperatures below about 1000 K. Second, at the lower temperatures a competing reaction (not listed) destroys hydrogen atoms. The net result is that this crucial reaction effectively does not occur at temperatures much below 1000 K. And it is undoubtedly for this reason that hydrocarbon flames do not exist in mixtures that cannot release enough heat to raise the temperature to about that level.

As a result of the chain of reactions in figure VII-5(a) the gas flowing out of the primary zone contains carbon monoxide, plus amounts of oxygen and hydrogen atoms and hydroxyl radicals that are far in excess of the chemical equilibrium values. There are also the unused oxygen, a small amount of hydrogen, and a large amount of water vapor. A good way of characterizing the situation is to say that the primary zone is a flame in which methane is burned to produce the fuel - carbon monoxide - for a second flame.

Things are considerably simpler in the secondary zone because the fuel has now been converted to smaller molecules that have fewer possibilities for reaction. Figure VII-5(b) summarizes the secondary zone reactions. The first one listed is responsible for converting carbon monoxide to the final product, carbon dioxide. While this is happening, the chain carriers shuffle their identities by means of the next four reactions, which now proceed in both directions because the temperature and the chain-carrier concentrations are high. In fact, the chain carriers tend to remain in a state of chemical equilibrium among themselves by means of these reactions, while at the same time their population decreases. This decrease is effected by the two recombination reactions, in which M denotes a third body whose function is to absorb the recombination energy and thus to stabilize the newly formed oxygen or water molecule. Because three-body colli-

sions are relatively infrequent, the recombination reactions are slow and continue after the carbon monoxide has been converted. For that reason, they have been assigned to a third zone, but with the understanding that recombination actually begins in the secondary zone.

Combustion Scheme for Excess Methane

The chemistry presented in the preceding section was for the case in which oxygen is in stoichiometric excess. If the situation is reversed and methane is in excess there are only a few changes; these are summarized in figure VII-6. The main attack on the fuel is now by hydrogen atoms rather than hydroxyl radicals. The product is methyl radical, as before, but its fate is less clear than in the excess-oxygen case. However, it does seem clear that methyl radical is chiefly attacked by oxygen atoms in fuel-rich mixtures with subsequent rapid conversion to carbon monoxide. Except for these changes, the primary zone reactions are as shown in figure VII-5(a).

In the secondary zone, carbon monoxide reacts with hydroxyl radicals as before, but some of it appears as a final product because of the deficiency of oxygen in these mixtures. Finally, figure VII-6 lists a new recombination reaction that is the source of some of the hydrogen appearing in the combustion products.

Combustion Scheme for Other Hydrocarbons in Excess Oxygen

The discussion so far has pertained to methane. Suppose the fuel is some other hydrocarbon? If it is a saturated hydrocarbon belonging to the alkane family, and if it burns in the presence of excess oxygen, much of the combustion scheme is the same as for methane.

As indicated in figure VII-7, such a fuel is mainly attacked by hydroxyl radicals. The resulting hydrocarbon free radical quickly undergoes thermal decomposition to an olefin and a methyl radical. The reactions of the latter, with the final evolution of carbon monoxide, are as shown in figure VII-5(a). The carbon in the olefin also appears in carbon monoxide, following initial attack by oxygen atoms and subsequent reactions which, although not yet known in detail, are fast compared to the corresponding sequence for methyl radicals. The evidence for this greater speed is the fact that flame sampling reveals only the

intermediate from methyl radicals, formaldehyde. No higher-molecular-weight aldehydes, ketones, or alcohols are detected.

Summary of Important Combustion Reactions

In figure VII-8 are listed the reactions that have been identified as important ones in hydrocarbon combustion. Clearly, they are not the whole story. The detailed combustion schemes have yet to be worked out for unsaturated and cyclic compounds, and for the heavier saturated hydrocarbons when burned in a deficiency of oxygen. Nevertheless, enough is already known to deal with many practical situations. And considering the enormous complexity that could in principle have been discovered for even so simple a fuel as methane, it is very encouraging to find that the really important reactions reduce to the small number shown in figure VII-8.

RATES OF COMBUSTION REACTIONS

With many of the important reactions identified, it is now pertinent to consider the state of knowledge of their rates. In doing so, the recombination reactions (fig. VII-8) are omitted. They are in a special category because their rates depend on the identity of the third body, M. A subsequent paper by Dr. Warshay discusses work designed to get a more basic understanding of the role of the third body in such reactions.

Rates at Low Temperatures

Of the remaining reactions, most are fast enough to be studied at room temperature to a few hundred K by any of a number of good experimental methods. In this class are (1) the reaction of hydroxyl radicals with fuel, (2) the first three chain-branching reactions, and (3) the one responsible for converting carbon monoxide to carbon dioxide. Consequently, the state of knowledge of these rates is quite good at low to moderate temperatures.

As an example of this, table VII-1 shows the results of five recent measurements of the rate of one of the chain-branching reactions at 300 K. Three different techniques were used to follow either the disappearance of a reactant (OH) or the appearance of a product (H or H_2O). The values listed for the rate coefficient

show a gratifyingly small range. Even the workers who encountered the largest experimental scatter obtained values fairly close to the most precise ones, much closer than the order-of-magnitude agreement that would have been gratefully accepted prior to the introduction of modern methods of studying free-radical reactions. Critical examination of the results listed in table VII-1 shows that the room-temperature rate of this reaction is well established. The same can be said of several others of the reactions that have appreciable low-temperature rates.

Rates at High Temperatures

For one reason or another, all of the experimental methods that work so well at low to moderate temperatures fail long before combustion temperatures are reached. And since rate coefficients increase exponentially with temperature, long extrapolations of low-temperature results are likely to be in error. There is a need for reliable, direct measurements at the higher temperatures.

At present, two experimental approaches have been developed to a point such that they can meet this need: flame sampling and shock tubes. The two are comparable with respect to the ranges of temperature and characteristic reaction times over which they can be applied. At this laboratory, shock tubes have been chosen as more direct and flexible tools for high-temperature rate measurements. In preparation for the next two papers, shock-tube operation is briefly described.

Shock Tubes for Measurement of High-Temperature Reactions Rates

As shown schematically in figure VII-9, a shock tube contains two sections separated by a metal or plastic diaphragm. Both sections are first evacuated. The gas mixture in which a reaction is to be studied is then admitted to the driven section. The driver section is filled with high-pressure gas and the diaphragm is burst. This generates a shock wave, which travels into the driven gas at several times the speed of sound. The shock compresses and heats the reaction mixture, and also sets it into motion following the shock. Near the end of the tube are windows and an array of instruments.

Figure VII-10 shows how the temperature changes as the heated reacting gas flows past the windows. It jumps almost instantaneously at the shock front from ambient to an elevated temperature, which may be several thousand degrees

and which is determined by the velocity of the shock. It is therefore essential to measure the velocity by carefully timing the arrival of the shock at two detectors (fig. VII-9). The flow of hot gas, in which reaction is occurring, lasts for about a millisecond in typical shock tubes. The temperature falls and the reaction is terminated when the cold, expanded driver gas moves past the window (fig. VII-10).

The course of reaction is followed spectroscopically by means of the instruments shown below the shock tube in figure VII-9. This is done by observing changes in the intensity of light, either emitted or absorbed, that are directly related to a changing concentration. An optical system gathers the light and isolates an appropriate wavelength. The light is detected by a photomultiplier and its signals are displayed on an oscilloscope, where they are photographed. This mode of recording must be used because of the exceedingly brief duration of the hot flow in a shock tube.

It was mentioned earlier that the temperature behind a shock depends on the shock velocity. This is not strictly true. For two reasons the temperature can change while a reaction is being observed. One of the reasons is that the heat of reaction may affect the temperature. This effect, however, can generally be reduced to minor proportions by diluting the reactive gases with a large amount of inert gas, such as argon, which serves as a constant-temperature bath. The other source of changing temperature is less obvious and has only recently come to be appreciated. Because the gas behind the shock is moving, a boundary layer develops along the walls of the tube. The effect of this layer is to increase the temperature in the core of the flow as indicated by the dashed line in figure VII-10. Furthermore, the pressure rises and the time scale of the reaction is distorted. All these effects of the boundary layer, if neglected, can cause serious errors in shock-tube rate measurements. Fortunately, the theory for dealing with these changes exists and recent tests show that it is quite adequate.

CONCLUDING REMARKS

Great progress has been made during the past 15 years in elucidating combustion chemistry and in making it a quantitative rather than a merely descriptive science. In many hydrocarbon-burning combustion systems of practical interest, the important reactions have been identified. All of these reactions involve highly reactive atoms or free radicals. Reliable measurements of the rates of these reactions, at both low and high temperatures, are steadily accumulating. The two kinds of information - chemical mechanisms and rate data - provide the ability to predict, and thus, to control, the behavior of complex combustion systems.

BIBLIOGRAPHY

Combustion Reactions

Friedman, Raymond; and Burke, Edward: Measurement of Temperature Distribution in a Low-Pressure Flat Flame. J. Chem. Phys., vol. 22, 1954, pp. 824-830.

Fristrom, R. M.; and Westenberg, A. A.: Flame Structure. McGraw-Hill Book Co., Inc., 1965.

Rates of Combustion Reactions

Schofield, K.: An Evaluation of Kinetic Rate Data for Reactions of Neutrals of Atmospheric Interest. Planet. Space Sci., vol. 15, 1967, pp. 543-670.

Baulch, D. L.; Drysdale, D. D.; and Lloyd, A. C.: Critical Evaluation of Rate Data for Homogeneous, Gas-Phase Reactions of Interest in High-Temperature Systems. Rep. 1, Dept. Phys. Chem., Leeds Univ., May 1968.

Baulch, D. L.; Drysdale, D. D.; and Lloyd, A. C.: Critical Evaluation of Rate Data for Homogeneous, Gas-Phase Reactions of Interest in High-Temperature Systems. Rep. 2, Dept. Phys. Chem., Leeds Univ., Nov. 1968.

Baulch, D. L.; Drysdale, D. D.; and Lloyd, A. C.: Critical Evaluation of Rate Data for Homogeneous, Gas-Phase Reactions of Interest in High-Temperature Systems. Rep. 3, Dept. Phys. Chem., Leeds Univ., Apr. 1969.

Shock Tubes

Greene, Edward F.; and Toennies, J. Peter: Chemical Reactions in Shock Waves. Academic Press, 1964.

Mirels, H.: Flow Nonuniformity in Shock Tubes Operating at Maximum Test Times. Phys. Fluids, vol. 9, no. 10, Oct. 1966, pp. 1907-1912.

Warshay, Marvin: Effects of Boundary Layer Buildup in Shock Tubes upon Chemical Rate Measurements. NASA TN D-4795, 1968.

TABLE VII-1. - RATE COEFFICIENTS AT 300 K

$$\left[\begin{array}{c} OH + H_2 \rightarrow H_2O + H \\ d[H_2O]/dt = d[H]/dt = k[OH][H_2] \end{array}\right]$$

Investigator	Method	Rate coefficient, k, cm^3/mole-sec
Kaufman (1963)	OH, UV absorption	$(4.3 \pm 1.0) \times 10^9$
Wise (1964)	H, ESR spectrometry	$(5.7 \pm 0.7) \times 10^9$
Dixon-Lewis (1966)	OH, ESR spectrometry	$(3.9 \pm 0.2) \times 10^9$
Greiner (1969)	OH, UV absorption	$(4.1 \pm 0.2) \times 10^9$
Wong (1970)	H_2O, mass spectrometry	$(5.0 \pm 3.0) \times 10^9$

CS-53165

Figure VII-1. - Premixed hydrocarbon flame.

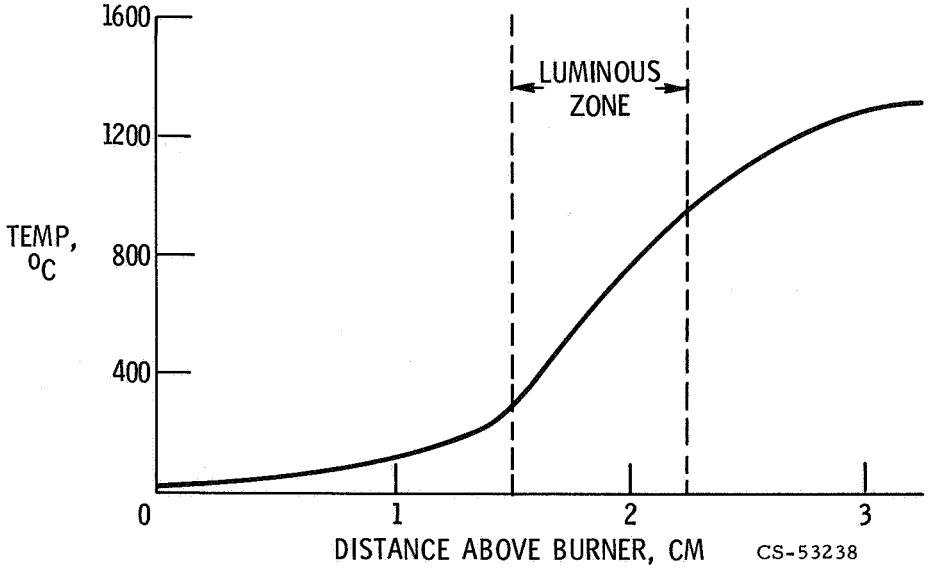

Figure VII-2. - Temperature profile of a flame. Propane-air; pressure, 0.06 atmosphere; A/F = 29.

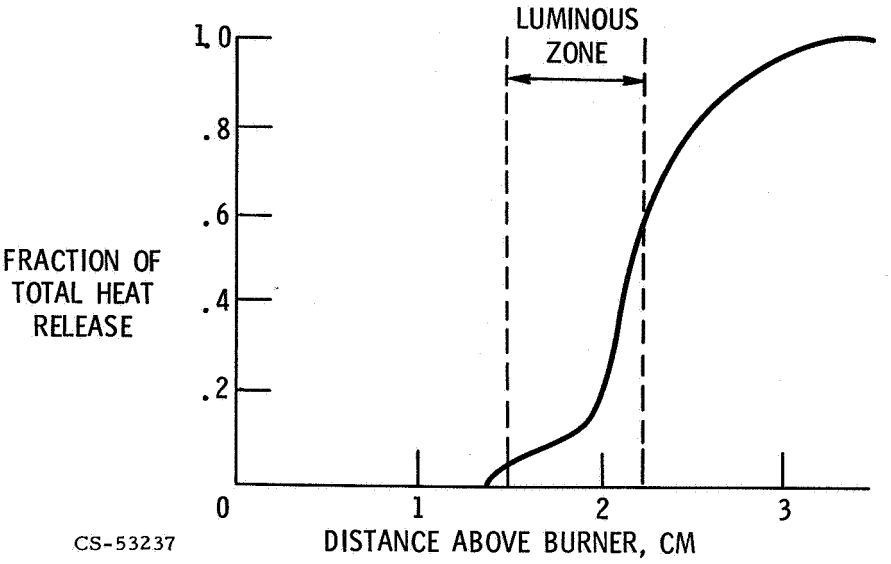

Figure VII-3. - Heat release in a flame (derived from temperature profile).

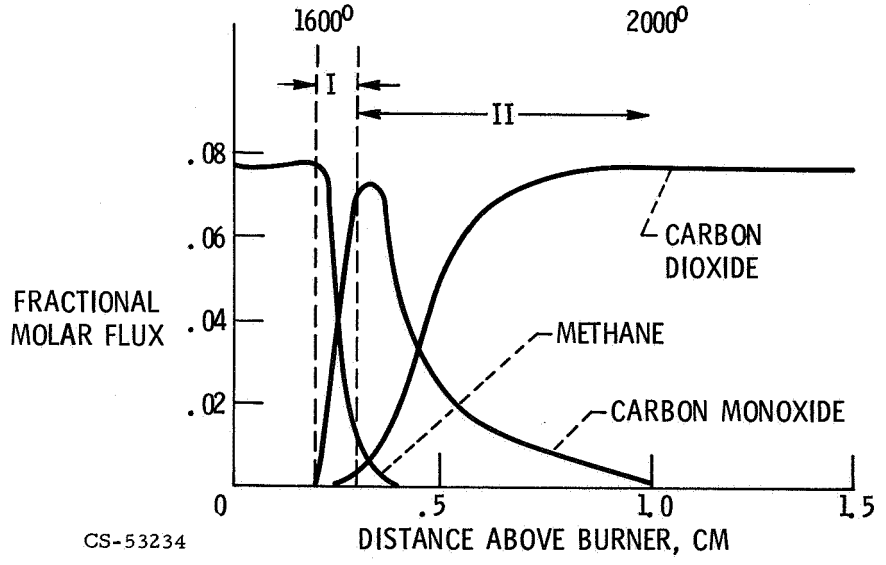

Figure VII-4. - Composition profile of a flame. Methane in excess oxygen; pressure, 0.1 atmosphere.

PRIMARY ZONE: ATTACK ON CH_4 AND O_2

MAIN ATTACK ON O_2:

$$H + O_2 \rightarrow OH + O \quad *$$

MAIN ATTACK ON CH_4:

$$OH + CH_4 \rightarrow CH_3 + H_2O$$

FOLLOWED BY:

$$CH_3 + O_2 \rightarrow OCH_2 + OH$$
$$OCH_2 + O \rightarrow HCO + OH \quad *$$
$$HCO \rightsquigarrow CO$$
$$CH_4 + H \rightarrow CH_3 + H_2$$
$$O + H_2 \rightarrow OH + H \quad *$$
$$OH + H_2 \rightarrow H_2O + H$$
$$O + H_2O \rightarrow OH + OH \quad *$$

} CO, OH, O, H, O_2, H_2O, H_2 ↓ SECONDARY ZONE

CS-53241

SECONDARY ZONE: ATTACK ON CO

MAIN ATTACK ON CO:

$$OH + CO \rightarrow CO_2 + H$$

SHUFFLE REACTIONS OF CHAIN CARRIERS:

$$H + O_2 \rightleftharpoons OH + O$$
$$O + H_2 \rightleftharpoons OH + H$$
$$OH + H_2 \rightleftharpoons H_2O + H$$
$$H_2O + O \rightleftharpoons OH + OH$$

RECOMBINATION ZONE

$$O + O + M \rightarrow O_2 + M$$
$$H + OH + M \rightarrow H_2O + M$$

CS-53242

Figure VII-5. - Combustion scheme for methane with excess oxygen.

PRIMARY ZONE:

MAIN ATTACK ON CH_4:

$$H + CH_4 \rightarrow CH_3 + H_2$$

ATTACK ON CH_3:

$$CH_3 + O \rightsquigarrow CO$$

SECONDARY ZONE:

NO CHANGE

RECOMBINATION ZONE:

$$H + H + M \rightarrow H_2 + M$$

CS-53243

Figure VII-6. - Changes in combustion scheme for methane with excess methane.

$$C_nH_{2n+2} + OH \rightarrow C_nH_{2n+1} + H_2O$$

$$\downarrow$$

$$C_{n-1}H_{2n-2} + CH_3$$

$$O \swarrow \text{(FAST)} \quad \downarrow O_2$$

$$CO \qquad OCH_2 + OH$$

EVIDENCE:

ONLY FORMALDEHYDE, OCH_2, FOUND IN FLAMES

CS-53232

Figure VII-7. - Behavior of heavier hydrocarbons with excess oxygen.

1. CHAIN-BRANCHING AND ATTACK ON O_2: $H + O_2 \rightarrow OH + O$

2. ATTACK ON FUEL: $C_nH_{2n+2} + OH \rightarrow C_nH_{2n+1} + H_2O$
$C_nH_{2n+2} + H \rightarrow C_nH_{2n+1} + H_2$

3. OTHER CHAIN-BRANCHING REACTIONS: $O + H_2 \rightarrow OH + H$
$OH + H_2 \rightarrow H_2O + H$
$OCH_2 + O \rightarrow HCO + OH$
$O + H_2O \rightarrow OH + OH$

4. CONVERSION OF CO: $CO + OH \rightarrow CO_2 + H$

5. RECOMBINATION: $O + O + M \rightarrow O_2 + M$
$H + OH + M \rightarrow H_2O + M$
$H + H + M \rightarrow H_2 + M$

CS-53235

Figure VII-8. - Summary of important combustion reactions.

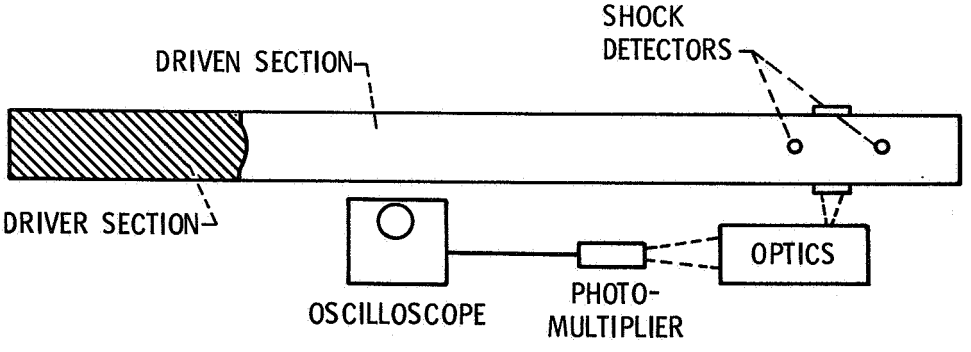

CS-53240

Figure VII-9. - Shock tube for rate measurements.

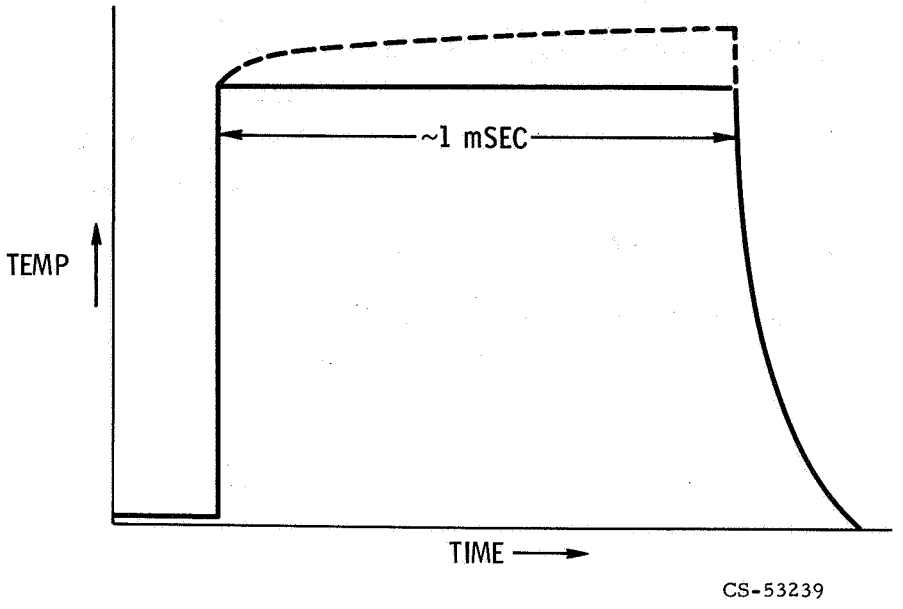

Figure VII-10. - Temperature history in a shock wave.

VIII. RATE CONSTANTS FROM IGNITION STUDIES OF THE H_2-CO-O_2 SYSTEM

Theodore A. Brabbs, Frank E. Belles, and Richard S. Brokaw

When a mixture containing hydrogen, carbon monoxide, and oxygen is subjected to a temperature and pressure pulse in a shock tube, small concentrations of atoms and free radicals are first formed by processes such as

$$CO + O_2 \rightarrow CO_2 + O$$

These concentrations may then grow exponentially by way of the well-known branched chain scheme

$$OH + H_2 \xrightarrow{k_1} H_2O + H \qquad \text{(I)}$$

$$H + O_2 \xrightarrow{k_2} OH + O \qquad \text{(II)}$$

$$O + H_2 \xrightarrow{k_3} OH + H \qquad \text{(III)}$$

$$H + O_2 + M \xrightarrow{k_4} HO_2 + M \qquad \text{(IV)}$$

$$OH + CO \xrightarrow{k_5} CO_2 + H \qquad \text{(V)}$$

Theory shows (refs. 1 and 2) that the oxygen atom concentration increases as $[O] \cong A \exp \lambda t$ (except very early in the reaction), where λ is the positive root of the cubic equation

$$\lambda^3 + (\nu_1 + \nu_2 + \nu_3 + \nu_4 + \nu_5)\lambda^2 + \left[(\nu_1 + \nu_5)(\nu_3 + \nu_4) + \nu_3\nu_4\right]\lambda - \nu_3(\nu_1 + \nu_5)(2\nu_2 - \nu_4) = 0 \qquad (1)$$

Here $\nu_1 \equiv k_1[H_2]$, $\nu_2 \equiv k_2[O_2]$, $\nu_3 \equiv k_3[H_2]$, $\nu_4 \equiv k_4[O_2][M]$, and $\nu_5 \equiv k_5[CO]$. Thus the exponential growth constant λ depends on the gas composition and the rate constants of reactions I to V. This paper reports measurements on mixtures chosen to permit determinations of the rates of reactions I, II, III, and V. Mixtures were selected by analyzing equation (1).

EXPERIMENTAL ASPECTS

Growth constants were obtained by measuring the blue carbon monoxide flame band emission behind incident shocks. The intensity of this radiation is proportional to the product of carbon monoxide and oxygen atom concentrations (ref. 3), and since very little carbon monoxide is consumed, the light monitors the increase of oxygen atom concentration with time.

Gas mixtures contained varying amounts of hydrogen, carbon monoxide, oxygen and in some mixtures carbon dioxide, diluted five to tenfold with argon. Hydrogen, oxygen, and argon were high purity tank gases and were used without further purification. Carbon monoxide was condensed at liquid nitrogen temperature; about one-quarter of the condensate was pumped off and discarded. Dry ice served as a convenient source of carbon dioxide. It was purified by subliming three-quarters of a sample into a liquid nitrogen cooled trap. The first quarter of this trapped fraction was discarded and the middle half used for mixture preparation.

Recently we showed that boundary layer effects must be considered in analyzing data obtained behind incident shocks; the growing boundary layer causes increases in temperature, density, and residence time with increasing distance behind the shock. Conditions behind the shocks, in the region of the experimental measurements, were obtained from a computer program which integrated the equations of chemical change for a shocked gas accounting for the effects of boundary layer buildup. In general, the extent of chemical reaction was small, and changes in gas properties were brought about largely by the gas dynamics associated with boundary layer growth.

Exponential growth constants were obtained from plots of the logarithm of observed light intensity against gas time; the relation between gas and laboratory times was obtained from the computer calculations.

SELECTION OF GAS MIXTURES

Let us turn now to the rationale used to select gas mixtures by analysis of

equation (1). To begin with, under our experimental conditions ν_4 is generally small in comparison with the other ν's and can be neglected for purposes of a qualitative discussion. Secondly, λ turns out to be a small positive root - of the order of the smaller ν values and small compared with the larger ν values. Thus, we neglect λ^3 in comparison with the other terms and rewrite equation (1):

$$\left[(\nu_1 + \nu_5) + \nu_2 + \nu_3\right]\lambda^2 + \nu_3(\nu_1 + \nu_5)\lambda \cong 2\nu_2\nu_3(\nu_1 + \nu_5) \tag{2}$$

If the amount of hydrogen in a mixture is large in comparison to oxygen, ν_1 and ν_3 are large and the term involving λ^2 may be neglected; in this event,

$$\lambda \cong 2\nu_2 \tag{3}$$

On the other hand, if only a trace of hydrogen is present, ν_3 is small, the term involving λ may be neglected, and

$$\lambda^2 \simeq \frac{2\nu_2\nu_3(\nu_1 + \nu_5)}{\nu_2 + (\nu_1 + \nu_5)} \tag{4}$$

If we choose a mixture with a large amount of carbon monoxide, ν_5 is large and

$$\lambda \sim \sqrt{2\nu_2\nu_3} \tag{5}$$

Whereas if there is a large amount of oxygen, ν_2 is large and

$$\left.\begin{aligned} \lambda &\sim \sqrt{2\nu_3(\nu_1 + \nu_5)} \\ &\to \sqrt{2\nu_3\nu_1} \qquad [H_2] > [CO] \\ &\to \sqrt{2\nu_3\nu_5} \qquad [CO] > [H_2] \end{aligned}\right\} \tag{6}$$

This, then, outlines a strategy for obtaining rates of reations I, II, III, and V. First, a mixture rich in hydrogen is used to determine k_2. Next, with k_2 known, a mixture with a trace of hydrogen and rich in carbon monoxide is used to determine k_3. Finally, with k_3 known, mixtures with excess oxygen and varying pro-

portions of hydrogen and carbon monoxide are used to isolate k_1 and k_5.

The foregoing discussion indicates a qualitative procedure for selecting gas mixtures. However, we also need a quantitative measure of the sensitivity of the growth constant for a particular mixture to the various rate constants. For example, we know that to isolate k_3 we want a mixture with a trace of hydrogen, a small amount of oxygen, and carbon monoxide in excess. But for a candidate composition, is the hydrogen concentration small enough, and is carbon monoxide sufficently in excess? A quantitative measure of the sensitivity to the various rates can be obtained by logarithmic partial differention of equation (1). For example,

$$\left(\frac{\partial \ln \lambda}{\partial \ln \nu_3}\right) = \frac{1}{2} - \frac{1}{2}\,\frac{\lambda^2 + 2\nu_3\lambda + (\nu_1 + \nu_5)(\nu_3 - \nu_4) + \nu_3\nu_4}{3\lambda^2 + 2(\nu_1 + \nu_2 + \nu_3 + \nu_4 + \nu_5)\lambda + (\nu_1 + \nu_5)(\nu_3 + \nu_4) + \nu_3\nu_4} \tag{7}$$

Equation (7) shows the growth constant will depend on something less than the square root of ν_3 - a somewhat weaker dependence than that suggested by equation (5).

The mixture compositions selected are shown in table VIII-1 along with sensitivities calculated for a pressure of 1 atmosphere and temperatures near the midpoints of the ranges of the experimental data. These mixtures were chosen on the basis of (1) high sensitivity to the rate constant being determined, (2) minimized sensitivity to the other rate constants, (3) growth constant in a convenient range for measurement (5×10^3 to 7×10^4 sec^{-1}), and (4) sufficient content of minor rate limiting constituents to permit accurate mixture preparation.

It was necessary to include in each mixture sufficient infrared-active gas so that the arrival of the contact surface could be detected by the cessation of infrared emission. (The position of the contact surface between driver and driven gas is needed in the boundary layer analysis.) Mixtures 2, 3, and 5 have substantial carbon monoxide concentrations; carbon dioxide was added to mixture 1 to achieve adequate infrared activity. Carbon dioxide was also added to mixtures 3 and 5 to ensure vibrational relaxation of the carbon monoxide. (In preliminary experiments on a composition similar to mixture 3, but without carbon dioxide, carbon monoxide was not relaxed and rate constants gave an activation energy of 15 kilocalories for reaction III, much higher than literature values (ref. 4). Results from mixture 3, with added carbon dioxide, show that the preliminary data were too low, particularly at the lower temperatures.)

CALCULATION OF RATE CONSTANTS FROM EXPONENTIAL GROWTH CONSTANTS

Rate constants were obtained from the experimental growth constants by means of equation (1), which was rearranged and solved for the rate constant being sought from the mixture in question - k_2 from mixture 2, k_3 from mixture 3, etc. Mixture 2 was studied first because the growth constants for this mixture depend almost exclusively on k_2 and are only slightly affected by the rates of the other reactions (see table VIII-1). Values of ν_4 were calculated from the k_4 suggested by the Leeds group (ref. 5). Trial values of k_1, k_3, and k_5 were also taken from the Leeds recommendations (refs. 4 to 6), but final values were taken from our own determinations. This involves an interative procedure, since our values of k_3 depend, in turn, on our values k_2, and to a lesser extent k_5. Two iterations sufficed to establish k_2.

Next k_3 was obtained by analyzing the growth constants for mixture 3, then k_1 from mixture 1, and finally k_5 from mixture 5. Three iterations around the k_3-k_1-k_5 loop were required.

A least squares fit to the Arrhenius equation was made for each set of rate constants; these equations were then used in subsequent calculations.

RESULTS AND DISCUSSION

The experimental results will be discussed in the order in which the data were obtained - first k_2, followed by k_3, k_1, and k_5. This order is also, approximately, the order of decreasing precision.

Rate constants for reaction II are plotted against reciprocal temperature in figure VIII-1. The least squares line through the data is

$$k_2 = 1.25\times10^{14} \exp\left(\frac{-16.3 \text{ kcal}}{RT}\right) \text{cm}^3 \text{ mole}^{-1} \text{ sec}^{-1} \qquad (8)$$

The standard deviation (ref. 7) of $\ln k_2$ is ± 0.094, or about 10 percent; the standard deviation (ref. 7) of the activation energy is 1.1 kilocalories. Rates given by equation (8) fall somewhat below most previous high temperature ($T >$ 1000 K) determinations and as a consequence lie about 30 percent below the recommendation of the Leeds group (ref. 5), but well within their suggested error limit of ± 50 percent. The activation energy of 16.3 kilocalories is

slightly more than the endothermicity of reaction II (16.15 kcal at 1300 K) in contrast to several other recent shock tube studies (refs. 5 and 7) which have yielded substantially lower activation energies. Indeed, equation (8) extrapolated to room temperature predicts rate constants which are straddled by the discordant results of Clyne and Thrust (ref. 9) and Kaufman and Del Greco (ref. 10) (see fig. VIII-2).

It should be emphasized that these satisfying results are obtained only when the effects of boundary layer growth are considered. If we ignore the boundary layer by using the temperature and pressure immediately behind the shock in the data reduction, rate constants for reaction II are 20 to 60 percent larger with an apparent activation energy of only 11.9 kilocalories. This is shown as a dashed line in figure VIII-1. The data without boundary layer corrections extrapolated to room temperature are too high by about two orders of magnitude, as shown by the dashed line in figure VIII-2.

Rate constants for reaction III are plotted in figure VIII-3. The least squares line through the data is

$$k_3 = 2.96\times10^{13} \exp\left(\frac{-9.8 \text{ kcal}}{RT}\right) \text{cm}^3 \text{ mole}^{-1} \text{ sec}^{-1} \qquad (9)$$

The standard deviation of $\ln k_3$ is ± 0.184, or about 20 percent; the standard deviation of the activation energy is 1.3 kilocalories. It is to be expected that errors in k_3 are roughly double those for k_2, since for mixture 3 the growth constants depend on the 0.4 power of k_3, whereas for mixture 2 the growth constants are very nearly proportional to k_2 (see sensitivities in table VIII-1).

Rates calculated from equation (9) fall among other high temperature determinations (ref. 4); they are about 50 percent above the Leeds recommendation (ref. 4) which is somewhat outside their suggested error limit of ±30 percent. (The Leeds recommendation appears to be based almost entirely on data from temperatures below 900 K.) On the other hand, equation (9) is only about 10 percent above an extrapolation of the more recent data of Westenberg and de Haas (ref. 11). The activation energy of 9.8 kilocalories appears reasonable since it lies between the recommendations of the Leeds group (9.45 kcal) and Westenberg and de Haas (10.2 kcal). As a consequence, equation (9) extrapolated to much lower temperatures predicts rate constants generally in accord with other experiments (ref. 4). Such an extrapolation is shown in figure VIII-4, which includes the data of Westenberg and de Haas (ref. 11).

Rate constants for reaction I are plotted against reciprocal temperature in figure VIII-5. The solid least squares line through the data is

$$k_1 = 1.9\times10^{13} \exp\left(\frac{-4.8 \text{ kcal}}{RT}\right) \text{cm}^3 \text{ mole}^{-1} \text{ sec}^{-1} \quad (10)$$

The standard deviation of $\ln k_1$ is ± 0.41, or about 40 percent; the standard deviation of the activation energy is 1.7 kilocalories.

In the temperature range of the experimental data, 1100 to 1600 K, equation (10) is in near-perfect accord with the Leeds recommendation (ref. 4). The activation energy is somewhat lower than the 5.15 kilocalories suggested by Leeds, so that equation (10) extrapolated to room temperature predicts rate constants about 50 percent too high; this extrapolation is shown in figure VIII-6. This can be rectified by including in the least squares analysis a recent value of $k_1 = 4.1\times10^9$ at 300 K due to Greiner (ref. 12). This gives

$$k_1 = 2.1\times10^{13} \exp\left(\frac{-5.1 \text{ kcal}}{RT}\right) \text{cm}^3 \text{ mole}^{-1} \text{ sec}^{-1} \quad (11)$$

The standard deviation of $\ln k_1$ remains ± 0.41, but the standard deviation of the activation energy is reduced to 0.3 kilocalorie. Equation (11) is shown as dashed lines in figures VIII-5 and VIII-6. Equations (10) and (11) differ by less than 4 percent in the experimental temperature range.

Rate constants for reaction V are plotted in figure VIII-5. The solid least squares line through the data is

$$k_5 = 1.0\times10^{12} \exp\left(\frac{-3.7 \text{ kcal}}{RT}\right) \text{cm}^3 \text{ mole}^{-1} \text{ sec}^{-1} \quad (12)$$

The standard deviation of $\ln k_5$ is ± 0.28, or about 30 percent; the standard deviation of the activation energy is 1.9 kilocalories. For the temperature range of 1300 to 1900 K, equation (12) gives rate constants 10 to 35 percent below the Leeds recommendation (ref. 6). The 3.7-kilocalorie activation energy is almost certainly too large; recent low temperature studies (refs. 12 and 13) suggest 0.2 to 1.0 kilocalories. As a consequence equation (12) extrapolated to room temperature predicts a rate two orders of magnitude smaller than Greiner (ref. 13) recent 300 K value of $k_5 = 8.6\times10^{10}$ (see fig. VIII-6). By including Greiner's datum in the least squares analysis we obtain

$$k_5 = 4.2\times10^{11} \exp\left(\frac{-1.0 \text{ kcal}}{RT}\right) \text{cm}^3 \text{ mole}^{-1} \text{ sec}^{-1} \quad (13)$$

The standard deviation of ln k_5 remains about the same, ±0.29, but the standard deviation of the activation energy is only 0.2 kilocalorie. Equation (13) is shown as dashed lines in figures VIII-5 and VIII-6. To the eye, equation (13) seems almost as good a representation of the data as equation (12). In the experimental temperature range equations (12) and (13) differ by at most 15 percent. Thus, equation (13) seems preferable.

CONCLUDING REMARKS

In this paper we have shown how to make systematic measurements so as to isolate the rates of individual bimolecular reaction steps in the complex of six reactions which describe the ignition behavior of the hydrogen - carbon monoxide - oxygen system.

We have obtained what we believe are quite accurate measurements of the rates of the reactions $H + O_2 \rightarrow OH + O$ and $O + H_2 \rightarrow OH + H$. An essential has been a proper accounting of the effects of boundary layer growth on the pressure, temperature, and residence time behind the shock wave. Our measurements of the rates of $OH + H_2 \rightarrow H_2O + H$ and $OH + CO \rightarrow CO_2 + H$ are less precise but are perhaps the most direct determinations of these rates for temperatures above 1100 K (previous high temperature determinations of these rates have been based on flame sampling).

REFERENCES

1. Brokaw, Richard S.: Analytic Solutions to the Ignition Kinetics of the Hydrogen-Oxygen Reaction. Tenth Symposium (International) on Combustion. Combustion Inst., 1965, pp. 269-278.

2. Brokaw, Richard S.: Ignition Kinetics of the Carbon Monoxide-Oxygen Reaction. Eleventh Symposium (International) on Combustion. Combustion Inst., 1967, pp. 1063-1073.

3. Clyne, M. A. A.; and Thrush, B. A.: Mechanism of Chemiluminescent Combination Reactions Involving Oxygen Atoms. Proc. Roy. Soc. (London), ser. A, vol. 269, no. 1338, Sept. 25, 1962, pp. 404-418.

4. Baulch, D. L.; Drysdale, D. D.; and Lloyd, A. C.: Critical Evaluation of Rate Data for Homogeneous, Gas-Phase Reactions of Interest in High-Temperature Systems. Rep. 2, Dept. Phys. Chem., Leeds Univ., Nov. 1968.

5. Baulch, D. L.; Drysdale, D. D.; and Lloyd, A. C.: Critical Evaluation of Rate Data for Homogeneous, Gas-Phase Reactions of Interest in High-Temperature Systems. Rep. 3, Dept. Phys. Chem., Leeds Univ., Apr. 1969.

6. Baulch, D. L.; Drysdale, D. D.; and Lloyd, A. C.: High Temperature Reaction Rate Data. Rep. 1, Dept. Phys. Chem., Leeds Univ., May 1968.

7. Youden, William J.: Statistical Methods for Chemists. John Wiley & Sons, Inc., 1951, p. 42.

8. Schott, G. L.: Chain-Branching and Initiation Rates Measured by Spatially Integrated Light Emission During Reflected Shock-Wave Ignition. Twelfth Symposium (International) on Combustion. Combustion Inst., 1969, pp. 569-578.

9. Clyne, M. A. A.; and Thrush, B. A.: Rates of Elementary Processes in the Chain Reaction Between Hydrogen and Oxygen. I. Reactions of Oxygen Atoms. Proc. Roy. Soc. (London), ser. A, vol. 275, no. 1363, Oct. 29, 1963, pp. 544-558.

10. Kaufman, F.; and Del Greco, F. P.: Fast Reactions of OH Radicals. Ninth Symposium (International) on Combustion. W. G. Berl, ed., Academic Press, 1963, pp. 659-668.

11. Westenberg, A. A.; and deHaas, N.: Reinvestigation of the Rate Coefficients for $O+H_2$ and $O+CH_4$. J. Chem. Phys., vol. 50, no. 6, Mar. 15, 1969, pp. 2512-2516.

12. Greiner, N. R.: Hydroxyl Radical Kinetics by Kinetic Spectroscopy. V. Reactions with H_2 and CO in the Range 300 - 500 K. J. Chem. Phys., vol. 51, no. 11, Dec. 1, 1969, pp. 5049-5051.

13. Wong, Edgar L.; and Belles, Frank E.: Activation Energies for Reactions of Hydroxl Radicals with Hydrogen and Carbon Monoxide. NASA TN D-5707, 1970.

TABLE VIII-1. - MIXTURE COMPOSITIONS AND GROWTH CONSTANT SENSITIVITIES

	Mixture			
	1	2	3	5
	Reaction			
	$OH + H_2 \rightarrow$	$H + O_2 \rightarrow$	$O + H_2 \rightarrow$	$OH + CO \rightarrow$
Mixture composition, percent				
H_2	0.21	5	0.1046	0.1035
CO	.11	6	10.0	6.01
O_2	10.0	0.5	0.503	10.0
CO_2	5.0	----	4.99	5.0
Growth constant sensitivities				
$\partial \ln \lambda / \partial \ln \nu_1$	0.34	0.01	0.0	0.07
$\partial \ln \lambda / \partial \ln \nu_2$	.33	1.00	.64	.21
$\partial \ln \lambda / \partial \ln \nu_3$	.48	.06	.39	.49
$\partial \ln \lambda / \partial \ln \nu_4$	-.17	-.07	-.06	-.06
$\partial \ln \lambda / \partial \ln \nu_5$	.02	.00	.04	.29

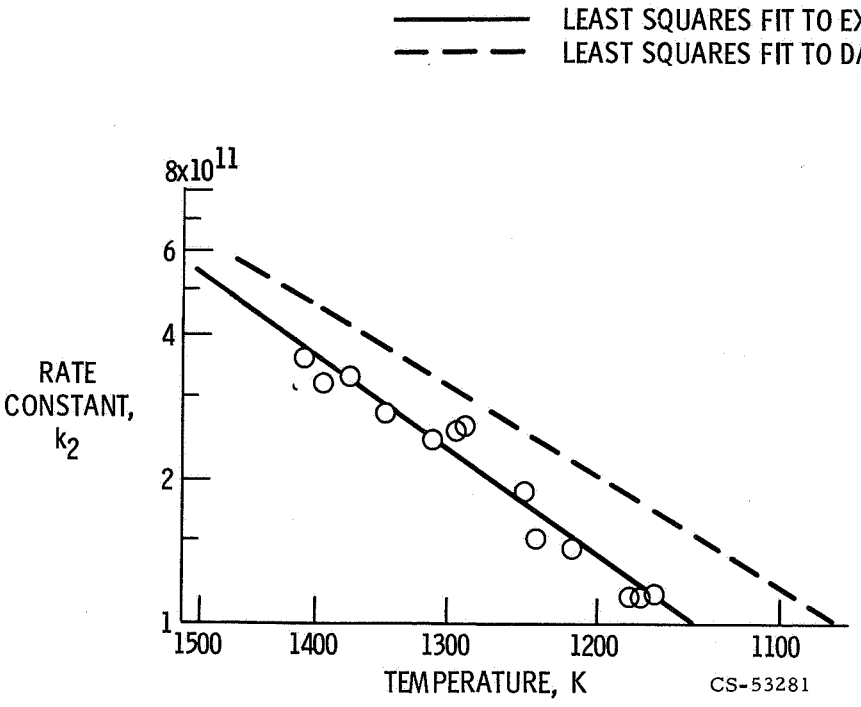

Figure VIII-1. - Rate constants for reaction II, $H + O_2 \rightarrow O + OH$.

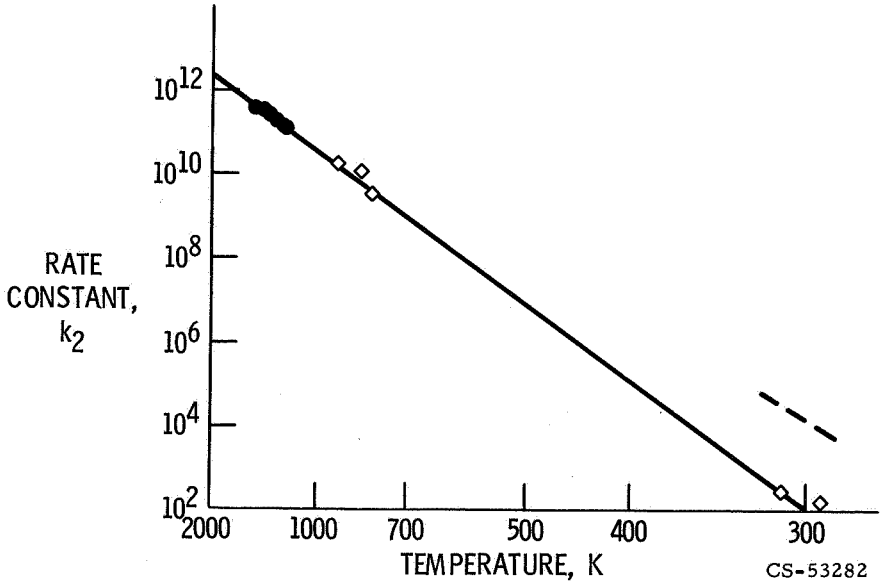

Figure VIII-2. - Rate constants for reaction II compared with low temperature data.

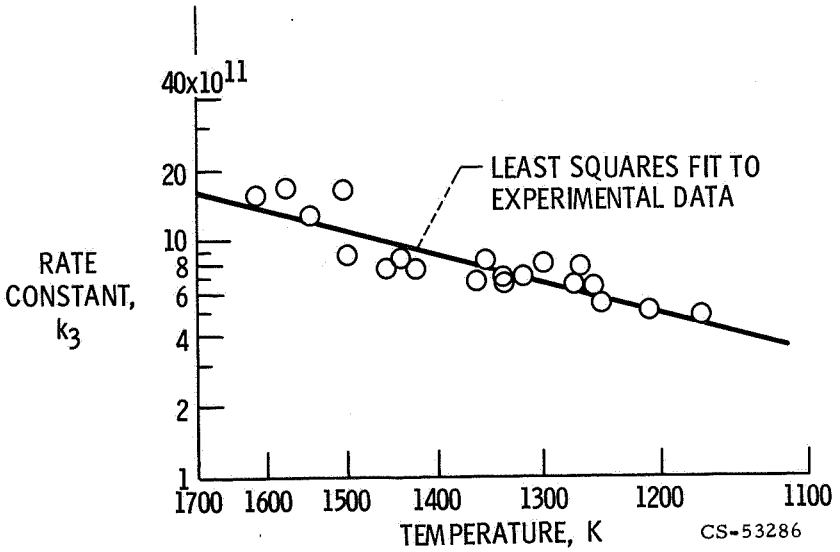

Figure VIII-3. - Rate constants for reaction III, $O + H_2 \rightarrow OH + H$.

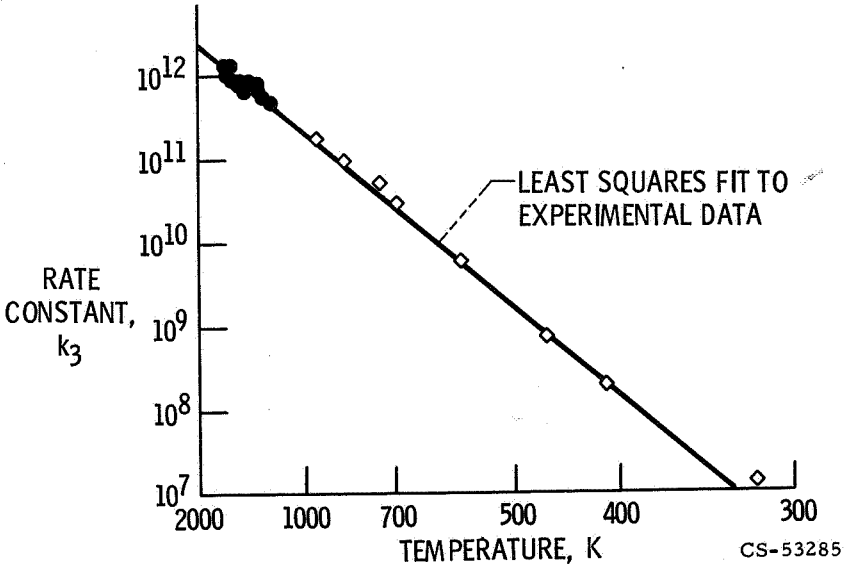

Figure VIII-4. - Rate constants for reaction III compared with low temperature data.

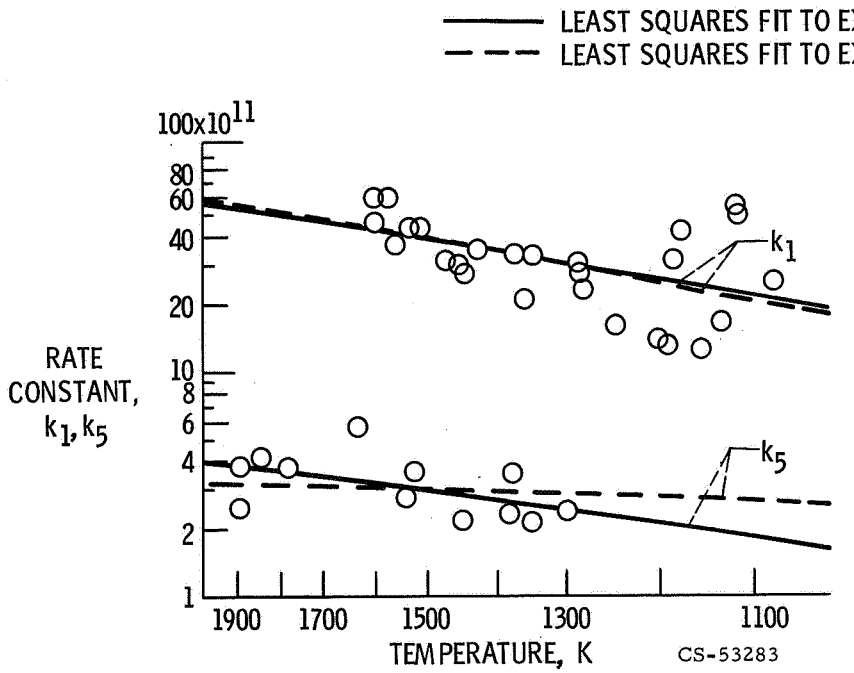

Figure VIII-5. - Rate constants for reaction I, $OH + H_2 \rightarrow H_2O + H$, and reaction V, $OH + CO \rightarrow CO_2 + H$.

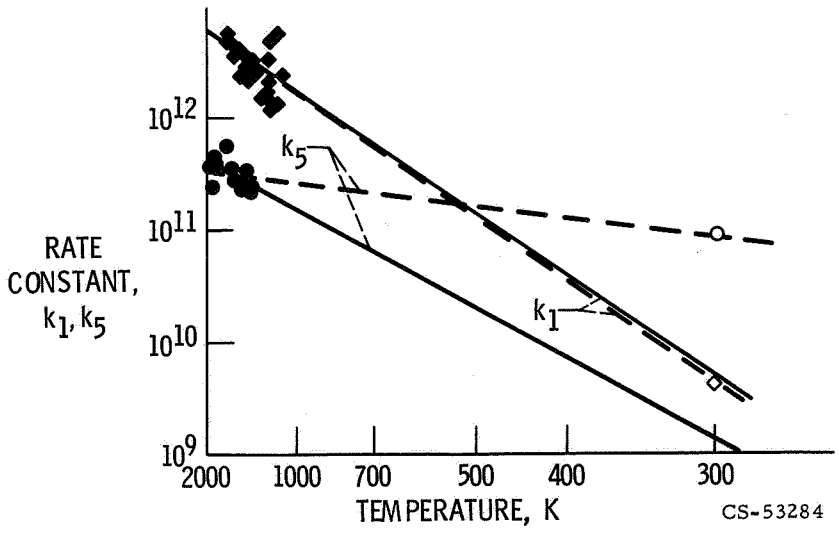

Figure VIII-6. - Rate constants for reactions I and V compared with low temperature data.

IX. KINETICS OF THE DISSOCIATION OF BROMINE

Marvin Warshay

The development of the modern shock-tube technique has enabled chemical kineticists to conduct quite a number of fruitful investigations. Over the last dozen years, the shock-tube method has been of special value for measuring the rates of dissociation of diatomic molecules. These experimental results have heightened interest in the theory of dissociation-recombination. A number of theoretical models have been proposed which attempt to describe the mechanism of dissociation and recombination, or in other words to understand the reactions from a microscopic-molecular viewpoint.

However, proper evaluation of these models and further progress in these areas have been hampered by two problems: (1) Insufficient data are available. (2) Shock-tube measurements of rate constants have often been imprecise. This second problem is illustrated in figure IX-1. This Arrhenius plot includes data from several early shock-tube investigations of bromine (Br_2) dissociation in argon (Ar).

First, as shown in figure IX-1, the data are scattered. Second, there is a lack of close agreement among the investigators. One illustration of the latter aspect of the problem is the 40-percent difference between the dotted and the solid lines. These curves represent the results of two experiments made by the same principal investigator in the same laboratory only a few years apart (see refs. 1 and 2).

The present investigator has measured the dissociation rates of Br_2 in the presence of high concentrations of noble gases. The experimental effort has achieved two aims: (1) improvement in the reliability of the shock-tube results, and (2) broadening the scope of the investigation of Br_2 dissociation.

Improvement in the Br_2 results was achieved by plain struggle coupled with great attention to experimental details. Avoidance of bromine-metal contact, design of a stable photomultiplier, and achieving a stable light source beam were essential features of this effort. The present work, of course, relied heavily on the pioneering Br_2 investigations. Those by Palmer and Hornig (ref. 3) and Britton and Davidson (ref. 4) were of particular value.

This is the first investigation of Br_2 (or any diatom for that matter) in the presence of all five nonradioactive noble gases. In conducting the experiments

with helium (He) through xenon (Xe), the mass range 4 to 131 was covered.

Bromine dissociation was selected for theoretical interest - not for direct commercial or space applications. Reliable experimental measurements of Br_2 dissociation help further our general understanding of diatomic dissociation-recombination. In the case of theoretical models, establishing in what ways a model successfully predicts the rates of the elementary case (diatomic, for example) aids in the development of models which will be able to accurately predict the more complex case.

Studying the dissociation in the presence of high concentrations of five noble gases provides useful information on the influence of the collision partner in the dissociation reaction. Similar experimental studies have been reported in the literature on halogen recombination. Most of these studies were performed at room temperature. Recently, Ip and Burns (ref. 5) extended the recombination measurements to higher temperatures.

Collision-partner efficiencies in dissociation and recombination have been predicted by several theoretical models. These predictions are examined later.

Bromine, in many respects, is a convenient substance to work with. It is homonuclear; consequently, complicating side reactions are avoided. Also, it dissociates at relatively low temperatures, and it absorbs light strongly in the visible region, which provides a good means of following the course of reaction.

RESULTS

The Br_2 - noble gas mixture results are plotted in figures IX-2 to IX-6. The scatter of the data is much lower than that of the past investigations (see fig. IX-1). In these Arrhenius coordinates the data for all five mixtures display linear trends and are correlated quite well by the simple collisional form of the rate constant equation $AT^{1/2}e^{-Ea/RT}$.

After correcting the data for boundary layer buildup in the shock tube and for the contribution to dissociation due to Br_2-Br_2 collisions, the following rate constant equations were obtained:

$$k_{D,He} = 2.15\times10^{8}\ T^{1/2} \exp\left(\frac{-31.9\ \text{kcal/mole}}{RT}\right) \quad \text{liters/mole-sec}$$

$$k_{D,Ne} = 1.04\times10^{8}\ T^{1/2} \exp\left(\frac{-29.1\ \text{kcal/mole}}{RT}\right) \quad \text{liters/mole-sec}$$

$$k_{D,Ar} = 2.14\times10^{8}\ T^{1/2} \exp\left(\frac{-31.3\ \text{kcal/mole}}{RT}\right) \quad \text{liters/mole-sec}$$

$$k_{D,Kr} = 3.32\times10^{8}\ T^{1/2} \exp\left(\frac{-32.8\ \text{kcal/mole}}{RT}\right) \quad \text{liters/mole-sec}$$

$$k_{D,Xe} = 6.92\times10^{8}\ T^{1/2} \exp\left(\frac{-35.5\ \text{kcal/mole}}{RT}\right) \quad \text{liters/mole-sec}$$

The Br_2-Br_2 contribution was obtained by comparing the dissociation rate in a 3-percent Br_2 - 97-percent Xe mixture with the rate in the 1-percent Br_2 - 99-percent Xe mixture.

DESCRIPTION OF THEORETICAL MODELS

Our understanding of the apparently simple reaction, $A_2 \rightarrow A + A$, has progressed from the initial breakthrough of explaining how the unimolecular reaction gets its energy for dissociation, the Lindemann-Hishelwood mechanism:

$$A_2 + M \rightleftarrows A_2^* + M \quad \text{(activation)}$$

$$A_2^* \rightarrow A + A \quad \text{(reaction)}$$

$$A_2 + M \rightarrow A + A + M \quad \text{(overall)}$$

Today, there are many sophisticated descriptions of the collision mechanism, involving A_2 plus M, accompanied by mathematical predictions of the rate of dissociation or of the reverse process (the rate of recombination).

Various theoretical models have been proposed for dissociation-recombination. Some important examples are given in figure IX-7. The analysis was limited to those models with which calculations of absolute reaction rates could be made. Those models which expressed their rate constants in terms of unknown parameters could not be considered.

Two classical models were considered first. The nonadiabatic collision model of Nielsen and Bak can be thought of as hard spheres colliding. Collision of the molecule with a fast-moving atom transfers energy from the atom to the molecule,

energy necessary for dissociating the molecule.

In the adiabatic collision model of Light, the spheres are not hard. In fact, interaction between the atom and the molecule occurs while they are a considerable distance apart. Unless dissociation occurs during the rather long duration of collision, the molecule returns all of the energy that it got from the atom. In this case, there is no net energy transfer; that is, the process is adiabatic.

The third model is Bunker and Davidson's complex formation mechanism, which is a recombination model. In the first step the atom A reacts with the third body M to produce the complex AM^*, a species which has enough energy to redissociate. This excess energy is removed from the complex by another third body in the second step. Finally, the collision complex reacts with another atom to form the diatomic molecule A_2.

The energy transfer mechanism of Benson, Fueno, and Berend is also a recombination model. However, in this case no collision complex is formed. The first step consists of A plus A forming A_2^*, a highly energetic species which will redissociate unless it can give up some of its energy. It does this by transferring energy to third bodies in a series of steps. In their model, this transfer occurs essentially one quantum at a time (like one would normally descend the rungs of a ladder) until the ground state molecule is formed.

The theoretical treatment of Keck and Carrier reduces to equations which are analogous to thermal diffusion. They describe the rate at which A_2 plus M cross the phase space boundary to become the dissociated atoms A plus A.

EVALUATION OF MODELS

Now each of the theories claims to shed some light on the problems of (1) describing the mechanism of dissociation-recombination and of (2) being able to predict reaction rates. An important difficulty in evaluating the various theories is that developers of a theory seldom select that type of experiment result which will make their theory look bad. For example, if their theory predicts a negative temperature coefficient in recombination (a well-known characteristic of recombination), then they will use the "ability to predict negative temperature coefficient in recombination" as the criterion of "goodness of prediction". Other criteria will receive minimum attention or be ignored completely. This is human nature.

The experimental Br_2 dissociation results presented in this paper have been used as the basis for an evaluation of the five previously discussed theoretical models. Three models are essentially dissociation models (Nielson and Bak,

Light, and Keck and Carrier), while two are essentially recombination models (Bunker and Davidson, and Benson, Fueno, and Berend). All five models are compared as to how well they (1) predict the measured dissociation rate constants, (2) predict the effect of temperature on the rate constants, that is, the activation energy, and (3) predict the efficiencies of the noble gas collision partners.

We will soon discover that no model excels in all three of these categories of evaluation. The next few figures illustrate this threefold evaluation.

Figure IX-8 is a comparison of the experimental rate constant line for the Br_2-Ar case with the predictions of the five models. To make the comparison easier, the experimental dissociation rate constants were converted to recombination rate constants by dividing by the equilibrium constant at the proper temperatures. This is an application of the law of microscopic reversibility or detailed balancing as it is also known.

Four of the predictions come within an order of magnitude of the experimental result. The Keck-Carrier prediction overshoots by more than an order of magnitude.[1] However, one obvious flaw which all five models have is the inability to match the experimental slope, the temperature coefficient, which is related to the activation energy of the dissociation reaction. There is a growing body of experimental support for the activation energy not being equal to the dissociation energy. This has been found to be the case in polyatomic as well as in diatomic dissociation.

An indication of the relative efficiencies of the noble gas collision partners in Br_2 dissociation can be gained from figure IX-9. Here all five experimental lines, corresponding to equations (1) to (5), are plotted. The lines fan out at the low temperature end and tend to converge and cross at higher temperatures. It could be said that as a rough first-order statement there are no great differences among the efficiencies of the five noble gases - that is, nothing like an order of magnitude difference.

---

[1] During the discussion following the presentation of this paper, Professor John P. Appleton (M.I.T) reported that the Keck-Carrier paper contained errors which were responsible for its prediction of the Br_2 dissociation rates being much too high. He reported further that correcting these errors brought the prediction as close to experiment as the predictions of the other four models. Subsequently, in a letter, Professor Appleton states that the Keck-Carrier paper contained two errors. The first error was algebraic in nature (see footnote (17) in ref. 12). The second error was not including the additional statistical correction factor which accounts for recrossings of the phase space boundary (see ref. 13). This new calculation of Br_2 dissociation rates in the presence of Ar is soon to be published in a detailed paper by Ven H. Shui, John P. Appleton, and James C. Keck.

The bar graph in figure IX-10 compares the predicted against experimental efficiencies of the noble gas collision partners. The comparison is at 1500 K, a midrange temperature. The solid bars represent the predicted relative efficiencies, while the open bars are the experimental efficiencies. Efficiency is expressed as a ratio of rate constants. For ease of comparison with each model, the experimental efficiency bars are repeated all the way across.

The best prediction is by the Keck-Carrier model - the worst by the Bunker and Davidson model. The Bunker and Davidson model predicts a marked mass effect, very small for the lightest noble gas, He, and very large for the heaviest noble gas, Xe. This is obviously not the case.

The other three models rank somewhere in between these two extremes. If it were not for He, Light's model would rank higher. In fairness, it ought to be said that in his published paper Light stated that the adiabatic assumption probably does not apply to He.

SUMMARY AND CONCLUSIONS

An investigation of the dissociation rates of Br_2 in the presence of all five noble gases has been carried out. The experimental shock tube results were sufficiently precise to use as a basis for evaluating five recent theoretical dissociation-recombination models. The general conclusions are as follows:

1. All predictions of the absolute rate constants, except for the Keck-Carrier model, were within an order of magnitude of the experimental rate.

2. One common flaw which all five models had was predicting the wrong temperature coefficient of k_D, that is, the activation energy. In every case, the predicted activation energy for dissociation was higher than the experimental value.

3. Since the measured relative efficiencies of the five noble gases did not vary to a great extent, the model which predicted no variation, the Keck-Carrier model, came closest. Models such as those of Bunker and Davidson, which predicted a marked collision partner effect related to mass, were very far off.

Certainly diatomic collisions with inert atoms are not the whole story of dissociation-recombination. However, these results and the analysis made with them should aid the development of theoretical models and lead to a better understanding of dissociation and recombination.

REFERENCES

1. Britton, Doyle: Shock Waves in Chemical Kinetics: Further Studies in the Rate of Dissociation of Bromine. J. Phys. Chem., vol. 64, no. 6, June 1960, pp. 742-748.

2. Johnson, Charles D.; and Britton, Doyle: Shock Waves in Chemical Kinetics: The Use of Reflected Shock Waves. J. Chem. Phys., vol. 38, no. 7, Apr. 1, 1963, pp. 1455-1462.

3. Palmer, H. B.; and Hornig, D. F.: Rate of Dissociation of Bromine in Shock Waves. J. Chem. Phys., vol. 26, no. 1, Jan. 1957, pp. 98-105.

4. Britton, Doyle; and Davidson, Norman: Shock Waves in Chemical Kinetics. Rate of Dissociation of Molecular Bromine. J. Chem. Phys., vol. 25, no. 5, Nov. 1956, pp. 810-813.

5. Ip, J. K. K.; and Burns, George: Recombination of Br Atoms by Flash Photolysis Over a Wide Temperature Range. II. Br_2 in He, Ne, Ar, Kr, N_2, and O_2. J. Chem. Phys., vol. 51, no. 8, Oct. 15, 1969, pp. 3414-3424.

6. Nielsen, Svend Erik; and Bak, Thor A.: Hard-Sphere Model for Dissociation of Diatomic Molecules. J. Chem. Phys., vol. 41, no. 3, Aug. 1, 1964, pp. 665-674.

7. Light, John C.: Dissociation of Gaseous Diatomic Molecules: Classical Adiabatic Scattering Approach. J. Chem. Phys., vol. 36, no. 4, Feb. 15, 1962, pp. 1016-1030.

8. Bunker, Don L.; and Davidson, Norman: On the Interpretation of Halogen Atom Recombination Rates. J. Am. Chem. Soc., vol. 80, no. 19, Oct. 5, 1958, pp. 5090-5096.

9. Benson, Sidney W.; and Fueno, Takayuki: Mechanism of Atom Recombination by Consecutive Vibrational Deactivations. J. Chem. Phys., vol. 36, no. 6, Mar. 15, 1962, pp. 1597-1607.

10. Benson, Sidney W.; and Berend, George C.: Vibrational Energy Exchange of Highly Excited Anharmonic Oscillators. J. Chem. Phys., vol. 40, no. 5, Mar. 1, 1964, pp. 1289-1298.

11. Keck, James; and Carrier, George: Diffusion Theory of Nonequilibrium Dissociation and Recombination. J. Chem. Phys., vol. 43, no. 7, Oct. 1, 1965, pp. 2284-2298.

12. Appleton, J. P.; Steinberg, M.; and Liquornik, D. J.: Shock-Tube Study of Nitrogen Dissociation using Vacuum-Ultraviolet Light Absorption. J. Chem. Phys., vol. 48, no. 2, Jan. 15, 1968, pp. 599-608.

13. Shui, Ven H.; Appleton, John P.; and Keck, James C.: The Dissociation and Recombination of Nitrogen; A Comparison Between Theory and Experiment. Publ. No. 70-2, Fluid Mech. Lab., Dept. Mech. Eng., Mass. Inst. Tech., Feb. 1970.

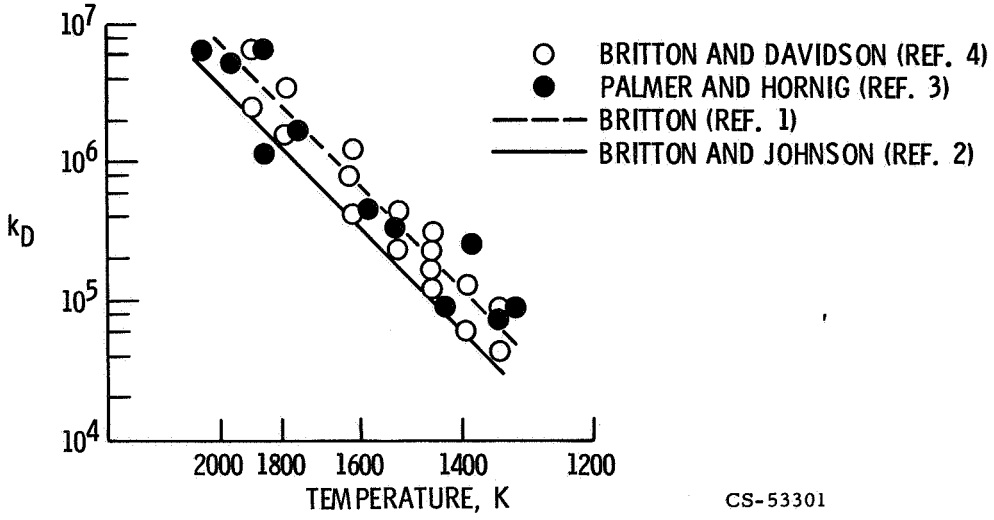

Figure IX-1. - Reported results (refs. 1 to 4) of bromine dissociation rate constant in presence of argon. The experimental mixtures varied from 1 to 10 percent Br_3. (Not all experimental data included for refs. 3 and 4.)

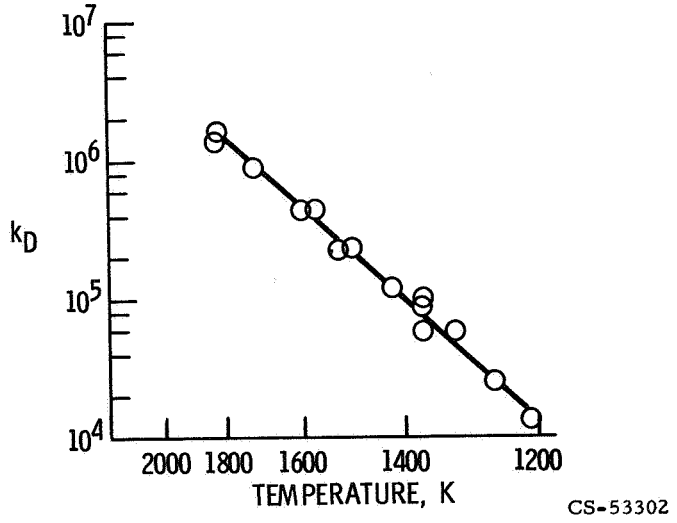

Figure IX-2. - NASA results of bromine dissociation rate constant in presence of argon (1 percent Br_2 - 99 percent Ar).

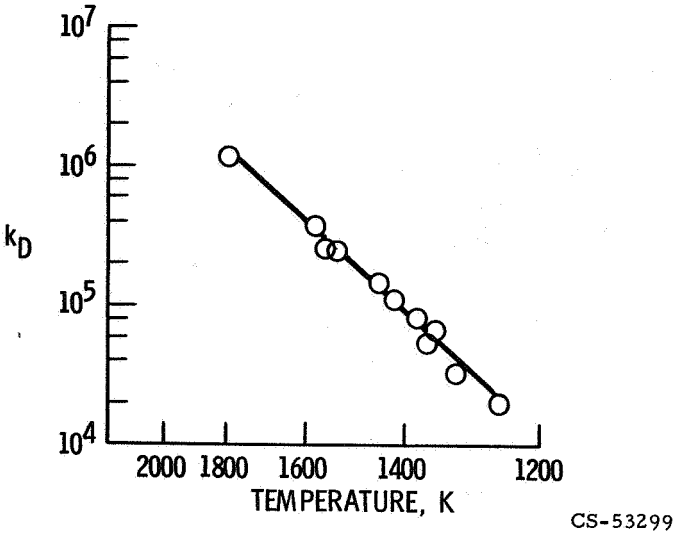

Figure IX-3. - Bromine dissociation rate constant in presence of neon (1 percent Br_2 - 99 percent Ne).

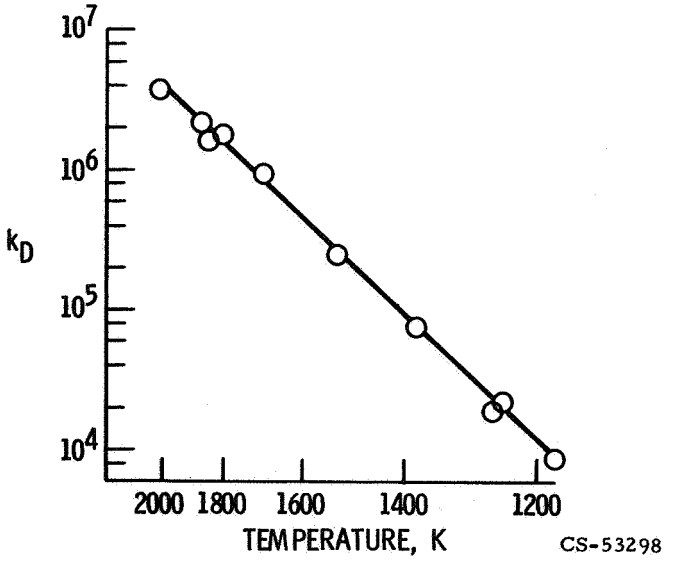

Figure IX-4. - Bromine dissociation rate constant in presence of krypton (1 percent Br_2 - 99 percent Kr).

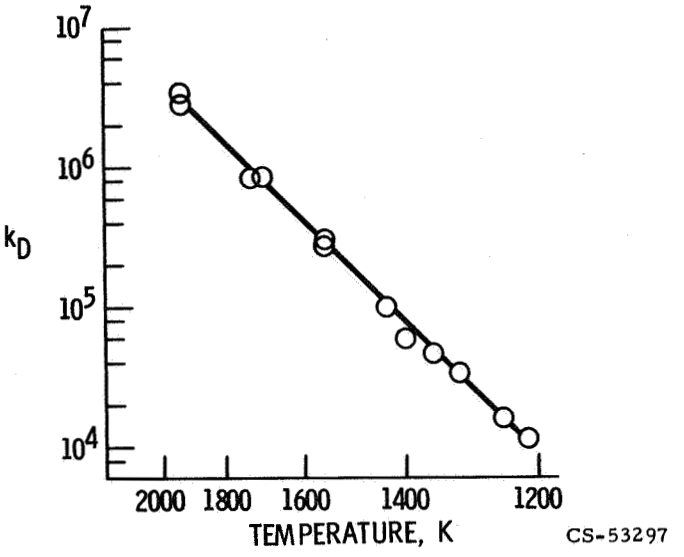

Figure IX-5. - Bromine dissociation rate constant in presence of xenon (1 percent Br_2 - 99 percent Xe).

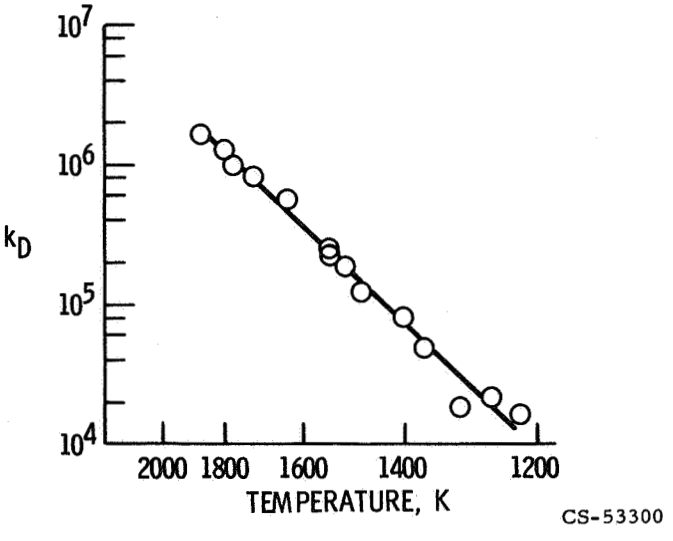

Figure IX-6. - Bromine dissociation rate constant in presence of helium (1 percent Br_2 - 79 percent He - 20 percent Xe). Contribution of Br_2-Xe collisions to overall dissociation was accounted for by knowing $k_{D,Xe}$. Xenon contribution was assumed to be directly related to its mole concentration.

CLASSICAL SCATTERING

1. NONADIABATIC COLLISIONS - NIELSEN-BAK
2. ADIABATIC COLLISIONS - LIGHT

COMPLEX FORMATION

$$A + M \rightleftharpoons AM^*$$
$$AM^* + M \rightleftharpoons AM + M$$
$$AM + A \rightarrow A_2 + M$$

3. BUNKER-DAVIDSON

CS-53305

ENERGY TRANSFER MECHANISM

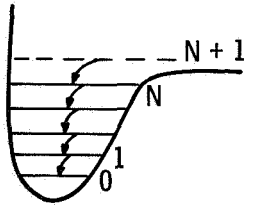

$$A + A \rightleftharpoons A_2^*$$
$$A_2^* + M \rightleftharpoons A_2^{(N)} + M$$
$$A_2^{(n)} + M \rightleftharpoons A_2^{(n-1)} + M$$
$$n = 1, 2, \ldots, N$$

4. LADDER DESCENDING - BENSON-FUENO-BEREND

DIFFUSIONAL THEORY

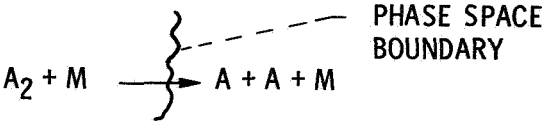

5. KECK-CARRIER

CS-53303

Figure IX-7. - Dissociation-recombination models.

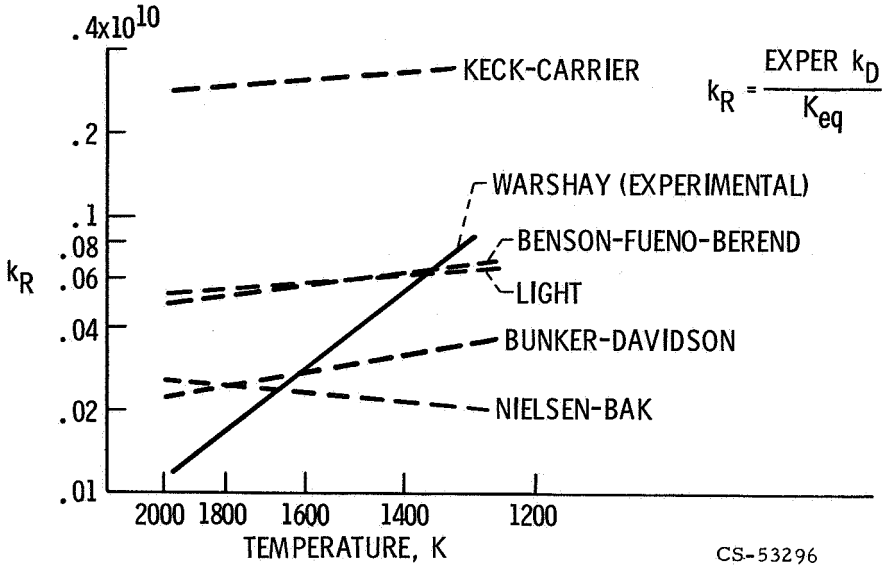

Figure IX-8. - Rate constant predictions against experiment.

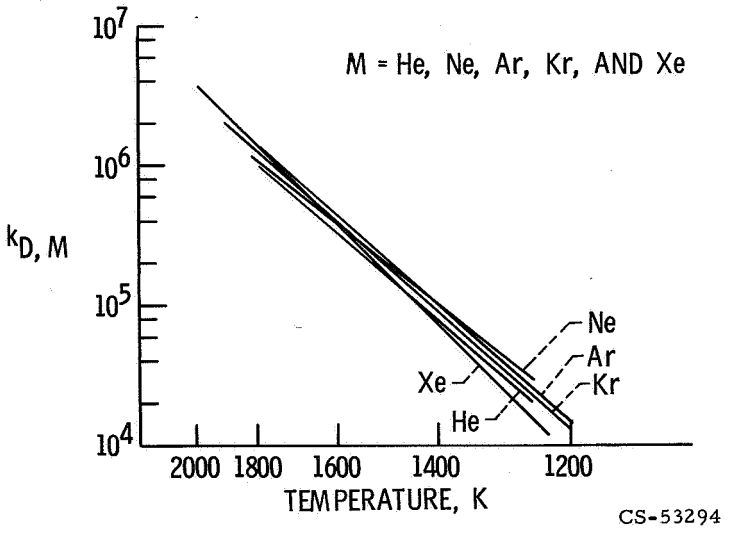

Figure IX-9. - Dissociation rate constants in noble gases.

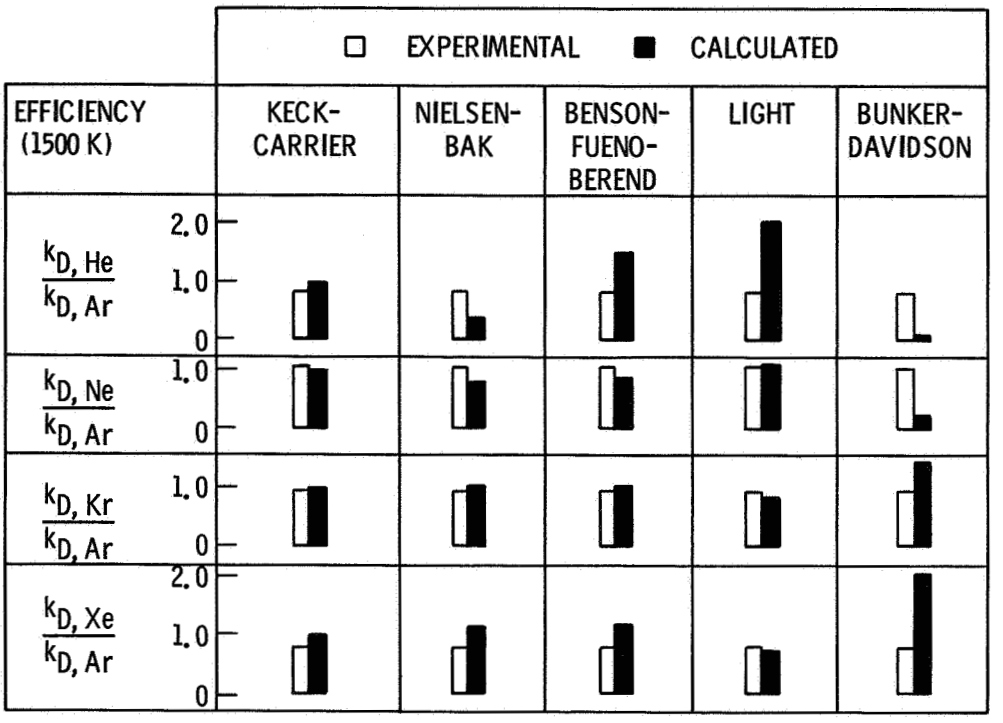

Figure IX-10. - Collision partner efficiencies (predicted against experimental).

X. CHEMICAL KINETIC COMPUTATIONS IN MULTIREACTION SYSTEMS

David A. Bittker

The previous papers have shown that the changes occurring in a complex reacting gas are the result of many individual chemical reactions occurring at the same time. Recently there has been considerable interest in being able to calculate accurately the time history of these complicated reactions. If we want to do this without neglecting some of the less important steps, we will have to solve a system of differential equations, usually on a digital computer. This type of exact kinetic calculation is useful in many types of problems. Two different approaches can be used: First, reliable experimental data can be used to study the details of a reaction mechanism and to determine individual rate constant values. This is done by studying

(1) Kinetics behind a shock wave

(2) Kinetics of reaction in a complex static system

On the other hand, known or estimated rate constants can be used to calculate practical things such as

(1) Kinetic rocket performance

(2) Ignition delays in combustible mixtures

(3) Ignition lengths and nozzle performance in supersonic flow

An example of each of these approaches is given later.

THEORY AND PRACTICAL PROBLEMS

The fundamental equations of kinetics, thermodynamics, and fluid flow are well known. The mass continuity equations for each individual species are obtained from the chemical kinetics equations. As a typical example, consider a system containing the species H_2, O_2, O, H, and OH.

The following three reversible reactions can occur:

$$H + O_2 \underset{k_{-A}}{\overset{k_A}{\rightleftarrows}} OH + O \qquad (A)$$

$$O + H_2 \underset{k_{-B}}{\overset{k_B}{\rightleftharpoons}} OH + H \qquad (B)$$

$$H_2 + OH \underset{k_{-C}}{\overset{k_C}{\rightleftharpoons}} H_2O + H \qquad (C)$$

Each forward rate constant can be expressed by a three constant equation as a function of temperature T:

$$k_i = AT^n e^{-E_a/RT} \qquad (1)$$

where A is the preexponential factor, n the temperature exponent, E_a the activation energy, and R the universal gas constant. The law of detailed balancing is used to express the relation between forward and reverse rate constant as

$$\frac{k_i}{k_{-i}} = K_{eq} \qquad (2)$$

where K_{eq} is the equilibrium constant. From reactions A, B, and C the species continuity equation for production of H_2 at any time is

$$\frac{d[H_2]}{dt} = k_{-B}[OH][H] - k_B[O][H_2] + k_{-C}[H_2O][H] - k_C[H_2][OH] \qquad (3)$$

where the brackets indicate molar concentrations of the different species. Similar equations are written for each species present. For each reaction we define the net reaction rate X_i as the difference between the forward and the reverse rate. For reaction B,

$$X_B = k_B[O][H_2] - k_{-B}[OH][H] \qquad (4)$$

Each X_i is useful as a first estimate of the importance of a single reaction among the many occurring in a reacting gas.

In practice, the species continuity equations are combined with the momentum and energy continuity equations and the equation of state for the gas mixture. The

result is a set of differential equations that must be integrated numerically.

The major practical problem in this work is finding an integration technique that will not only give good answers but give them efficiently in all experimental situations (ref. 1). The most difficult conditions to handle are the extremes of either very slow or very fast reaction. An example of slow reaction is an ignition process with a long delay. The near-equilibrium flow in a rocket nozzle is a good example of fast reaction.

EXAMPLES OF COMPUTATIONS

Using Experimental Data to Study Single Reactions

As a first application of exact kinetic calculations, we used some recently published experimental data to study the detailed mechanism of the hydrogen-oxygen reaction. Shown in figure X-1 are the data of Baldwin and his coworkers (ref. 2) giving H_2O_2 production and pressure change during the reaction of hydrogen and oxygen. The reaction took place in a static system at constant volume. The gas temperature was held constant at 500° C, and the starting mixture contained an excess of H_2 (86 mole percent). Baldwin used an approximate kinetic analysis to predict only the maximum peroxide concentration that would occur in any single experiment. This is much easier than calculating the complete H_2O_2 concentration and pressure change against time curves. We performed computations to find out whether, indeed, both the curves shown in figure X-1 could be calculated for the experiment using a single set of reaction rate constants.

Table X-1 shows the complete reaction mechanism used to describe this reacting mixture. Of the 12 listed, reactions II, III, and IV have rate constants which are quite accurately known. They have been discussed in the earlier paper by Brabbs. Our first calculations showed that there are only five reactions which really have a significant effect on the observed results. These have been marked with an asterisk in table X-1. The reaction

$$H_2 + O_2 \rightleftarrows OH + OH \qquad \text{I}$$

is the initiation step that provides the free radicals which participate in a branching chain mechanism. This is the same mechanism described in the previous

paper by Belles. The resulting radicals are used in the following reactions which control H_2O_2 production and pressure change:

$$H + O_2 + M \rightleftarrows HO_2 + M \qquad V$$

$$HO_2 + H_2 \rightleftarrows H_2O_2 + H \qquad IX$$

$$H_2O_2 + M \rightleftarrows OH + OH + M \qquad VII$$

$$HO_2 + HO_2 \rightleftarrows H_2O_2 + O_2 \qquad VIII$$

The rate constants for these reactions are not accurately known, so that they may be changed within limits if necessary.

Figure X-2(a) shows our first attempt to calculate, independently, both the experimental curves in figure X-1. For these calculations the best available literature rate constants were used for all the reactions in table X-1. The agreement between calculated and experimental curves is quite poor for both H_2O_2 mole fraction and the pressure change Δp. We then made many repeat calculations of these two curves, using each time a different set of changed rate constants for the five reactions just listed as important. We must emphasize that the rate constant changes were always within the uncertainty limits given in the literature. A modified set of rate constants was finally found which gave much better agreement between calculation and experiment. The comparison for this new set of rate constants is shown in figure X-2(b).

The necessary percentage change for each rate constant is shown in table X-2. That the largest change was needed for the $H_2 + O_2$ initiation step is not surprising, for no experimental value exists in the literature for its rate constant. Moreover, the estimates available are quite approximate. On the other hand, the peroxide decomposition rate constant was found to need no change at all after several trials. The rate constant given for this reaction VII in the Leeds University rate constant survey was found to do the best job of reproducing the experimental results. This is a rather interesting coincidence, since the Leeds survey indicates a rather large uncertainty in this rate constant. Of course, a single reaction cannot really be isolated in this type of study. Therefore, in making any judgment interactions have to be considered among all of the reactions I, V, VII, VIII, and IX. No quantitative error analysis was used. We judged "goodness of fit" for each trial by inspection of very accurate graphs. One qualitative factor considered was how

well any calculated H_2O_2 concentration curve followed the shape of the experimental curve, especially near its maximum.

In summary, what can be concluded? First, we are able to suggest small adjustments in the literature values of four rate constants to make a better fit with the overall results from one experiment. However, we recognize that the rough fitting of two simple curves using five adjustable constants does not define these constants with great precision. But if one or two additional sets of experimental data were added and the constants adjusted to give a good fit for the two or three overall reactions, then the several detailed kinetic rates could be established with good precision. Therefore the importance of this work is to suggest that the back calculation, by high speed computer methods, of detailed kinetic rates from two or three careful experiments can be a very powerful tool in establishing these rates precisely.

Using Known Rate Constants for Practical Computations

As mentioned before, rate constants can be used to calculate a quantity that depends on them in a complicated way. As an example, we show how rocket performance is calculated for a complicated propellant system, oxygen difluoride (OF_2) and diborane (B_2H_6). The engine is shown schematically in figure X-3. Propellants mix and react in the chamber, where the residence time (~10 msec) is long enough for all reactions to reach equilibrium. Many high energy species, atoms and free radicals, are formed at the combustion temperature of 4143 K. The combustion mixture is then expanded into the diverging nozzle section where the gases are rapidly accelerated and cooled. Rocket performance is really measured simply by the velocity of the hot gas at the nozzle exit point. It is clear, then, that the kinetic energy of the nozzle gas must be kept as high as possible. This kinetic energy is increased by the chemical recombination reactions which occur in the nozzle. These reactions convert the high potential energy atoms and free radicals into low energy stable molecules. Because residence time is very short (~1 msec) in the nozzle, there may not be enough time for all the possible recombinations to take place. Therefore, to accurately calculate rocket performance we must know what chemical reactions occur and also the rate of each one.

To see what important reactions occur in the nozzle we can look at the partial gas compositions shown in table X-3. These two compositions are calculated for the chamber and for the nozzle exit position at equilibrium conditions. Comparing these two compositions shows two things. First, only seven or eight species make up at least 97 percent of the gas mixture, even in this complicated system. Second,

there are only two important composition changes between chamber and nozzle exit: the H atoms are converted to H_2 molecules and the BOF mole fraction increases.

Table X-4 shows the important part of the reaction mechanism that was used in our kinetic performance calculations. Several of the minor species were used in these reactions so that no small effects would be neglected. For each reaction two importance rating factors were calculated. The first is the net reaction rate X_i illustrated in equation (4). This factor shows that the first two reactions are about equally important in controlling the results. We mentioned, however, that heat release is an important factor to be considered in rocket performance. The heat of reaction ΔH has, therefore, been listed in table X-4 for each reaction. These values show that the three-body recombination reactions like H + H + M have much larger heats of reaction than the bimolecular shuffle reactions such as BO + HF. We have used ΔH to calculate a second rating factor, the energy release rate. This factor is proportional to the product of the net reaction rate and ΔH for each reaction, and it is a much more realistic performance rating factor. It is given on a percentage basis in table X-4.

Using the energy release rate significantly changes the quantitative ranking of the first two reactions in the table. Now the H + H + M recombination clearly predominates over all other reactions. It accounts for half of the total heat release into the expanding gases. This is a very fortunate thing because the rate constant for this reaction is the best known of any of the reactions listed. A few calculations showed that most of the other rate constants for the reactions of table X-4 had to be known only to order of magnitude accuracy for our present purposes.

The results of these performance calculations are shown in figure X-4 plotted as vacuum specific impulse against oxidant-fuel ratio. The top curve shows the best performance obtainable from the OF_2-B_2H_6 combination. This calculation assumes fast reaction rates in the nozzle, so equilibrium is maintained. The bottom curve assumes that all reaction rates are zero in the nozzle. The gas composition stays the same as it was in the chamber. The kinetic curve is closer to the equilibrium line, but still well below it. The data points shown are unpublished experimental measurements obtained by the Rocketdyne Laboratory under NASA contract. They have been corrected for various losses including friction and heat transfer losses in the nozzle and combustion inefficiencies in the chamber. The nozzle corrections are those calculated by U. A. C. Research Laboratories (ref. 3), while the combustion inefficiencies are the experimental values measured by Rocketdyne. The experimental data agree with the kinetically calculated curve to about 1 percent or four to six impulse points. The discrepancy may be due to experimental error in the combustion efficiency measurements as well as computa-

tion uncertainties. The important result is that we have been able to predict rocket performance fairly accurately for this one system. The ability to predict specific impulse accurately is important to rocket designers. Especially in upper stage vehicles, useful payload depends very strongly on specific impulse.

This example shows that a complex reaction can sometimes be studied without knowing all the rate constants involved. This can be done when only one or two reactions are controlling and when these rate constants are accurately known.

COMPUTER PROGRAM

A new computer program for general chemical kinetics computations has been developed at the Lewis Research Center. This program can be used for the following types of kinetics problem:

(1) Reaction behind a shock wave

(2) Ignition kinetics

(3) Reacting one-dimensional flow

  (a) All subsonic

  (b) All supersonic

(4) Reaction in a complex static mixture

The program is designed for special convenience in performing shock kinetics and ignition kinetics computations. A flow problem that this general kinetics program will not handle is one in which the flow velocity changes from subsonic to supersonic values. It will not, then, be useful for a complete rocket nozzle expansion through a sonic throat. We have a separate program specially made to perform these rocket nozzle calculations.

Next some of the special features of the general chemical kinetics program will be described.

General Chemistry

Any chemical system can be studied. The gas mixture may contain any species with known thermodynamic properties. And any chemical reaction among these species may be used, if the reaction's rate constant is known.

Computation Efficiency

A modified implicit integration technique was developed for this program by Vincent J. Scullin of the Lewis Research Center. It is designed to work efficiently for all reaction conditions, slow or fast.

Area Profile

Any one-dimensional area profile may be assigned in a flow reaction. The user may submit a list of individual area against distance coordinates, or one of the two built-in area equations may be used. These are, first, a cubic polynomial in distance, x:

$$A = c_0 + c_1 x + c_2 x^2 + c_3 x^3 \tag{5}$$

Second, the special equation

$$A = \frac{1}{1 - \left(\frac{x}{L_m}\right)^{\eta}} \tag{6}$$

where L_m and η are constants. This equation is used only in shock kinetics calculations. It applies the corrections for boundary layer buildup in the shock tube according to the theory of Mirels (refs. 4 and 5).

Optional Constraints

In any reaction being studied, the temperature or volume or both may be held constant.

Convenience Features

We have made the program easy to use in several ways. Input data cards are simple to prepare. The user has a choice of three different sets of units for input and output. One of these is the Systemé International. In addition, the program

performs equilibrium combustion and nonreacting shock computations. The program has an option to use the results of these frozen shock calculations to start a kinetic shock computation. Finally, the user has a choice of integration variable: Either time or distance may be used as the fundamental integration variable in any problem.

SUMMARY

We have shown the usefulness of exact chemical kinetic computations for complex mixtures by illustrating two different approaches. These are (1) using experimental data with the computations to evaluate individual rate constants in a mechanism and (2) using known rate constants to compute practical things like rocket performance. The need for a good integration technique for all conditions was briefly mentioned and a computer program is described which performs many types of kinetic calculation quite efficiently.

REFERENCES

1. Lomax, Harvard; and Bailey, Harry E.: A Critical Analysis of Various Numerical Integration Methods for Computing the Flow of a Gas in Chemical Nonequilibrium. NASA TN D-4109, 1967.

2. Baldwin, R. R.; Rossiter, B. N.; and Walker, R. W.: Hydrogen Peroxide Yields in the Hydrogen + Oxygen Reaction. Trans. Faraday Soc., vol. 65, no. 556, Apr. 1969, pp. 1044-1050.

3. Sarli, V. J.; Bender, L. S.; Aceto, L. D.; and Burwell, W. G.: Kinetic Flow Performance in Nozzles. Rep. H910666-15, United Aircraft Corp. (NASA CR-72600), Dec. 5, 1969, p. 14.

4. Mirels, H.: Flow Nonuniformity in Shock Tubes Operating at Maximum Test Times. Phys. Fluids, vol. 9, no. 10, Oct. 1966, pp. 1907-1912.

5. Mirels, Harold: Shock Tube Test Time Limitation Due to Turbulent-Wall Boundary Layer. AIAA J., vol. 2, no. 1, Jan. 1964, pp. 84-93.

TABLE X-1. - MECHANISM FOR

HYDROGEN-OXYGEN REACTION

Reaction number	Reaction
I	$^{*}H_2 + O_2 \rightleftarrows OH + OH$
II	$H_2 + OH \rightleftarrows H_2O + H$
III	$H + O_2 \rightleftarrows OH + O$
IV	$O + H_2 \rightleftarrows OH + H$
V	$^{*}H + O_2 + M \rightleftarrows HO_2 + M$
VI	$H + HO_2 \rightleftarrows OH + OH$
VII	$^{*}H_2O_2 + M \rightleftarrows OH + OH + M$
VIII	$^{*}HO_2 + HO_2 \rightleftarrows H_2O_2 + O_2$
IX	$^{*}HO_2 + H_2 \rightleftarrows H_2O_2 + H$
X	$H + H_2O_2 \rightleftarrows H_2O + OH$
XI	$OH + H_2O_2 \rightleftarrows H_2O + HO_2$
XII	$O + H_2O \rightleftarrows OH + OH$

TABLE X-2. - RATE CONSTANTS FOR H_2-O_2 SYSTEM

Reaction number	Reaction	Rate constant at T = 500° C (CGS units)		
		Literature values	Adjusted values	Percent change
I	$H_2 + O_2 \rightleftarrows OH + OH$	23.6	7.01	70
V	$H + O_2 + M \rightleftarrows HO_2 + M$	3.05×10^{15}	1.63×10^{15}	47
VII	$H_2O_2 + M \rightleftarrows OH + OH + M$	1.61×10^{4}	1.61×10^{4}	0
VIII	$HO_2 + HO_2 \rightleftarrows H_2O_2 + O_2$	1.8×10^{12}	1.3×10^{12}	28
IX	$HO_2 + H_2 \rightleftarrows H_2O_2 + H$	1.58×10^{6}	1.15×10^{6}	27

TABLE X-3. - GAS COMPOSITION FOR OF_2-B_2H_6 ROCKET PROPELLANT

[Mole fractions assuming fast reactions.]

Species	Chamber	Exit
H	0.2910	0.0744
HF	.2521	.2648
BOF	.1955	.3049
H_2	.1417	.3281
BF	.0423	.0168
BO	.0258	.0007
F	.0152	.0001
O	.0075	.0000

TABLE X-4. - RANKING OF REACTIONS IN OF_2-B_2H_6 MECHANISM

[Equivalence ratio = 1.63.]

Reaction	Net reaction rate, percent	ΔH, kcal/mole	Energy release rate, percent
$H + H + M \rightleftarrows H_2 + M$	32.3	-104	53.1
$BO + HF \rightleftarrows BOF + H$	26.8	-33	13.9
$H + F + M \rightleftarrows HF + M$	5.1	-136	11.1
$H + OH + M \rightleftarrows H_2O + M$	5.2	-119	9.8
$BF + OH \rightleftarrows BOF + H$	3.9	-58	3.5
$F + H_2 \rightleftarrows HF + H$	4.5	-32	2.3
$H_2 + OH \rightleftarrows H_2O + H$	9.7	-15	2.3
$BF + O \rightleftarrows BO + F$	9.3	+8	1.2
$H + BF_2 \rightleftarrows HF + BF$	2.4	-25	1.0
$BO + F + M \rightleftarrows BOF + M$	.3	-169	.7
$BF + O + M \rightleftarrows BOF + M$	.2	-160	.6
$O + H + M \rightleftarrows OH + M$	.3	-102	.5
Total	100.0		100.0

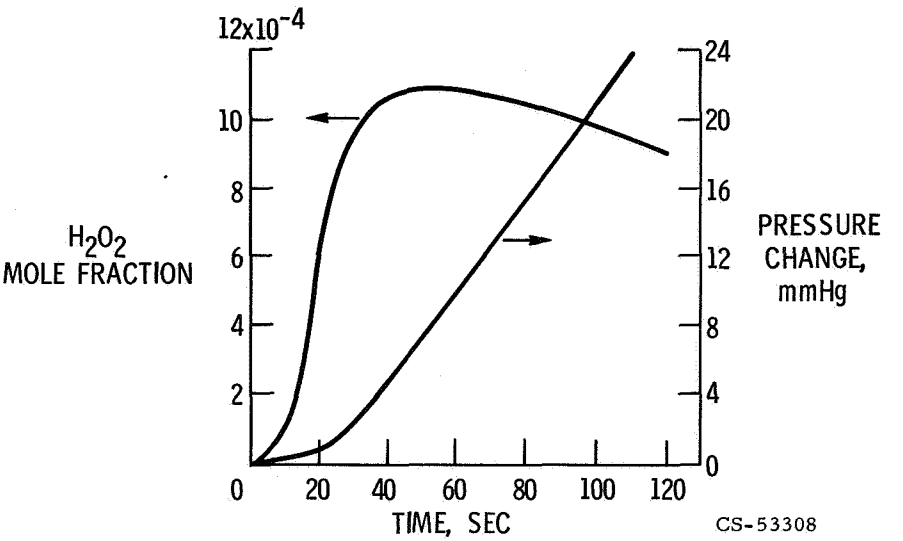

Figure X-1. - Hydrogen-oxygen reaction at constant temperature and volume. Data from reference 2; temperature, 500° C; pressure, 500 millimeters of mercury; 86 mole percent H_2 and 14 mole percent O_2.

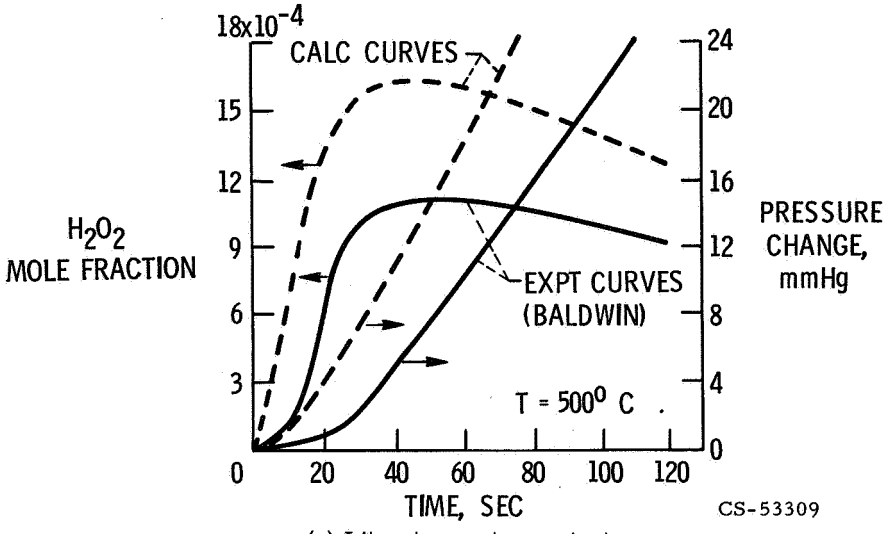

(a) Literature rate constants.

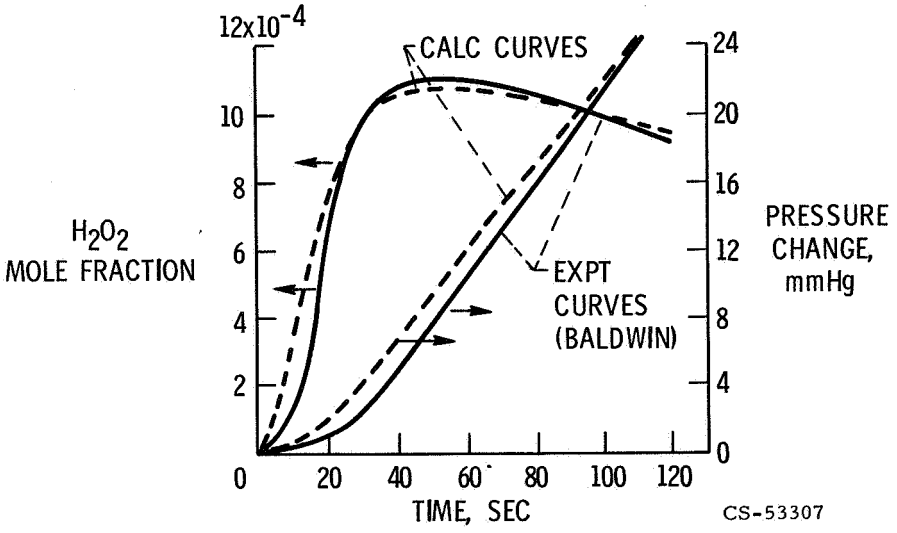

(b) Adjusted rate constants.

Figure X-2. - Calculated and experimental results for hydrogen-oxygen. Temperature, 500° C.

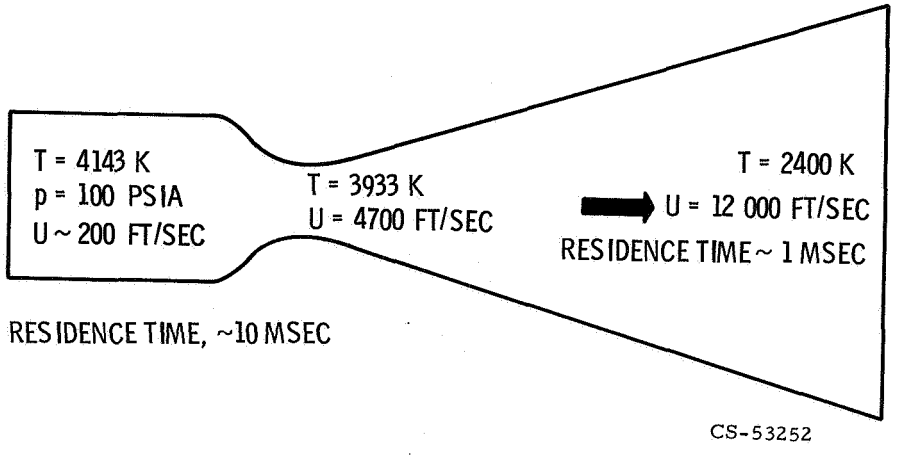

Figure X-3. - Rocket engine conditions for OF_2-B_2H_6 propellant. Equivalence ratio, 1.63.

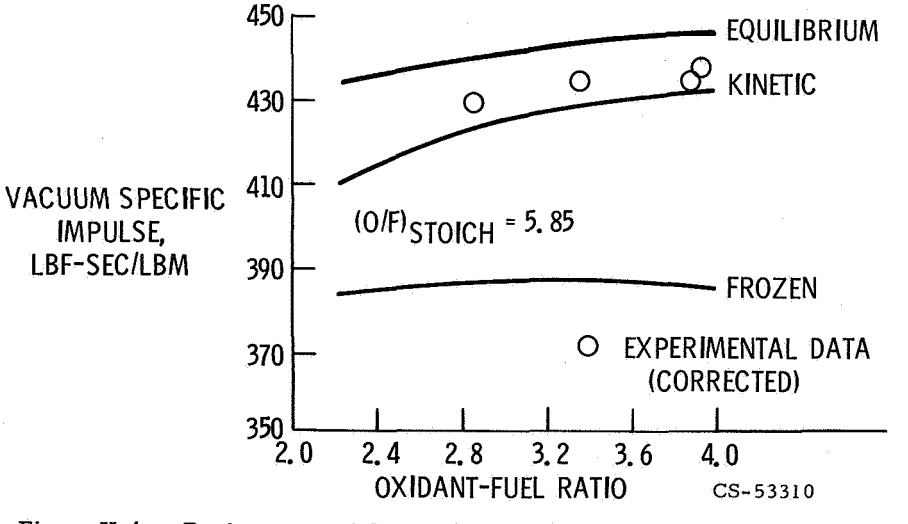

Figure X-4. - Performance of OF_2-B_2H_6 rocket propellant. Chamber pressure, 100 psia.

NASA-Langley, 1970 —— 33 E-5596